EFFECT OF SURFACE ROUGHNESS ON FLOW OVER A CIRCULAR
CYLINDER AT HIGH REYNOLDS NUMBER

BY

MD. DURUL HUDA

A Thesis
Submitted to the Department of Mechanical Engineering
in partial fulfilment of the requirements for the degree
of
MASTER OF SCIENCE IN MECHANICAL ENGINEERING

MAY, 1987.

EFFECT OF SURFACE ROUGHNESS ON FLOW OVER A CIRCULAR CYLINDER AT HIGH REYNOLDS NUMBER
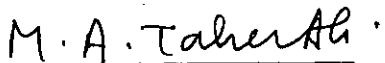
A Thesis

by

Md. Durul Huda

Approved as to style and contents by

(Dr. Dipak Kanti Das)
Professor,
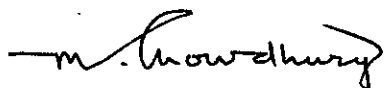Department of Mechanical Engg.
BUET, Dhaka.

Chairman

(Dr. M.A. Taher Ali)
Professor and Head
Department of Mechanical Engg.
BUET, Dhaka.

Member

Dr. Md. Quamrul Islam)
Associate Professor
Department of Mechanical Engg.
BUET, Dhaka.

Member

(Dr. Mohiuddin Chowdhury)
Professor and Head
Department of Naval Architecture
and Marine Engineering
BUET, Dhaka.

Member

May, 1987

ABSTRACT

The effect of surface roughness on the flow over a circular cylinder at high Reynolds number was investigated. The development of wake behind the cylinder was also investigated.

The experiment was done in a subsonic wind tunnel of test section 45.72 cm (18 in.) x 45.72 cm (18 in.). A wooden circular cylinder of diameter 69.85 mm (2.75 in.) was used for the experiment treating as smooth cylinder. Sand grains of average size of 1.785 mm (.0703 in.) and 3.57 mm (.14035 in.) were used as the roughness element and the roughness parameter was taken by r/d. So two roughness parameter 2.644×10^{-2} and 5.155×10^{-2} were used. Reynolds number was calculated on the basis of free stream velocity and the diameter of the cylinder. The flow parameters were measured at four Reynolds number Viz. 1.0535×10^{5}, 1.038×10^{5}, 9.726×10^{4} and 9.316×10^{4}.

Roughness of surface thickened the boundary layer and earlier separation was taken place. It also increased the drag coefficient. The drag coefficient measured by integration of local pressure around the cylinder, from momentum equation and from wake are almost equal but the method "by integration of local pressure around the cylinder" was more accurate.

The centre- line velocity increased with increase of axial distance and with decrease of roughness parameter. The rms error decreased gradually with increase of axial distance and with increase of Reynolds number and with the decrease of roughness parameter.

To My Parents

ACKNOWLEDGEMENTS

TABLE OF CONTENTS

LIST OF FIGURES

FIGURES

LIST OF TABLES

LIST OF APPENDICES

LIST OF PLATES

MOMENCLATURE

Symbols   Meaning

Latin Letters

A   Position locating pressure head connection in pitot static tube at the upstream side.

a   Constant in empirical equation.

B   Position locating total head connection in pitot static tube

b'   Const.

b   Width of the mixing zone.

C_f Coefficient of friction $\tau/\frac{1}{2}\rho U^2$

C_p Coefficient of pressure $\Delta P/\frac{1}{2}\rho U^2$

C_{pb} base pressure coefficient

C_{pm} minimum pressure coefficient.

C_p' fluctuating component of C_p

C_d drag coefficient $D/\frac{1}{2}\rho U^2 . d$

d   diameter of the cylinder.

D   drag force per unit length of the cylinder.

H   Shape factor

K_s Equivalent surface roughness

L   Length between upstream and downstream section.

P   Mean static pressure.

P_o total pressure.

Latin Letters

P_a Atmospheric pressure.

R   radius of the cylinder.

r   Average size of the sand grain.

Re_d Reynolds number based on the diameter of cylinder
and the free stream velocity - Ud/ν

u   mean axial velocity.

U   free stream velocity.

U*   Shear velocity.

W   width of the fist section.

$y_{\frac{1}{2}}$ half width of the wake

x,y   co-ordinate system

GREEK LETTERS

∂ boundary layer thickness

∂*   displacement thickness

θ momentum thickness

θ Angular position of the tapping holes

K   vonkarman constant in log-law of wall.

μ absolute viscosity of gas.

GREEK LETTERS

ν kinetic viscosity of gas.

ρ density of gas.

τ shear stress.

τ_o shear stress at surface.

Subscripts

a   air

C   Centre-line.

i   axial direction.

o   at surface.

rms   root mean square.

CHAPTER - I

1.1 INTRODUCTION:

In fluid mechanics the flow around and behind the cylinder is very important problem from fundamental and applied points of view. The flow over rough cylinder is of more interest from the application point of view. The flow over rough cylinder is quite different from the potential flow and needs a thorough investigation due to its complicated nature of flow. Besides this, the wake generated behind the circular cylinder reveals the characteristics of flow which is needed for designing hydraulics structures, ship, submarine to minimize the energy losses associated with wakes.

1.2 MOTIVATION BEHIND THE SELECTION OF THE PROBLEM:

The flow past circular cylinder at high Reynolds numbers has long been a subject of intense attention both from academic and practical points of view. For example important reductions in the magnitude of the mean peak suction in cooling tower shells can be obtained if the surface is roughened by external ribs. Heat transfer and presssure drop of heat exchanger working in nuclear reactors are generally influenced by the surface roughness of the tubes because of the high Reynolds numbers. Tall buildings, columns of bridges and barrages, oil rigs, large

ships may be broadly considered to be roughened cylinders acting in open space and subjected to fluid flow with high Reynolds number. Present exercise attempts to analyse the effect of roughness over cylinders under simmulated conditions. For the same intension, wakes are investigated.

1.3 OBJECTIVES:

The above discussions suggest for designing wind loading model, the flow characteristics are needed around the smooth and rough cylinder and in the wake behind the cylinder. The objectives of the present research programmes are:

1) To measure the pressure distribution around the cylinder for smooth and rough circular cylinder and mean flow characteristics in wakes.

The above objectives include the traverging of velocity profile, calculation of shear stress, drag coefficient, pressure coefficient, velocity defect in wake and prediction of flow preservation.

1.4 OUTLINE OF INVESTIGATION:

The flow was carried out in the test section of a wind tunnel over circular cylinder of diameter 69.85 mm (2.75 in.). The cylinder surface was roughened by sand particle of average size 1.785 mm and 3.57 mm. Nineteen holes are made on the upper half part of the cylinder at 10° interval. The flow was fully

developed in front of the cylinder and the flow development
was checked by the universal log-law of velocity distribution
near the wall.

The drag and pressure coefficients were calculated and the
position of separation point was observed by the flow visuali-
zation method and the development of wake for both smooth and
roughed cylinder was analysed. The possible explanations of
the obtained results were made and also compared with the
investigations of the similar problems.

CHAPTER - II

LITERATURE REVIEW

2.1 Number of experiments were carried out by several researchers and the effects of roughness on flow past circular cylinder were investigated. Some important works are presented below.

2.2. Experimental Investigation on Flow Over Smooth Circular Cylinder:

Flow investigation was carried out over smooth cylinder by Anatol Roshko (30) Achenbach (1), P.W. Bearman (8), J.P. Batham(7), V.C. Patel (18), Nakayama (28), Michio Nishioka (29) and others.

Anatol Roshko (30) performed his experiment in a pressurized wind tunnel at Reynolds number from 10^6 to 10^7. The drag coefficient increased from its low supercitical value to a value 0.7 at R = 3.5 x 10^6 and then become constant. He also measured the Strouhal number for R >3.5 x 10^6, definite vortex shedding occured with Strouhal number 0.27.

E. Achenbach (1) investigated the flow around single cylinders at Reynolds number 6 x 10^4 <Re <5 x 10^6. He measured local pressure and skin friction distribution around the cylinder and from these results total drag, pressure drag & friction drags were calculated. By means of the skin friction distribution the position of the separation points, separation bubbles or

transition points could be localized. He classified the flow
from the data, the subcritical flow where the boundary layer
separated laminarly, the critical flow in which a separation
bubble followed by a turbulent reattachment occured and the
supercritical flow where an immediate transition from the
laminar to the turbulent boundary layer was observed at a
critical distance from the stagnation point. He connected the
drag coefficient at the subcritical region measured by weise-
lsberger, Fage Warsap (11) with his result and also connected
with the supercritical range in which Roshko carried out his
experiment.

P.W. Bearman (8) examined the flow at Reynolds number
10^5 to 7.5 x 10^5. He observed the Narrow-band vortex shedding
upto a Reynolds number of 5.5 x 10^5 i.e. well into the critical
regime. At the Reynolds number the Strouhal number reached the
unusually high value of 0.46. Spectra of the velocity fluctua-
tion measured in the wake were also taken for several values
of Reynolds number.

Michio Nishioka and Hiroshi Satu (29) investigated the
flow behind a circular cylinder at low Reynolds number from
10 to 80. He observed that Takami and Keller's numerical
solution for the velocity distribution in the wake shows good
agreement at low Reynolds number and fair agreement at high

Reynolds numbers. The measured velocity defect distributions were well representated by the following theoretical distribution for the wake by assuming similarity

$$\frac{U - u}{U - u_c} = \exp \{- 0.693 \ (y/Y_{\frac{1}{2}})^2 \}$$

H.H. Fernholz and J.D. Vagt (13) measured the tubulence characteristics in an adverse pressure gradient three-dimensional turbulent boundary layer along a circular cylinder. He showed that the normal stresses $\overline{u'_i{}^2}$ and the shear stress component $\overline{u'v'}$ behaved qualitatively much as those in a two dimensional adverse pressure gradient boundary layer. The other components $\overline{v'w'}$ and $\overline{u'w'}$ both characteristic of three dimensional flow and caused by the circumferential pressure gradient were influenced in different ways by the streamwise and circumferential pressure gradients. Spectra of u' fluctuations were again similar to those obtained from two-dimensional boundary layers. Mean velocity profiles obyeyed the linear and logarithmic law of the wall known from two-dimensional boundary layer. This was for the streamwise pressure gradient dominated over the circumferential pressure gradient in that experiment. Again the ratio of Reynolds shear stress and turbulent kinetic energy was no longer approximately constant as was assumed for two-dimensional boundary layer.

Alfred Ayoub and K. Karamcheti (6) measured the surface pressure and wake velocity fluctuations at the Reynolds number .85 x 10^5, 1.8 x 10^5 and 7.7 x 10^5. The above measurements revealed the existance of a shedding regime in the tip region that was distinct from the one prevailing on the main body of the cylinder. In particular this regime could be unstable and intermittent, could have a cellular structure in the wake or could be subcritical when the main flow was supercritical.

The effect of the free-stream turbulence on the flow past a circular cylinder wasstudied experimentally in the subcritical and critical regimes by Masarukiya Yasuhiro Suzuki, Mikio Arie(24). The critical Reynolds number R_c at which the time-mean drag coefficient obtained the value of .8 was found to satisfy the relation $R_c^{1.34}$ T = 1.98 x 10^5 where T is the Tailor number defined in terms of longitudinal integral scale. The time mean drag coefficient, the base-pressure coefficient and the Spanwise correlation length of the surface pressure fluctuations in the vicinity of the separation point were fairly correlated with the parameter $R^{1.34}$ T, R being the Reynolds number and it was argued that the parameter $R^{1.34}$ T would control some aspects of the flow past a circular cylinder immersed in turbulent streams. Tailor's number T = $\{(u'^2)^{1/2}/U_x\}$ $(d/L_x)^{1/5}$ where L_x is the longitudinal integral scale.

G.S. West and C.J. Apelt (34) investigated the effects of tunnel blockage and aspect ratio on the mean flow past a circular cylinder at Reynolds number 10^4 to 10^5. He took the blockage ratio from 2 to 16% and of aspect ratios from 4 to 10. For blockage ratios less than 6%, it was shown that the effects of blockage in pressure coefficient and the drag coefficient are small and that the strouhal number was unaffected by blockage. But for blockage ratios in the range 6- 16%, there was considerable distortion of the flow due to blockage and the effects were complex. The pressure distribution was of a different form and the strouhal number changed. However, conflicting influences result in a blocked drag coefficient which was not very different from that at no blockage. Reduction in aspect ratio had effects on drag coefficient and on base pressure coefficient which were similar to those associated with increase in blockage ratio. The momentum method predicted the unblocked base pressure coefficient quite well. By momentum method $Cd_c/Cd = (1 - C_{Pbc})/(1- C_{pb})$.

C indicated the corrected value.

2.3 Experimental Investigation on Flow Over Rough Circular Cylinder:

Elmar Achenbach (2) investigated the influence of surface roughness on cross flow around a circular cylinder in a high

pressure wind tunnel at Reynolds numbers in between 4×10^4 to 3×10^6. He used a cylinder of diameter 150 mm and length 500 mm. The cross section of the test section was 500 x 900 mm. He took the sand particle for roughening the cylinder surface and performed the experiment by taking three roughness parameter Ks/D = 110×10^{-5}, 450×10^{-5} and 900×10^{-5}. He corrected the drag coefficient by applying the formula of Allen and Vincenti. The drag coefficient was a function of Reynolds number and was divided by four parts namely subcritical, critical, supercritical and transcritical flow regime according to the value of Reynolds number and each of these ranges was characterized by a special boundary layer behaviour. In subcritical flow regime Cd was not influenced by Reynolds number like transcritical flow regime but at critical flow regimes, Cd suddenly droped and then raised for the supercritical regime. The position of zero skin friction indicated the separation of boundary layer. He showed that the transition point between laminar to turbulent boundary layer became small for large roughness parameter than that of lower one. He also concluded that large values of separation angle meant the low drag coefficient and vice versa. Large separation angles occured for lower roughness parameter. Increasing roughness parameters caused decreasing critical Reynolds numbers and in the transcritical flow regime higher the drag coefficients corresponded to higher roughness.

J.P. Batham (7) measured the mean and fluctuating pressure distribution on long circular cylinders for smooth & rough surfaces at two Reynolds numbers 1.11×10^5 and 2.35×10^5 in both uniform and turbulent streams. He observed that pressure distributions on the rough cylinder were completely different in uniform and turbulent streams. The presence of turbulence increased the level of vortex shedding energy and made mean pressure distribution similar to those obtained on smooth cylinders at Reynolds numbers fo the order of 10^7. At both Reynolds numbers 1.11×10^5 and 2.35×10^5 the level of C_p' around the front of the cylinder was approximately constant up to the approach of separation turbulent stream. It was seen that after separation the distribution at the lower Reynolds numbers fell to the level observed on the rough cylinder in the uniform flow but at the higher Reynolds number the distribution was similar to that shown on a rough cylinder in turbulent flow at a Reynolds number of 7.1×10^5 tested by Tunstall.

Edmond Szechenyi (32) investigated the flow over circular cylinder at Reynolds numbers 2×10^5 to 6×10^6 in two different wind tunnels having working sections 1.77×1.75 m and $.78 \times .56$ m and used the cylinder .14, .10 and .06 m of diameter. Spherical glass beads of seven different sizes of diameter δ from .04 to .7 mm were used. He used the roughness Reynolds number and measured steady drag, fluctuating lift, and shedding strouhal number.

In sub and supercritical regimes, vortex shedding was periodic, resulting in an alternating circulation which genera- ted fluctuating pressures with a well defined frequency fs = $S_s V/d$ where fs is the shedding frequency and S_s is the strouhal number. But in transitional (critical) flow separation was neither regular nor periodic and the resulting fluctuating pressures were random. The separation point in transcritical flow was far down- stream from its position for the sub and supercritical regimes, so the wake became narrower, resulting in a smaller steady drag force. He observed that the change from transcritical to super- critical flow always occured at a value of R_s between 170 and 220 and in order to generate a supercritical flow by means of surface roughness the diametral Reynolds number must had a value of at least 10^5. Roughness Reynolds number was the only parame- ter determining the change in the flow regime from trans to supercritical which implied that the absolute roughness dimension was the only governing size parameter. The limit between the sub and the transcritical regimes was much less sensitive to surface roughness.

O. Guven, C. Farell and V.C. Patel (18) investigated the surface roughness effects on the mean flow past circular cylin- ders at Reynolds numbers range 7×10^4 to 5.5×10^5 for distri- buted roughness parameter of 2.5×10^{-3}, 3.11×10^{-3}, 4.18×10^{-3}, and 6.21×10^{-3}. They measured the mean pressure distributions

and discussed the effects of roughness in the light of boundary layer theory. He found a significance influence of surface roughness on the mean pressure distribution even at very large Reynolds number. He found that larger roughness gave rise to a thicker and more retarded boundary layer which separated earlier and with a smaller pressure recovery which was in agreement with Roshko, Achenbach. They classified the flow in four regions by the help of boundary layer theory.
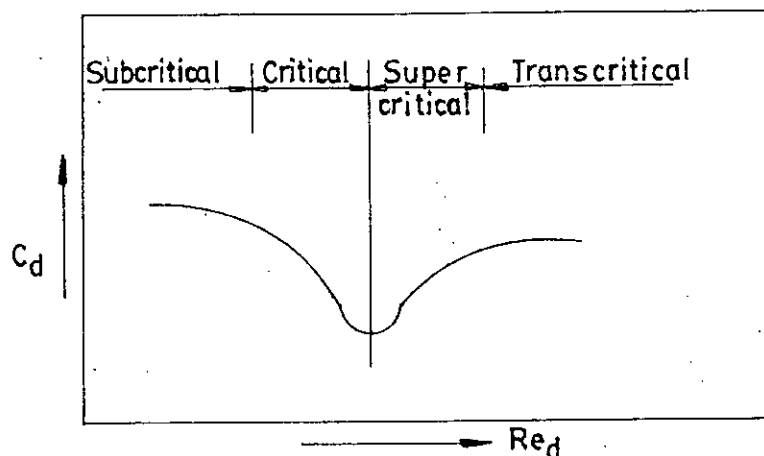
Four Reynolds number ranges relevant to the flow past circular cylinders.

In the region of subcritical Reynolds number, separation becomes purely laminar, in the critical range, laminar bubbles followed by turbulent reattachment and delayed final separation, in supercritical range, transition ahead of separation

and moving upstream and in transcritical region, transition
sufficiently close to the stagnation points in which the flow
became independent of Rd.

Y. NAKAMURA AND Y. TOMONARI (28) investigated the effects
of surface roughness on the flow past circular cylinders at
high Reynolds numbers. He measured the mean pressure distri-
bution and strouhal number on a smooth circular cylinder.
Circular cylinders with distributed roughness and circular cylin-
ders with narrow strips over a Reynolds number range 4.0×10^4
to 1.7×10^6 in a uniform flow. His results were in good agree-
ment with Achenbach. A successful high Reynolds number (trans-
critical) simulation for a smooth circular cylinder obtained
using a smooth circular cylinder with roughness strips and he
found that High Reynolds number simulation could only be obtained
by roughness strips and not by distributed roughness. The flow
characteristics were primarily functions of the roughness para-
meter r/D in the transcritical range. A similarity parameter
$(r/D)^{0.6}$ Rd could correlate the pressure distributions on cir-
cular cylinders with distributed roughness in the supercritical
range where the drag coefficient was increasing with Reynolds
number.

CHAPTER - III

THEORY

3.1 General:

Three methods are used to calculate the drag coefficient
and these three methods are dealt with in this chapter.

3.2 Draf Coefficient:

The drag coefficient is given by (C - 5)

$$Cd = \frac{D}{\frac{1}{2} \rho U^2 . d}$$ where D is the drag per unit length

of the cylinder and d is the hydraulic diameter of the cylinder.

The drag force is calculated by the following three methods

1) by momentum equation

2) by the integration of local pressure around the cylinder.

3) From the wake profile.

The drag force obtained by taking control volume over a
region containing upstream and downstream side is given by

$$D = P_1 h - \int_0^h P_2 dh - 2 \int \tau_0 dl + \rho_a \int_0^h u^2 dy - \rho_a \int_0^h v^2 dy \qquad 3.2.1$$

The drag force obtained by the integration of local pressure
around the cylinder is given by.

$$D = 2 \cdot R \int_0^{\pi/2} (P_2 - P_1) \, d\theta \qquad\qquad 3.2.2$$

The drag coefficient calculated from the velocity distribution in the wake of the cylinder is given by

$$C_D = \int 2 \frac{u}{U} \left(1 - \frac{u}{U} \right) d \left(\frac{y}{d} \right) \qquad\qquad 3.2.3$$

The details of derivation are given to the appendix A,B and C.

3.3 Development of Flow:

To check the flow fully developed the log-law wall was introduced. The straight line plotting u/U^* versus YU^*/ν in semilog scale proves the flow fully developed. The well known log law wall is

$$\frac{u}{U^*} = \frac{1}{k} \log \frac{YU^*}{\nu} + B' \qquad\qquad 3.3$$

The details of derivation are given in appendix D.

3.4 Development of Wake:

A wake is formed behind a solid body which is being draged through a fluid at rest or behind a solid body which has been immersed in a stream of fluid. The velocities in a wake are smaller than those in the main stream and the loss

in the velocity within the wake is amount to a loss of momentum which causes drag in the wake and it spreads in the axial direction. But at a certain distance the velocity defect and Reynolds stress become invariant with respect to axial distance if they are expressed in terms of the local length and velocity scale. The empirical equation which satisfies the flow in wake and self preservation is

$$\frac{U-u}{U-u_c} = \exp\{-\ln a \ (\ y/y_{\frac{1}{2}})^2\} \quad \text{where } a = 2 \qquad 3.4$$

CHAPTER - IV

EXPERIMENTAL SET UP AND PROCEDURE OF MEASUREMENT

4.1 General:

The objectives of this investigation are to study the

effect of surface roughness on flow over circular cylinder and

on wakes. All properties relating wake, mean axial velocities,

local pressure around the cylinder were measured experimentally

and compared with the existing theoretical & experimental

results.

The mean velocities were measured by a pitot static tube,

the local pressures around the cylinder (upper half part of

the cylinder) were sensed by the tappings on the circumference

of the cylinder. The main flow system is described in the

following sections of this chapter. Section (4.2) describes

the main flow facility used. Section (4.3) describes the

traversing mechanism of the sensing probe. Possible sources

of error are dealt with in section (4.4). Wind tunnel test is

described in (4.5) section. The process for observing separa-

tion and back flow are described in section (4.8) and in

section (4.7), the measured procedure are described.

4.2 The Wind Tunnel:

The wind tunnel used in this experiment was a 16.15 m

(53 feet)long open circuit subsonic wind tunnel with a test

section of .46 m (1.5 ft) x .46 m (1.5 ft) cross section.

The basic design of the wind tunnel was done by Islam (21) which was a closed circuit wind tunnel, later the design was modified by Khalil (22) to an open circuit tunnel and further modification and development was done by Hasan (19).

The wind tunnel and its different views are shown in Figure (4.1). The wind tunnel was made of a filter cum settling chamber, a bell mouth entry, an eddy breaker, a flow straightener and a 152.4 cm uniform upstream section, a test section, a diverging section, two counter rotary axial flow fans, a flow controlling valve and a silencer.

The filter cum settling chamber measuring 254 cm x 152.4 cm was made of wooden frames covered with 2.54 cm thick foam sheets. A cloth cover for the settling chamber was used in order to keep the foam clean and to prevent external damages. This chamber immunized the flow inside the tunnel against all outside disturbances and foreign particles. Even then at the front portion of the settling chamber about 91.44 cm away, a rectangular block was errected (152.4 cm x 304.8 cm) made by 1.27 cm foam for one layer and 2.54 cm foam for the other layer facing the settling chamber with wire net 8 sevies per cm in between these foam for removing all foreign particles.

The converging nozzle was 152.4 cm long and made of 15 SWG black sheet. The contraction ratio of the nozzle is 5:1. The honneycomb like flow straightner made of 2.54 cm diameter PVC pipes, 24 cm long stacked at the duct-entry and fixed with glue. Wire net with 2 holes/cm was fitted at the entrance of the nozzle played as the eddy breaker.

The test section was made of three wooden walls and one perspex wall of length 183 cm. The perspex wall was provided for observation of the probes and for setting the cylinder properly during the experiments. At the test section, a hole of 8.9 cm diameter was done to the 1.27 cm ($\frac{1}{2}$") thickness perspex sheet at its mid point and a .3175 cm (1/8") grove of 69.85 cm diameter was made to the opposite wood wall of the perspex sheet. For fastening the cylinder in the tunnel easily, the hole made in the perspex sheet became larger than that of cylinder diameter. Cylinder was pressed fitted to a flange of outer diameter 13.33 cm (5.25") which was fixed to the perspex sheet by the screw.

Two tappings, one for monitoring static pressure and other for that of temperature were made on the ceiling of the wind tunnel at a distance of 30.48 cm (1') & 60.96 cm (2') from the entrance end respectively. The static pressure

tapping was connected to a draft gauge and its deflection was observed time to time during the measurements. Any variation of mean flow caused mainly by the variation of fan speed, was detected in the monitoring draft gauge and was corrected by controlling the butterfly valve. The wooden section have 1.27 cm ($\frac{1}{2}$") continuous axial slot in the middle of the ceiling and transverse slot at four positions of the duct ceiling. These slots facilited the positioning of the sensing probes at different positions of the test section. The probe positioning arrangement was shown in Fig. 4.2.

The diverging section of the tunnel was 396.24 cm long and made of 15 SWG balck sheet. The angle of divergence was 6° which envisized, minimizing the expansion loss and reducing greatly the possibility of flow separation. The flow was produced by a two-stage contra-rotating axial flow fan (woods of colchester Ltd. England Type 38 JTE) of capacity 30,000 cfm at the head of 15.24 cm of water and rpm 1475. The position of the fan, downstream of the tunnel section produced an induced flow through it providing a more uniform, stable and undisturbed flow through the test section. The butterfly valve was used to control the flow, a screw thread mechanism was used to actuate the valve. Finally the silencer was fitted at the end of the tunnel to reduce the noise of the system.

The central longitudinal axis of the wind tunnel was maintained at a constant height from floor. A foam made isolator was placed between the fan unit and the diverging part so that the vibration of the rotating fan could not proceed towards the test section.

4.3 Traversing Mechanism:

The pilot-static tube was traversed in the air stream by Mitutoyo co-ordinate Measuring Machine (Type CX 652 code 198-402) with ranges X co-ordinate 60.96 cm (24 in), Y co-ordinate 50.8 cm (20 in.) and Z co-ordinate 25.4 cm (10 in.) (plate 4-2.). The mechanisms was actuated by a wheel through a rack and pinion arrangement and by the help of it a position was fixed upto an accuracy of .00127 cm (.0005 in.).

In order to prevent undue vibration of the sensing probe, the pilot-static tube was supported by a mild steel rod of diameter. 1.016 cm (.4 in.) as shown in fig. 4.3b. The rod was rigidly fixed to the holder fig. 4.3a which was again fixed with the traversing gear. The sensing point was kept 15.24 cm beyond the end of the rod to ensure that no major disturbances occured near the sensing point of the pitot tube by the presence of the rod.

4.4 Uncertainties and Their Analysis:

The uncertainies were introduced in the system of measurements. Errors were taken place during the measurement of the properties of the flow. The traversing mechanism could place the probe with an accuracy of $\pm$ .00127 cm. which could result in a maximum error of 0.50% in the mean velocity measurement.

For a particular valve setting the flow in the tunnel varied due to the variation of the fan speed and changes in the atmospheric conditions. To minimize the first effect the fan was kept running for half an hour before taking the actual reading. The flow was monitored time to time by recording the static pressure at the reference station of the wind tunnel. The flow was found to vary within .0254 cm of H_2O of static pressure in one experimental run and the flow reproducibility between different runs was also maintained within the same range. The analyses of uncertainties involved in different measurements are given in Appendix-E.

4.5 Test of the Wind Tunnel:

The origin of the co-ordinates used in the experiment is shown in the fig. 4.2. The origin is the middle point of the cylinder and x co-ordinate measured + tive in the downstream

direction and y co-ordinate is measured positive with upward

direction and Z is measured along the axis of the cylinder.

Before performing the actual experiments the mean velocity

and the mean static pressures were measured at $x/d = -4$ and -3

at different flow rates. From figure 5.6 a-b the flow was

found to be almost symmetric about the centre of line of the

test section. The mean velocity was found stable within 1.15%

of its value. The flow in the test section of the wind tunnel

was found almost absolutely free from any transverse pressure

gradient as evident from fig. 5.7. The mean velocity profiles

at different axial positions ($x/D = -2,-3,-4$) would coalesce

to a single curve justifying the attainment of a fully deve-

loped flow condition. To avoid overcrowding of experimental

points, however, the profiles are drawn shifting their origin

upwards as shown in fig. 5.8 a-d. The st. line nature of the

semilogarithmic plots of mean velocity also serve as strong

evidence of a fully developed flow condition, fig. 5.9.

The reproducibility of the flow condition and of

measurement by draft gauge was found to be 3.5% of mean centre

line velocity and 1% of a measured value of the instruments.

These variation were allowed in the experiment.

4.6 Measurement of Pressure Around the Circular Cylinder:

A wooden cylinder of 69.85 mm diameter made of teak wood

was used for the experiment. Nineteen holes were made on the

upper half part of the cylinder making 10° interval thus in 180° the nineteen tappings were made for measurement of the pressure on the surface of the cylinder. The holes were connected internally by the capilary tubes of .079 cm dia (1/32") which were fixed at the end by nipple. For suitability of measurement and for stability of the cylinder the holes were made at differents points on the cylinder placed diagonally shown by the diagram 4-6. During the experiment the stagnation point was fixed where the pressure readings became minimum. Pressure readings were taken at the downstream side $x/d = 4,6,7,8.5$ and 12.5 and to the upstream side at a distance $x/D = -4,-3$ by the pitot tube. After taking all readings, the smooth cylinder was turned up in the lathe machine. Sand particle of average radius of height .178 cm were distributed around the cylinder fixed with glue. At first a white cloth was wrapped around the cylinder, and was glued by Aica, then the cylinder was rotated on the pile of the sand particle. Only one particle will be placed to one place. Then all readings were taken in the similar way like smooth cylinder. The diameter of the cylinder remained const with deviation $\pm$ .5%. During making the roughness on the surface of the cylinder, the opening of the small holes were closed by the pin which were root up during taking reading.

4.7 Measurement of Mean Velocity and Pressure:

For measurement of axial mean velocity and mean static pressure, a hemispherical head of .317 cm (1/8 in.) O.D and 40.64 cm (16 in.) long united sensor pitot static tube Fig. 4.4 was used. According to Huston (20) a misalignment of the tip of the tube $\pm$ 10° from the flow direction have little effect on the measured value of total pressure. The pressure around the cylinder were determined from the pressure tappings made to the upper half part of the circumference of the cylinder and was measured by draft gauge.

The McMillan (27) correction factor for the effective displacement of the pitot tube centre towards the region of higher velocities was considered negligible due to the small tip height of the static tube used. The mean velocities were inferred from the total and static pressure data with the aid of incompressible Bernoulli's equation

$$u = \sqrt{2/\rho . \ (P_O - P)}$$

where P and P_O are the wall static pressure and stagnation pressure respectively.

4.8 Flow Visualisation:

The technique applied for observing flow separation and the flow around the cylinder is very simple but very effective.

For test at first the 30.48 cm (12 in.) x 30.48 cm (12 in.)
wind tunnel made of perspex sheet was used and presented a
clear view of the flow picture. Then this technique was
applied to the experimental wind tunnel. At first a white
paper was carefully fixed to the cylinder surface such that
no foldings and bulge portion were on the surface. Then a
mixture of kerosine and lamp-black was painted on the surface
and then the air was blown. After few minutes the required
pattern would be developed. During the experiment the concen-
tration of the mixture was to be carefully determined, if it
was too thin, all the lamp blacks would be washed away and if
it was thick, it would give no flow pattern. So the concentra-
tion of the mixture was determined by trial and error. To see
the back flow region the test section was placed in such way
that the cylinder axis remained in the bottom and ceiling
direction of the wind tunnel. Then a white paper was crefully
placed on the tunnel bed and was brushed with the mixture
and the air was blown. After few minutes of air blowing, a
clear picture of the pattern would be developed and it is
shown in Fig. 5-4-c,d.

CHAPTER - V

RESULTS AND DISCUSSION

5.1 General:

In this study, the flows are investigated around and behind the cylinder. The experiments were performed by varying the roughness parameter. All the experimental data have been analysed to obtain pressure coefficient, drag coefficient and information regarding the wake developments. The wooden cylinder of 69.85 mm diameter was smoothened in a lathe machine by brushing it with a smooth sand paper No. 0 and treated as smooth cylinder which was subsequently made rough by gluing sand particles of average size 1.785 mm and 3.57 mm along the circumference of the cylinder.

The results obtained are compared with the similar investigations made by different workers.

5.2 Measurement of Mean Flow Characteristics Around and Behind the Cylinder.

The mean flow characteristics were measured at four different Reynolds numbers viz Re_d = 1.0535 x 10^5, 1.0382 x 10^5, 9.726 x 10^4 and 9.316 x 10^4. These Reynolds numbers were taken since these were the max^m Reynolds number attained at the experimental wind tunnel.

· The measurements included mean axial velocity, local pressure around the circumference of the cylinder and coefficient of pressure, coefficient of drag, log-law parameters, and velocity defect distribution were determined.

5.2.1 Coefficient of Pressure:

The coefficient of pressure, C_p versus angular position, θ plots are shown in Fig.5.2-1 a-d. Each figure has three distinct portions. In the first portion C_p decreases because pressure on the front part of the cylinder decreases and after attaining the peak negative value, it starts increasing due to increase of pressure before it becomes constant at the trailing edge. The pressure coefficient C_{pb} is the base pressure coefficient defined as the average of the nearly constant pressure coefficient in the wake region and C_{pm} is the minimum pressure coefficient. In Fig. 5.2-1-d, the curves from measured value are different from Guven, Achenback because of different Re_d and roughness parameter.

The $|C_{pm}|$ increases with the increase of Reynolds number which is in agreement with Achenbach (1) and base pressure is independent of Reynolds number for large roughness parameter which is in agreement with Armit (5), Nakamura (28), Guven (18). At the stagnation point C_p becomes unity indicating the complete conversion of velocity head. At higher Re_d, C_p distri-

butions falls on a single line except at the negative peak.

From Fig. 5-2-1-e-h it is evident that $\left|C_{pm}\right|$ of smooth cylinder is always greater than that of rough cylinder but $\left|C_{pb}\right|$ of smooth cylinder is lower than that of rough cylinder indicating the delay of separation. With the increase of roughness, separation takes place earlier which is in agreement with the results of Guven (18), Acheback (1). The point from where C_p becomes constant indicates roughly the point of separation.

5.2.2 Coefficient of Drag

The coefficient of drag is measured by using three different methods. The coefficients of drag measured by the method of integration of local pressure around the cylinder have been shown in fig. 5.2.2a and they are in good agreement with Roshko (29), Guven (15), Achenback (1), Fage and Warsap (11). Fig. 5.2.2.b-f shows the variation of C_d with Reynolds number and roughness parameter, measured from momentum equation. These curves also show that coefficient of drag increases with the increase of roughness and of Reynolds number. The same conclusions can be drawn from the fig. 5.2.2.g-k where C_d is calculated from wake profile. Fig. 5.2.2.m shows that the drag coefficient measured by the method of integration of local pressure around the cylinder is almost equal to the

value obtained from wake profile and slightly smaller than

C_d measured from momentum equation.

All figures indicate that no critical Reynolds number are

attained both for smooth and Rough cylinder.

5.3 Wake Development:

5.3.1 Mean Velocity:

Fig. 5.3.1 (a to L) show the variation of mean velocity

distribution in wakes at Reynolds numbers Re_d = 1.0535 x 10^5,

1.035 x 10^5, 9.726 x 10^4, and 9.316 x 10^4 for smooth and rough

cylinders. All the figures show the development of the wakes

with increasing the width. Such a spread of the wake is logical

from the view point of energy transfer to the wake from the

surroundings.

Fig. 5.3.1 m, n show that drag coefficient remains constant

within the wake for a certain Reynolds number and increases

with Reynolds number. So indirectly it can be said that momen-

tum thickness increases with Reynolds number but remains cons-

tant within the wake which is in agreement with Chevary and

Kovasznay (9).

5.3.2 Half Width and Centre Line Velocity:

The half width is the vertical distance in the wake
where $(U-u)/(U-u_c) = .5$. It is an important geometrical dimen-
sion for length scale generally used for explaining the self
preserving flow. From the Figure 5.3.1 (a-1) it is seen that
half width increases with the increase of axial distances
indicating development of wake. According to Schlichting, H.
and Reichardt, H.(31) $y_{\frac{1}{2}} = \frac{1}{4}(x.c_d.d)^{\frac{1}{2}}$. However the present
results do not show a good agreement (Fig. 5.3.2a), since the
experiment carried on $x/c_d.d < 50$ unlike schlichting.

Dimensionless centre line velocity against the dimen-
sionless axial distance is plotted in Fig. 5.3.2 b, c,d,e.
It is observed that centre line velocity increases more rapidly
with axial distance in the case of smooth cylinder in compari-
son to rough cylinder. This indicates that wake behind a smooth
cylinder attains self preservation more quickly.

5.3.3 Self Preservation:

Dimensionless velocity distributions in the wake for
smooth cylinder are plotted in Fig. 5.3.3 a,b,c,d at Reynolds
number 1.0535×10^5, 1.0355×10^5, 9.726×10^4 and 9.316×10^4
to examine self preservation of flow. The half width $y_{\frac{1}{2}}$ is
used as length scale in the self preservation plot. The figures

show the near self preservation. The semiempirical equation
(3-4) derived by Gartshore and Keffer (15) for sinilarity
profile is superimposed to compare with the present results
and is shown in Fig. 5.3.3 a,b,c and d. The deviation of
the experimental results from the semiempirical equation
(3.4) is not too great. The rms error in respect of deviation
was calculated and found to decrease gradually with axial
distance and increasing Reynolds number. So the flow achieves
self preservation earlier with higher Reynolds number which
is in agreement with Gartshore (15) and shown from the follow-
ing tables and drawn in Fig. 5.3.e.

Table 5.1

rms error at various distance from the origin

$x/d \longrightarrow$ R_{ed}	4	6	7	8.5	12.5
1.0535×10^5	.337	.287	.258	.234	.215
1.0355×10^5	.351	.292	.278	.254	.222
9.726×10^4	.354	.313	.296	.286	.279
9.316×10^4	.3684	.339	.313	.311	.297

5.4 Separation:

Separation starts where $(\partial u/\partial y)_{y=0}$ is zero and at separation shear stress is zero. Separation cannot occur unless $\partial p/\partial x > 0$. From figure 5.2.1 a,b,c,d it is seen that pressure increases at the downstream surface of the cylinder. Achenbach[2], Guven [18] showed that separation starts earlier with increasing Reynolds number and Roughness parameter at the supercritical and transcritical region. Achenbach [2] showed separation at $\theta_s = 78^O$ for $Re_c = 10^5$, $\theta_s = 94^O$ for $Re_d = 2.6 \times 10^5$ at subcritical region. $\theta_s = 147^O$ for Re_d 8.5×10^5 at critical region and $\theta_s^O = 115^O$ at $Re_d = 3.6 \times 10^6$ at supercritical region and θ_s would be earlier with $Re_d > 3.6 \times 10^6$.

At the adverse pressure gradient the fluid particle could be brought to rest causing the neighbouring fluid to be deflected away from the boundary. This is roughly observed by the Figure 5.4. a,b. A white strip along the axis of the cylinder starts at about 75° indicating separation starts from 75°, was taken at Re = 1.035×10^5. This separation point is nearly equal to that one, found by Achenback [2].

Back flow starts from the separation point and vortex rings are developed. The vortices interact strongly and break down into turbulent eddies. The interaction of turbulent

eddies causes large scale vortical motion and these small scale vortical motions caused by viscosity and flow becomes straight. This is shown by the Figure 5.4.c,d. From Fig. 5.4.c it is shown that after 20.32 cm (8") from origin the flow becomes straight taken at Re = 1.035×10^5 and would be increased the distances with increase of Re_d.

CHAPTER - VI

CONCLUSIONS

6.1 General:

In this chapter the achievements of the present experimental investigation are presented and the scope of extension and development of the present study are suggested. The roughness parameters used in the present study is comparatively large from that used by the previous researchers. The effect of roughness on flow past circular cylinder, drag coefficient and other parameters was analysed.

6.2 Conclusions:

1. $\left|C_{pm}\right|$ is greater in the case of smooth cylinder than rough cylinder.

2. $\left|C_{pb}\right|$ at large Reynolds number for large roughness parameter is constant.

3. Separation starts earlier if the roughness parameter increases.

4. With increase of Reynolds number the separation starts earlier giving larger value of drag coefficient i.e., large momentum thickness.

5. Drag coefficients calculated from three different methods are almost same.

6. The drag coefficient increases with increase of roughness parameters.

7. Half width increases with increase of axial distance.

8. The flow over smooth cylinder becomes self preserving flow, earlier than that of rough cylinder.

9. The flow achieves self preservation earlier with higher Reynolds number.

6.3 Extension of the Present Work:

After completing the present study the following suggestions are made for the extension of the research topic.

1. The experiment should be taken in a pressurized wind tunnel due to attaining high Reynolds number.

2. Hot wire should be used for measuring the flow parameters in the wake.

3. Skin friction probe should be used to locate the separation point.

4. The similar flow characteristics can be made by using different roughness parameter with distributed roughness over whole surface and part of the surface of the cylinder.

REFERENCES

REFERENCES

1. ACHENBACH, E. "Distribution of local pressure and skin friction around a circular cylinder in cross flow up to Re = 5 x 10^6, J.F.M. 1968, Vol. 34, part 4, pp 625-639.

2. Achenbach, E. "Influence of surface roughness on the cross flow around a circular cylinder". Institute fur Reakterbamelements der Kernforschungsanlage, juich Gmblt, June, 1970, J.F.M.

3. Achenbach, E, and Heinecke, E. "On vortex shedding from smooth and rough cylinders in the range of Reynolds numbers 6 x 10^3 to 5 x 10^6". J.F.M. 1981 Vol. 109, pp. 239-251.

4. Achenbach, H. "The effect of surface roughness on the heat transfer from a circular cylinder to the cross flow of air" .J.H.M.T., Vol. 20, pp. 359-369.

5. Armit John, B.Sc. "The effect of surface roughness and free stream turbulence on the flow around a Model cooling Tower at Critical Reynolds Numbers". Symposium on Wind effects on buildings & structures organised by Loughborough university of technology, 1968.

6. AYOB ALFRED and KARAMCHETI, K. "An experiment on the flow part a finite circular cylinder at high subcritical and supercritical Reynolds numbers". Joint institute for Aeronautics and Acoustics, Department of Aeronautics and Astranautics, Stanford University, California 94305, U.S.A., 3 April - 1981, J.F.M.

7. Batham, J.P. "Pressure distributions on circular cylinders at critical Reynolds numbers". J.F.M. 1973, Vol. 57, part 2, page 209-228.

8. BEARMAN, P.W. "On vortex shedding from a circular cylinder in the critical Reynolds number regime". National physical laboratory, Teddington, Middlesex, 23 September 1968, J.F.M.

9. Chevray, R. and Kovasznay, L.S.G., "Turbulence measurements in the wake of a thin flat plate", AIAA Journal, vol. 7, No. 8, August, 1969, p. 1641.

10. Das, D.K. "Turbulent shear flows on rough surface with reliable overlayer or a macro element" Ph.D. Thesis.

11. Fage and Warsap, J.H. 1929, Aero Res. Comm. No. 1283.

12. FARUQUE OMAR "Experimental ivestigation of two dimensional wakes behind flat plates", M.Sc. thesis, BUET, November, 1983.

13. FERNHOLZ, H.H. & VAGT, J.D. "Turbulence measurements in an adverse pressure gradient three dimensional turbulent boundary layer along a circular cylinder".

14. FOX.W. ROBERT and McDONALD, T. ALAN "Introduction to fluid mechanics" Second edition, 1978.

15. Gartshere, I.S., "Two-dimensional turbulent wake", J. Fluid mechanics, Vol. 30, part 3, 1967, p. 547.

16. Guven, Oktay, Farell, C. and Patel, V.C. "Laboratory
    simulation of wind loading of round structures",
    Proc. I.A.SS. World Congress on space enclosures,
    Montreal, 1976.

17. Guven, O, Patel, V.C.; Farell, C. "A model for high
    Reynolds numbers flow part rough walled circular cylin-
    ders", Trans, ASME, J. Fluids Engs., 1977.

18. Guven, O.; Farell, C.; Patel, V-C. "Surface roughness effects
    on the mean flow part circular cylinders"; J. Fluid
    Mech., 1980, Vol. 98, part 4, p. 673-701.

19. Hasan Altaf "Study of turbulent boundary layer in a step
    change from smooth to rough surface", M.Sc. thesis,
    Bangladesh University of Engineering and Technology,
    1984.

20. Huston, W.B. "Accuracy of air speed measurements and slight
    calibration procedures", NACA Technical Report No.
    919, 1984.

21. Islam, S.M.N., "Design and construction of a closed circuit
    wind tunnel", M.Sc. thesis , Bangladesh University of
    Engineering and Technology, 1975.

22. Khalil, G.M. "The initial region of a plane turbulent
    mixing layer", Ph.D. thesis, Bangladesh University
    of Engineering and Technology, 1982.

23. Keffer, J.F., "A note on the expansion of turbulent wakes",
    J. Fluid Mech., Vol. 28, part 1, 1966, p. 183.

24. Kiya Masaru, Suznki Yanehiro, ARIE Mikio and Hagino

24. Kiya Masaru, Suznki Yanehiro, ARIE Mikio and Hagino
    Mitsutoshi, "A constribution to the free stream
    turbulence effect on the flow part a circular
    cylinder, 8 July, 1981, J.F.M.

25. Kline, S.J., and McClintock, F.A., "Describing uncertain-
    ties in single-sample experiments", Mechanical Engg.,
    Vol. 75, No.1, p. 3, 1958.

26. Massey, B.S. "Mechanics of fluid", 1970.

27. McMillan, F.A., "Experiments on pitot tubes in shear flow",
    Report Memor. Aeronantical and Research Council,
    London, No. 3028, 1956.

28. Nakamura, Y. and Tomonari, Y. "The effects of surface
    roughness on the flow part circular cylinders at
    high Reynolds numbers", 17 June, 1981, J.F.M.

29. Nishioka, Michio and Satu Hiroshi, "Study of flow behind
    a circular cylinder at low Reynolds number from 10 to
    30. J.F.M., 1973.

30. Roshko Anatol "Experiments on the flow part a circular
    cylinder at very high Reynolds number", 15 November,
    1960, J.F.M.

31. Schlichting, H. "Boundary layer theory", Seventh
    edition.

32. Szechenyi Edmond "Supercritical Reynolds number simulation
    for two dimensional flow over circular cylinders,
    J. Fluid Mech., 1975, Vol. 70, Part 3, pp. 529-542.

33. Townsend A.A. "Measurements in the turbulent wake of a cylinder", Emmanuel College, Cambridge, 17 December, 1946.

34. West, G.S. and Apelt, C.J. "The effects of tunnel blockage and aspect ratio on the mean flow part a circular cylinder with Reynolds number between 10^4 to 10^5", 13 May, 1981, J.F.M.

FIGURES

1   Settling chamber
2   Converging mouth
3   Perspex section with honycomb
4   Perspex section (Test section)
5   Wood section
6   Wood section
7   Fan section
8   Fan section
9   Butterfly section
10   Silencer
11   Diverging section
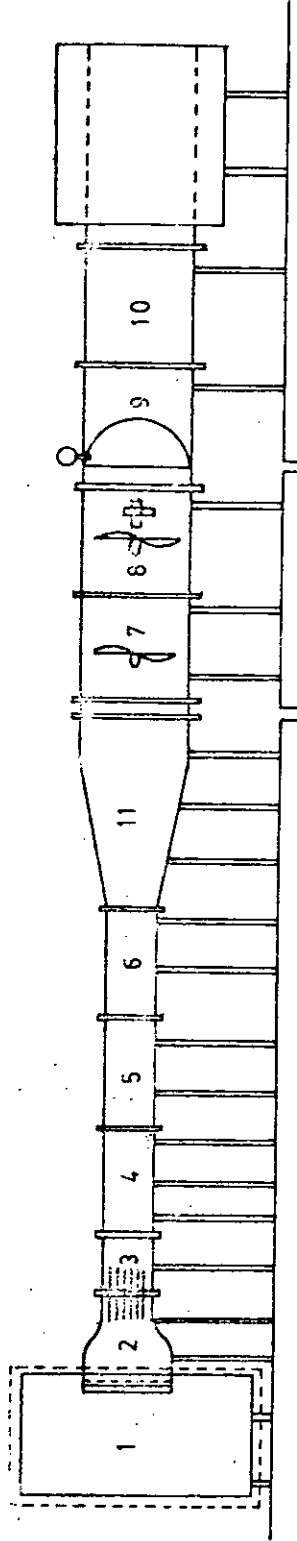
Fig. 4.1   Schematic diagram of wind tunnel
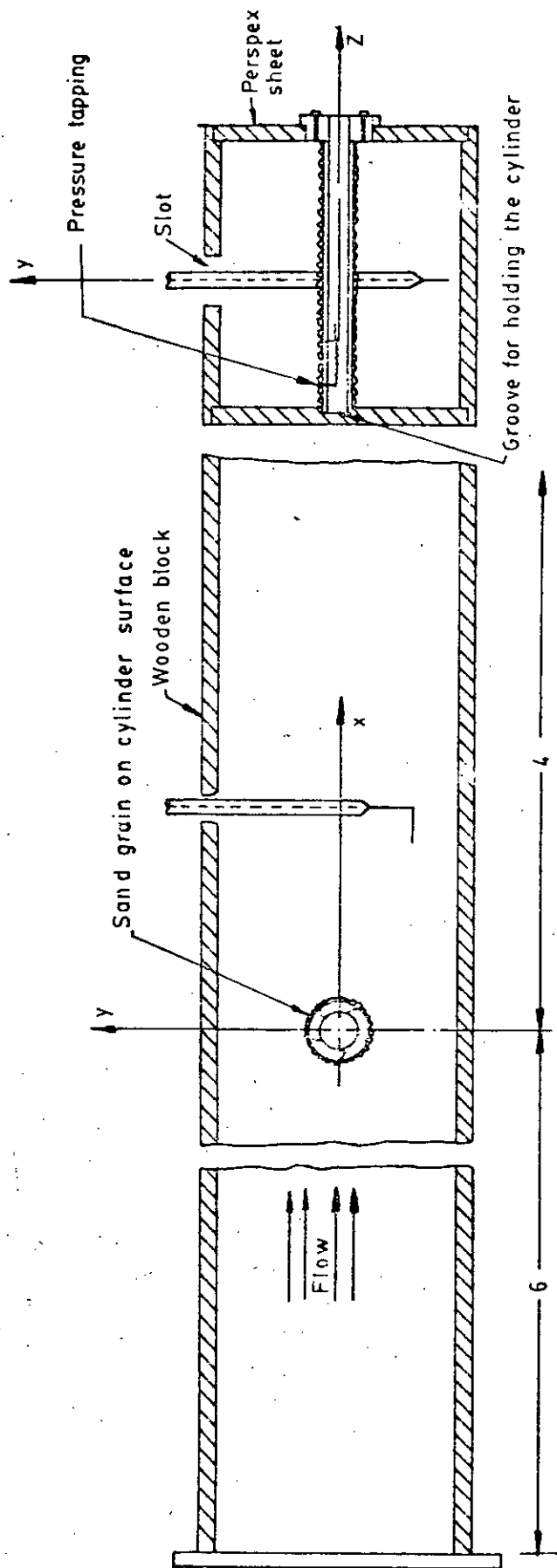
Fig. 4.2   Test section with sensing probe.

5·08 cm

·762 cm

7.62 cm

1905 cm

1016 cm

30·48 cm

11·43 cm

Groove to accomodate
pitot tube

1·015 cm

6·67 cm

7.9 cm

(a)

(b)
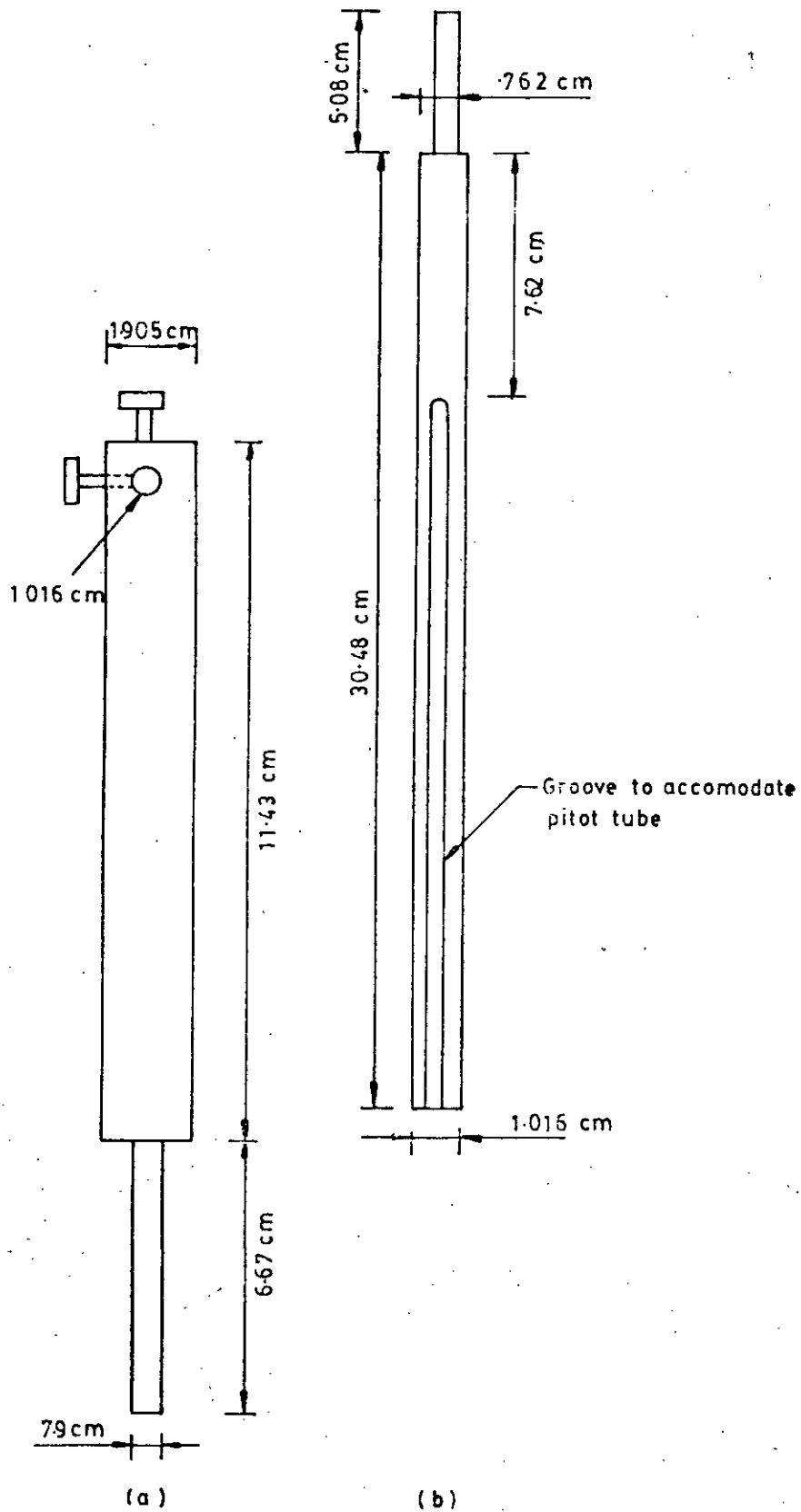
Fig. 4.3a   Pitot static tube holder
Fig. 4.3b   Pitot tube support hanger
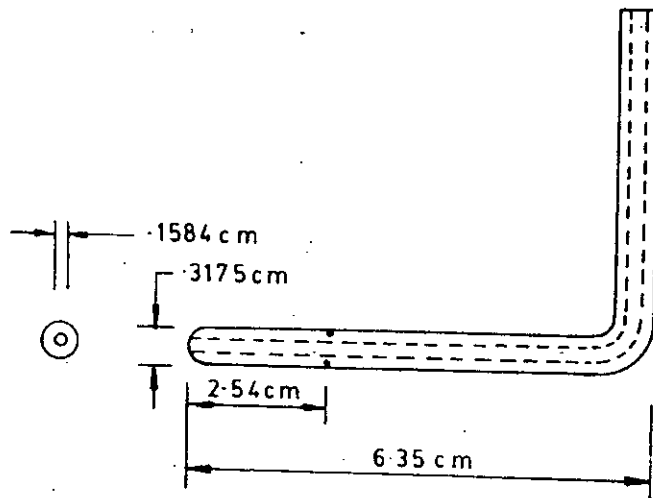
Fig. 4.4 Pitot static tube
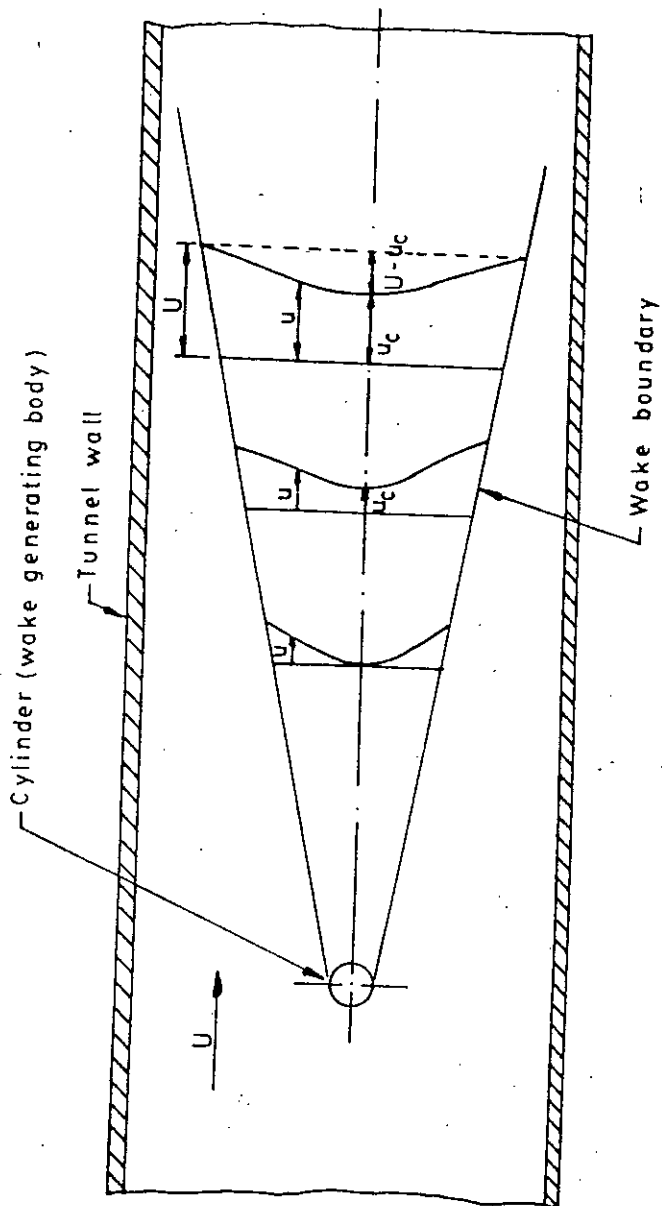
Fig.4.5a Wake geometry and nomenclature
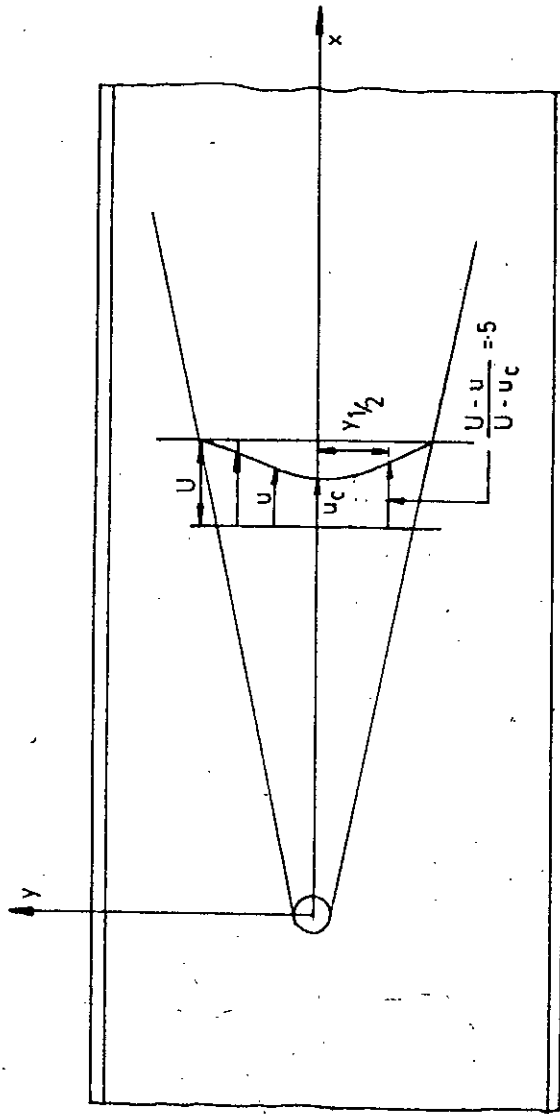
Fig. 4.5 b Co-ordinate system of wake
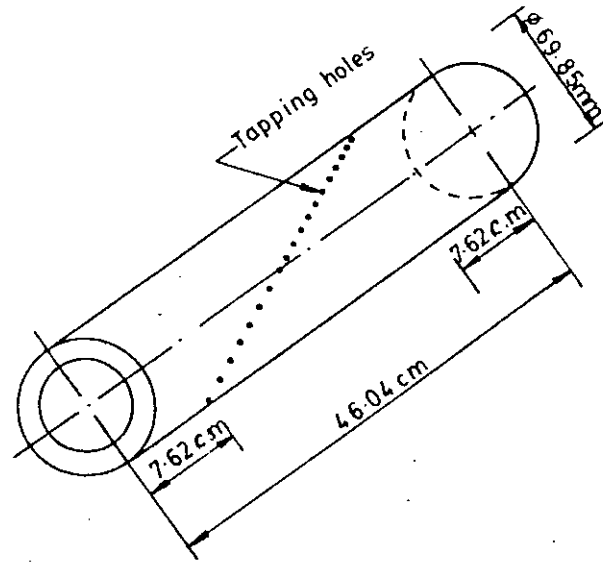
Fig. 4.6a   Nineteen tappings on(180°) the upper half part
of the cylinder.
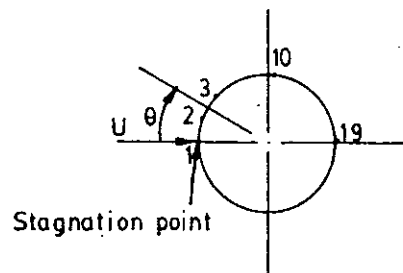
Fig. 4.6 b   X Section showing
angular position, θ
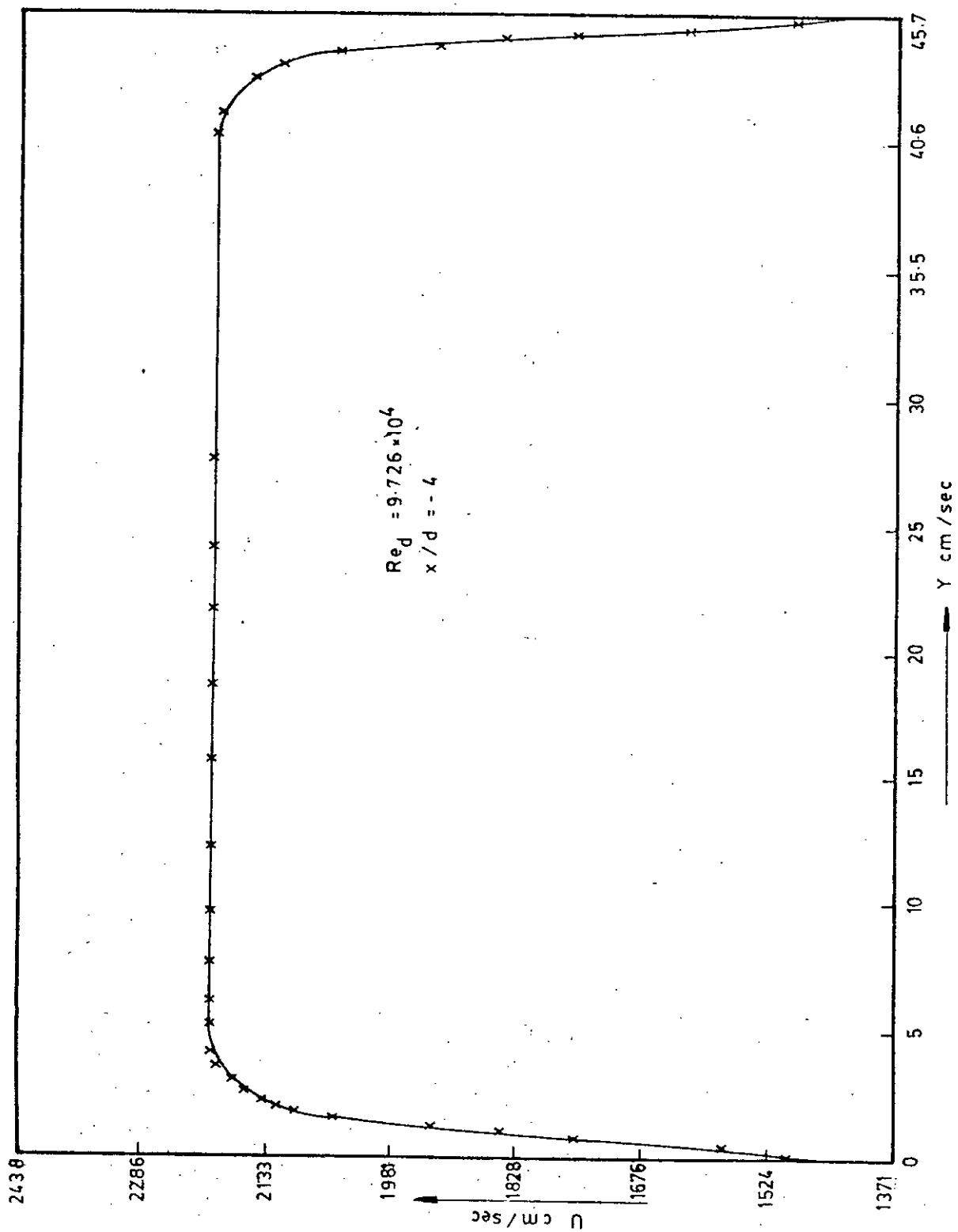
Fig. 5-6-a   Mean velocity profile over smooth surface in the test section (Upsteam side.)
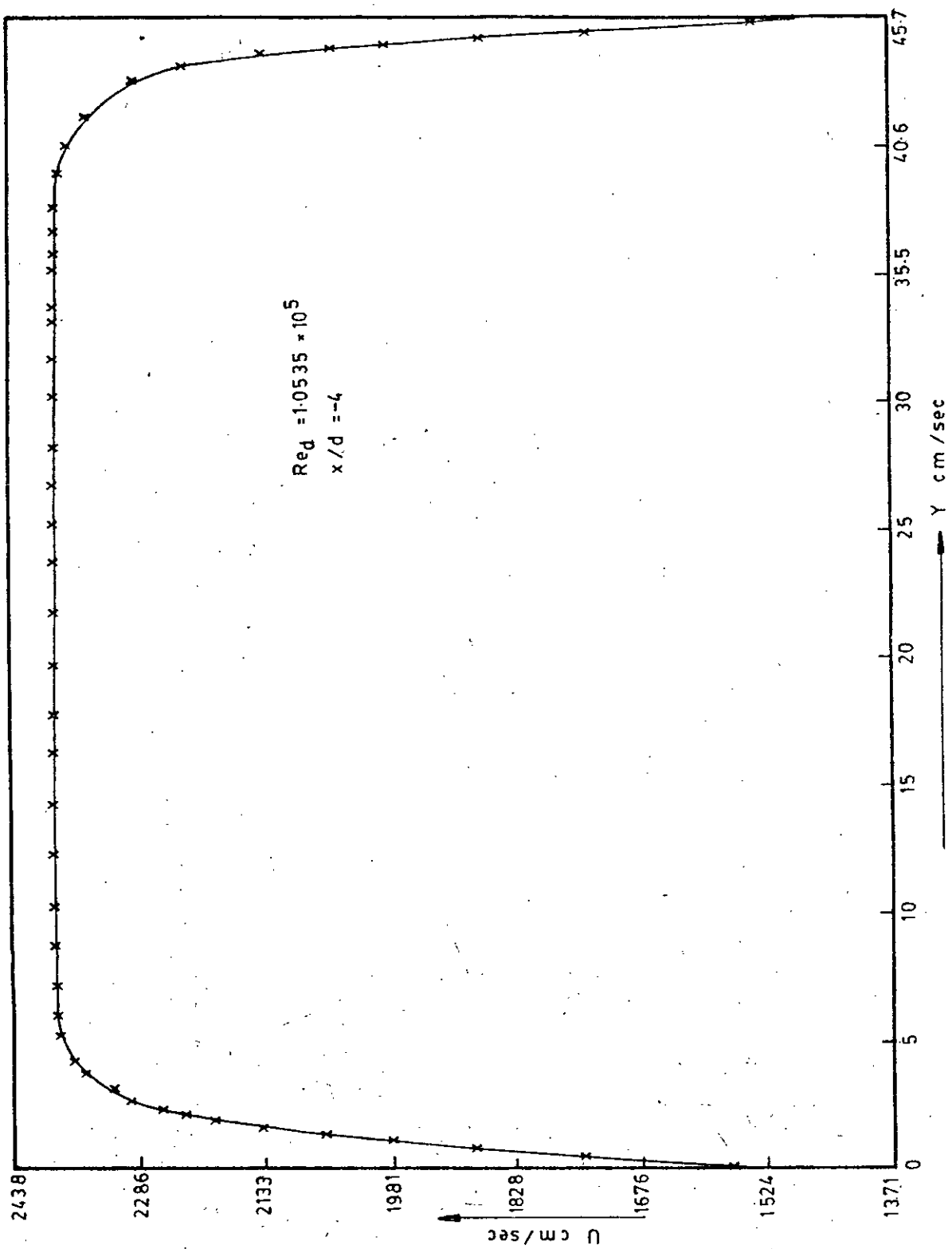
Fig. 5-6-b Mean velocity profile over smooth surface in the test section (Upsteam side)
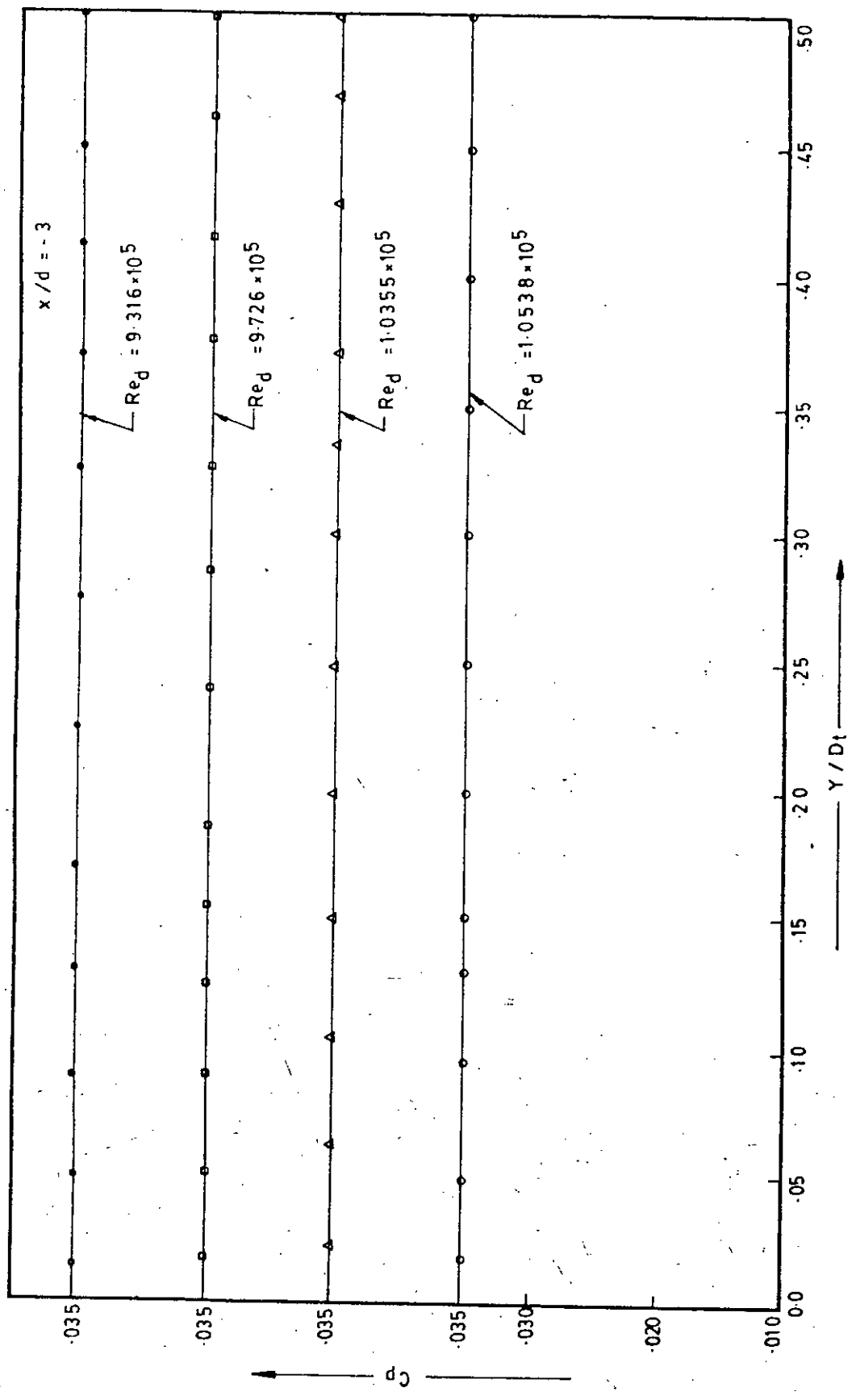
Fig. 5-7   Transverse pressure distribution in the test section with smooth surface.
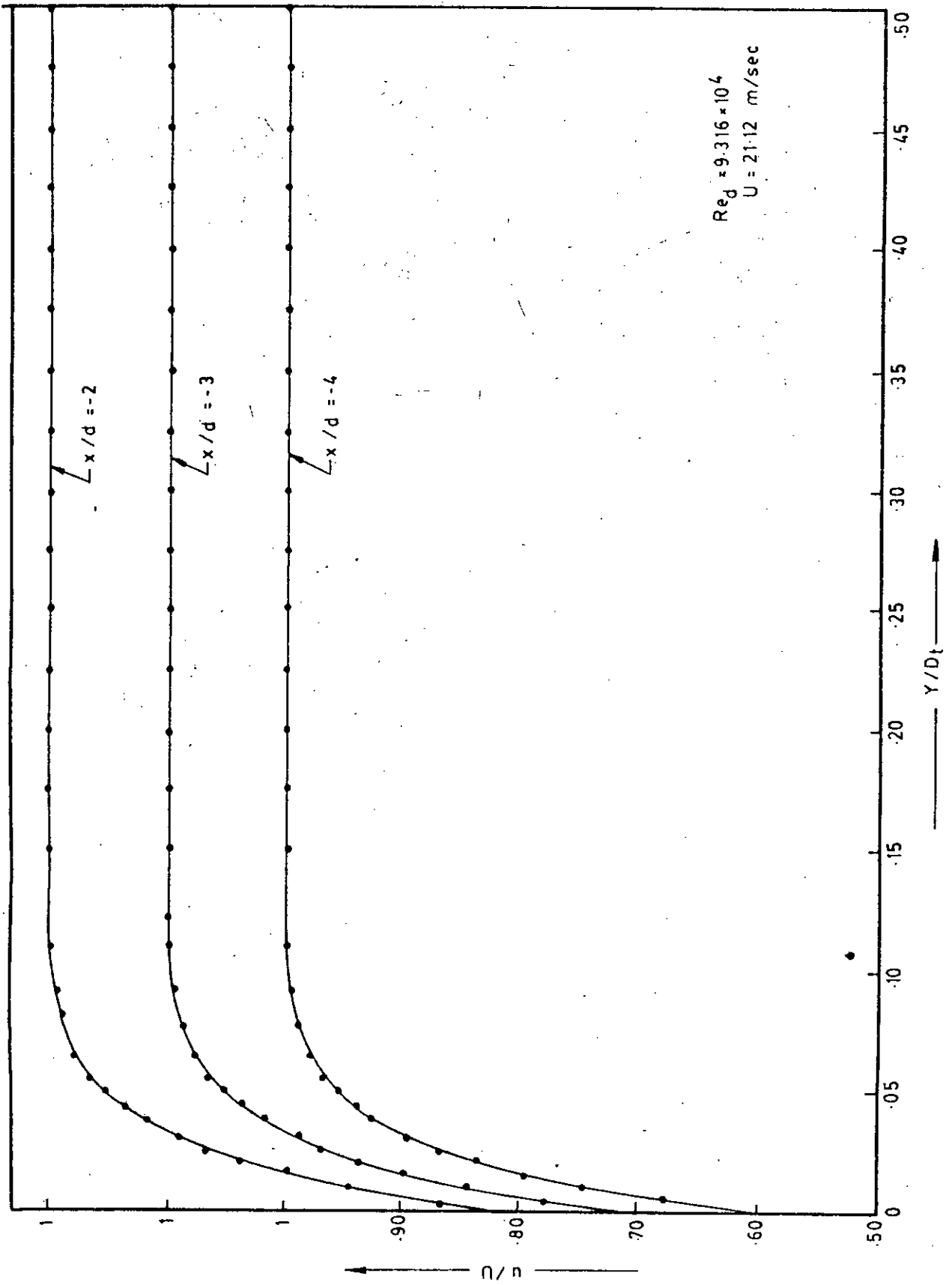
Fig. 5-8-a Mean velocity profile measured by pitot static probe over smooth surface (Upstream side)
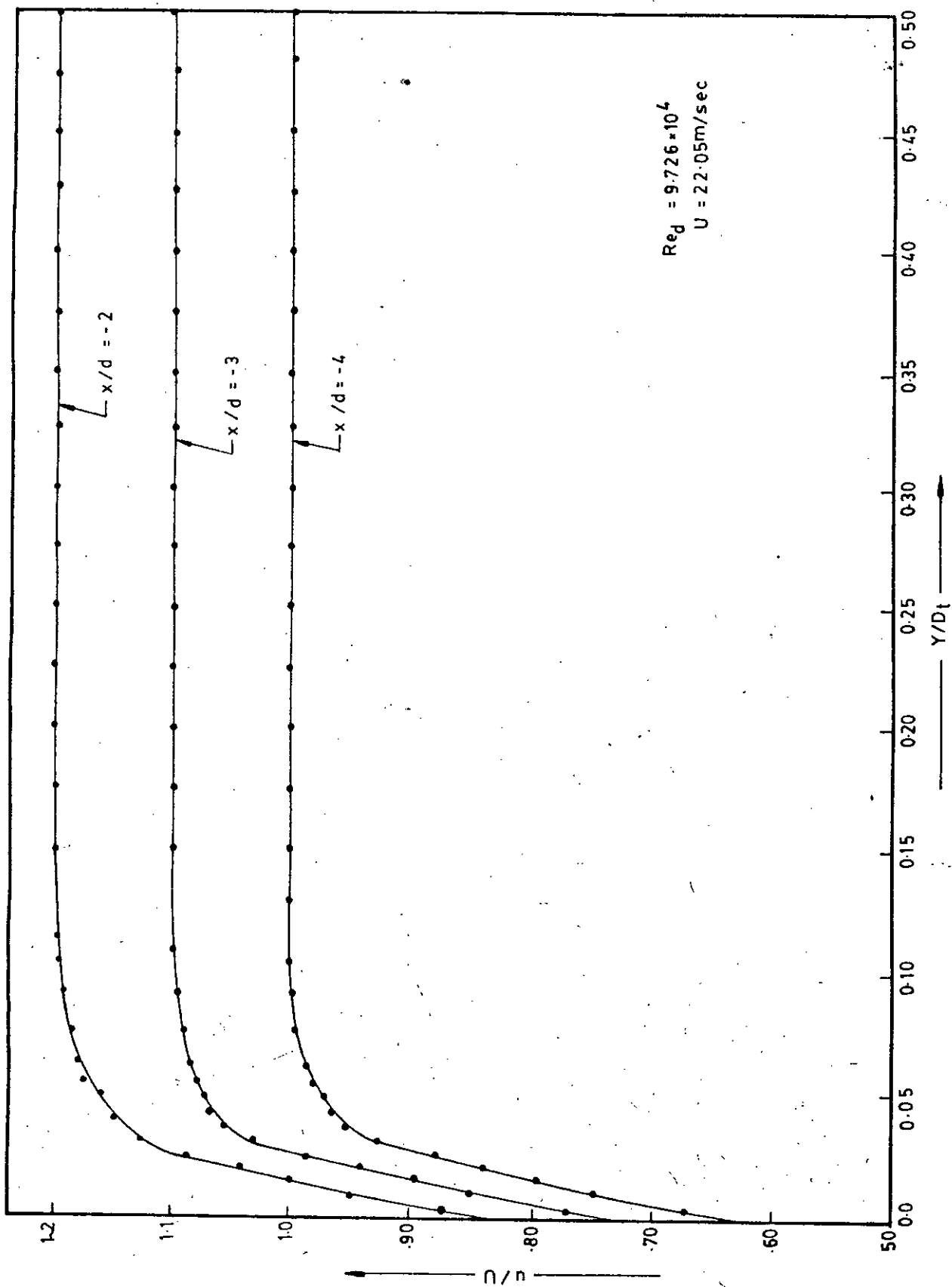
Fig. 5-8-b Mean velocity profile measured by pitot static tube over smooth surface (Upstream side)
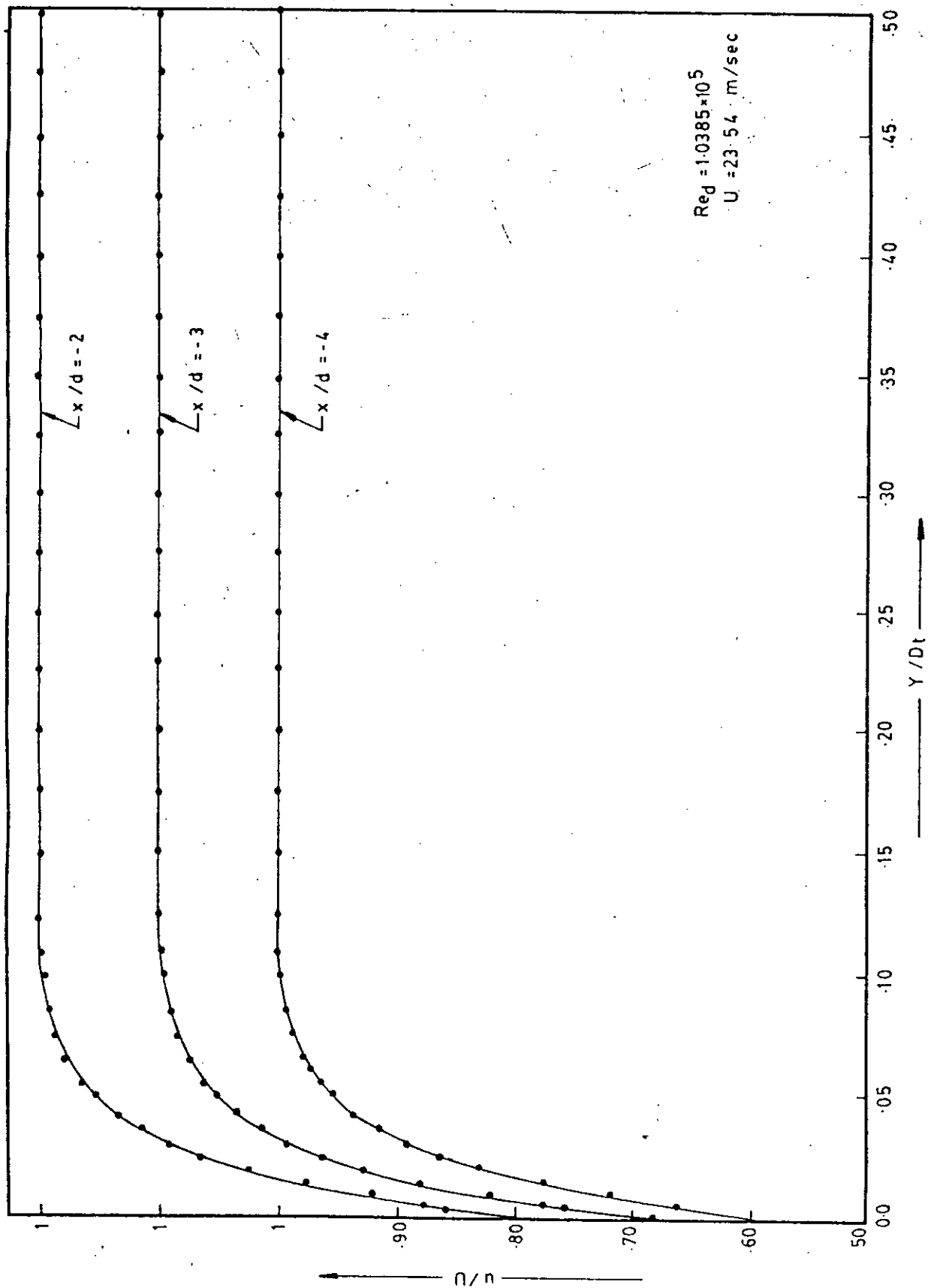
Fig. 5-8-c   Mean velocity profile measured by pitot static prove over smooth surface(Upstream side)
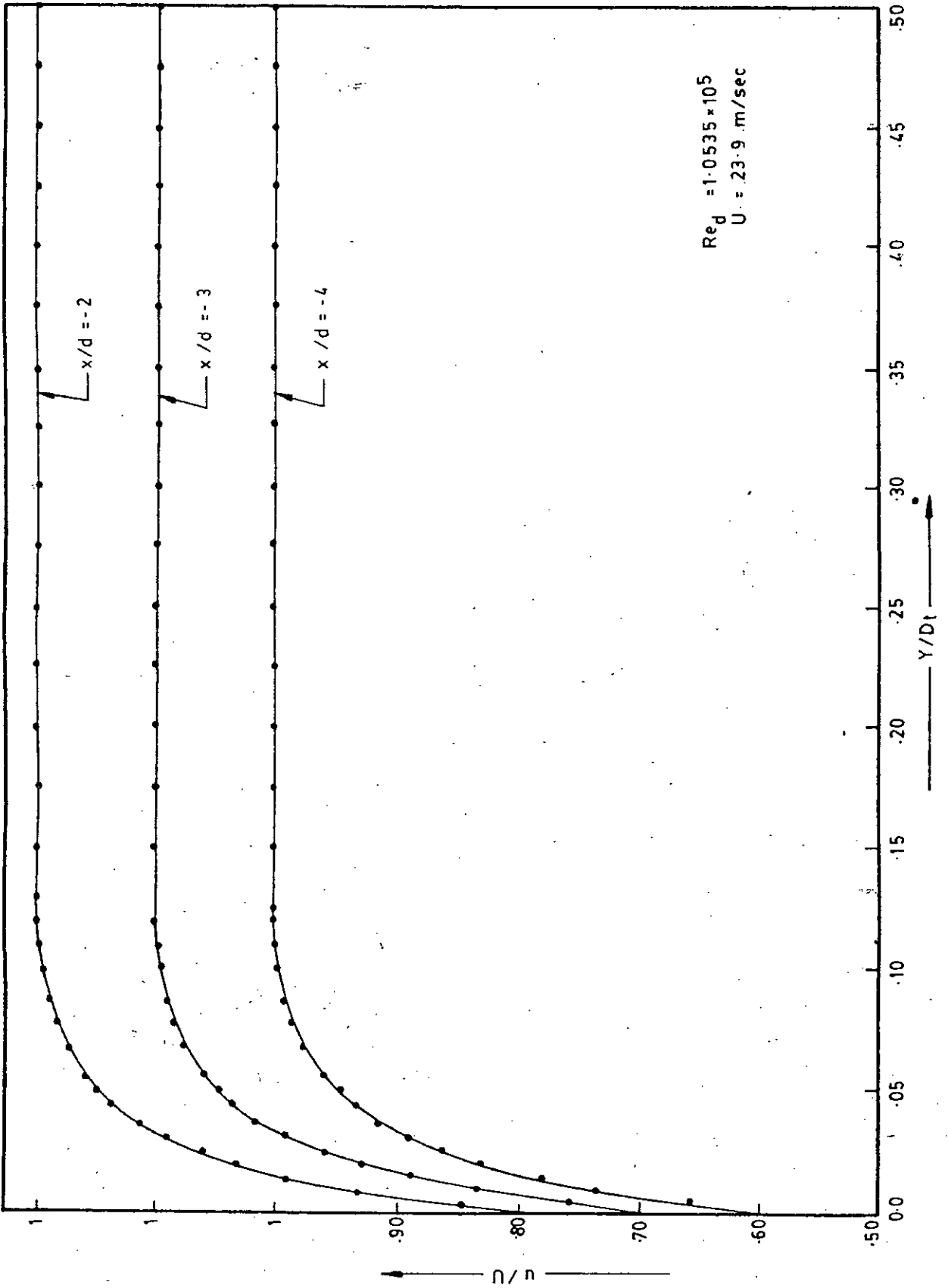
Fig. 5-8-d Mean velocity profile measured by pitot static probe over smooth surface (Upstream side)
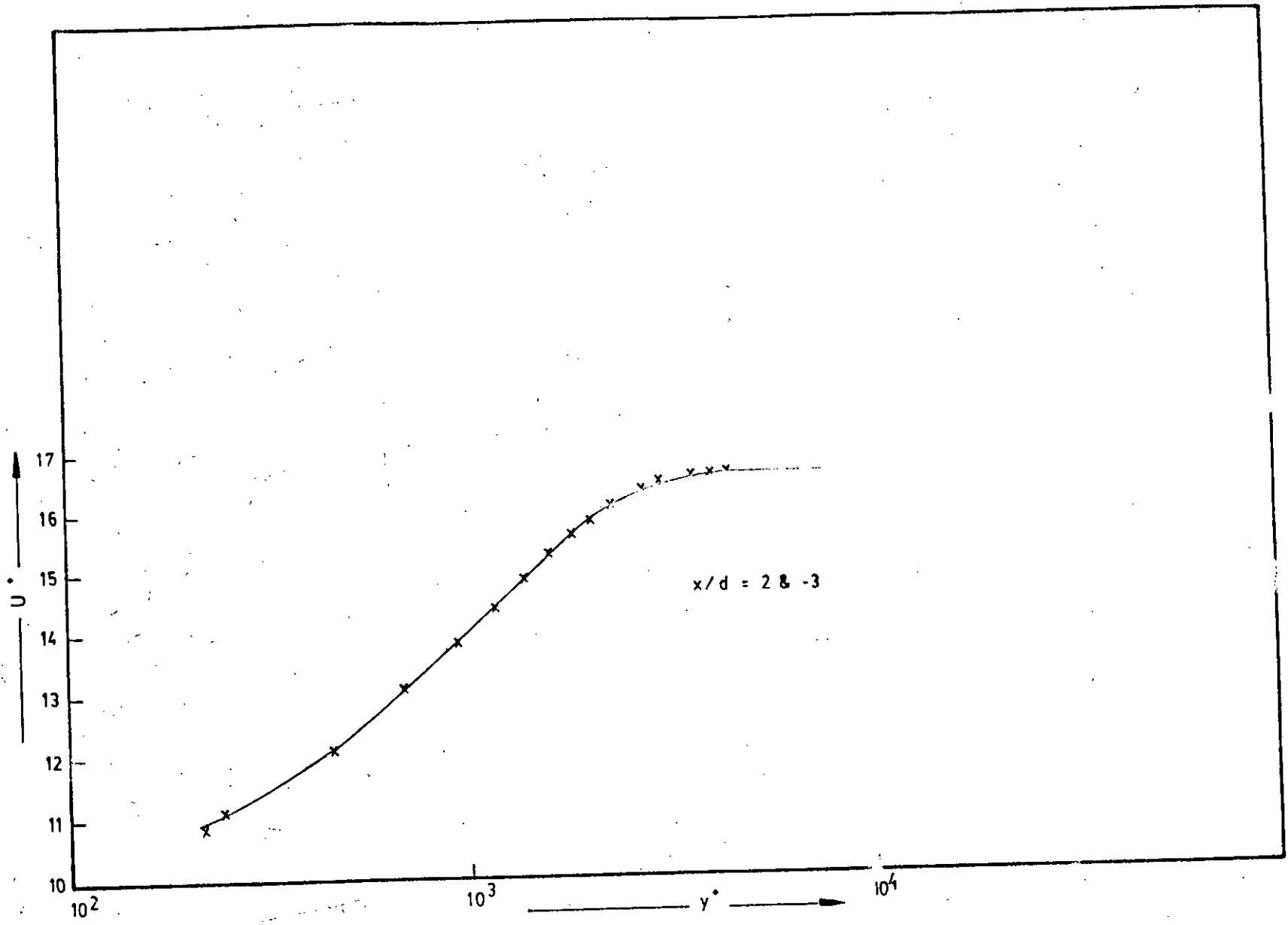
FIG. 5-9 LOGARITHMIC VELOCITY PROFILE AT THE UPSTREAM POSITION

The chart is labeled with $x/d = 2 \& -3$, with the vertical axis labeled U^* showing values 10 through 17, and the horizontal axis labeled y^* ranging from 10^2 to 10^4.
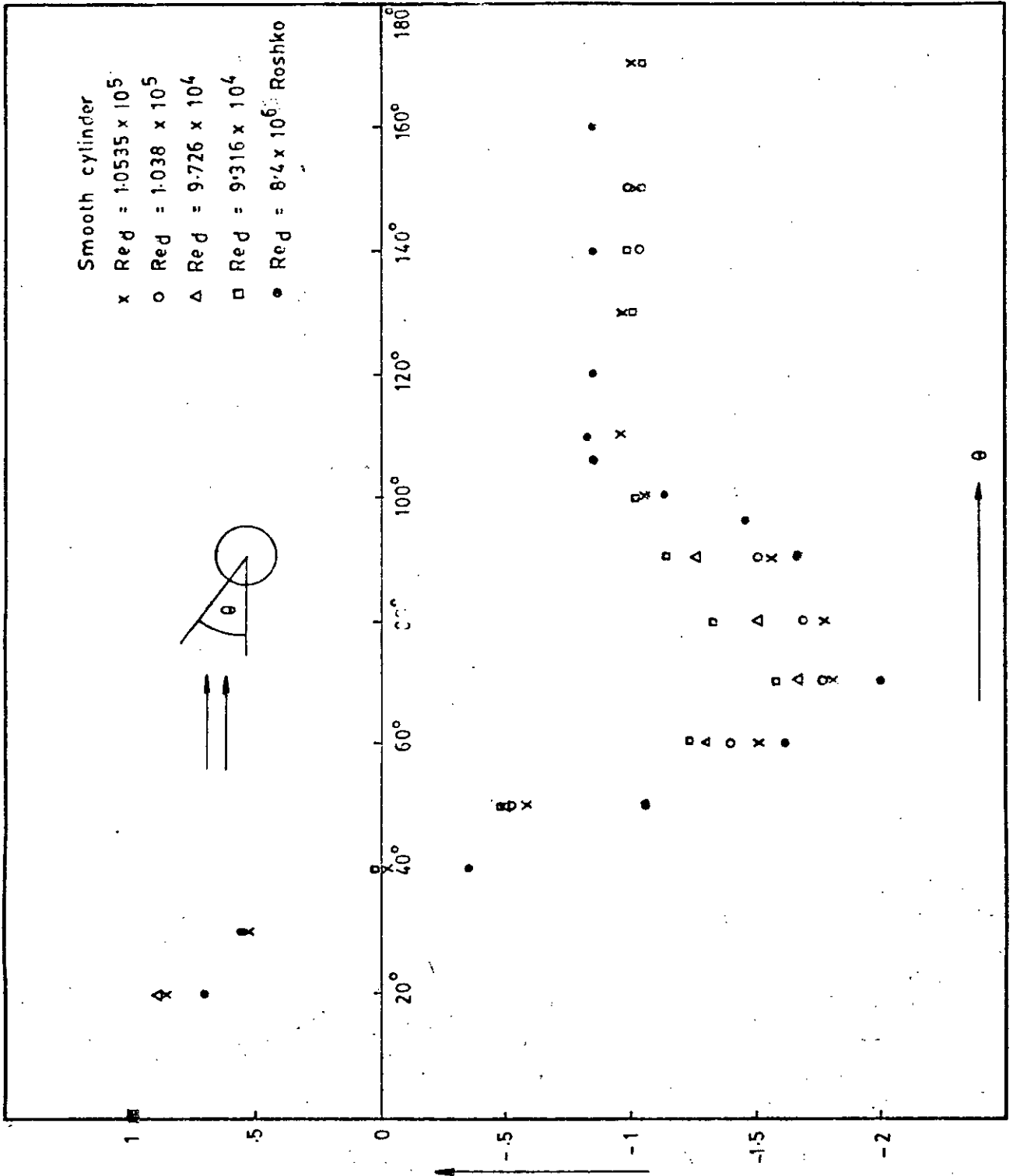
Fig. 5-2-1-a Pressure distribution around cylinder

Roughness parameter 2.644×10^{-2}

- x Re$_d$ = 1.0535×10^5
- o Re$_d$ = 1.0382×10^5
- △ Re$_d$ = 9.726×10^4
- □ Re$_d$ = 9.316×10^4
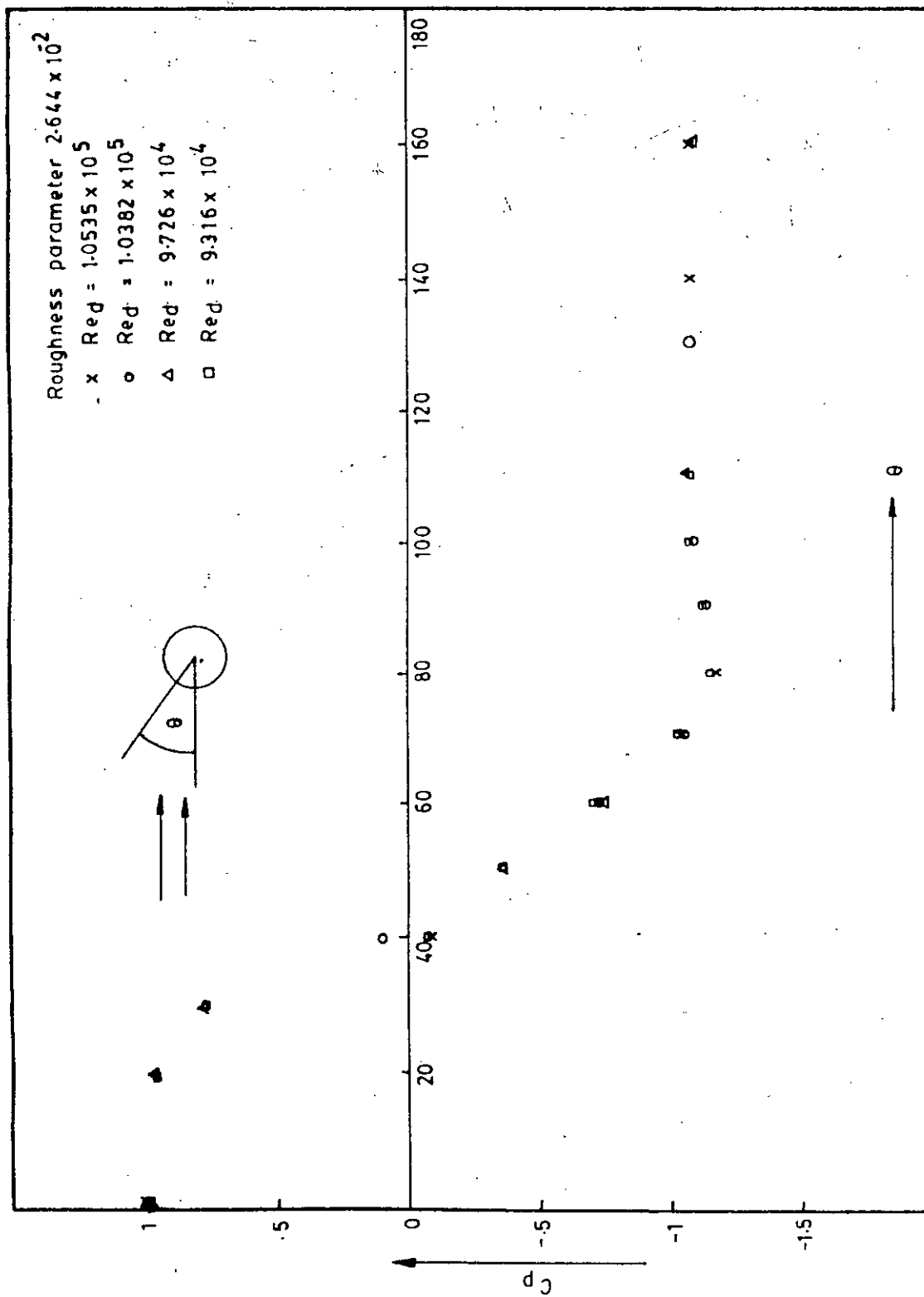
Fig. 5-2-1-b   Pressure distribution around cylinder
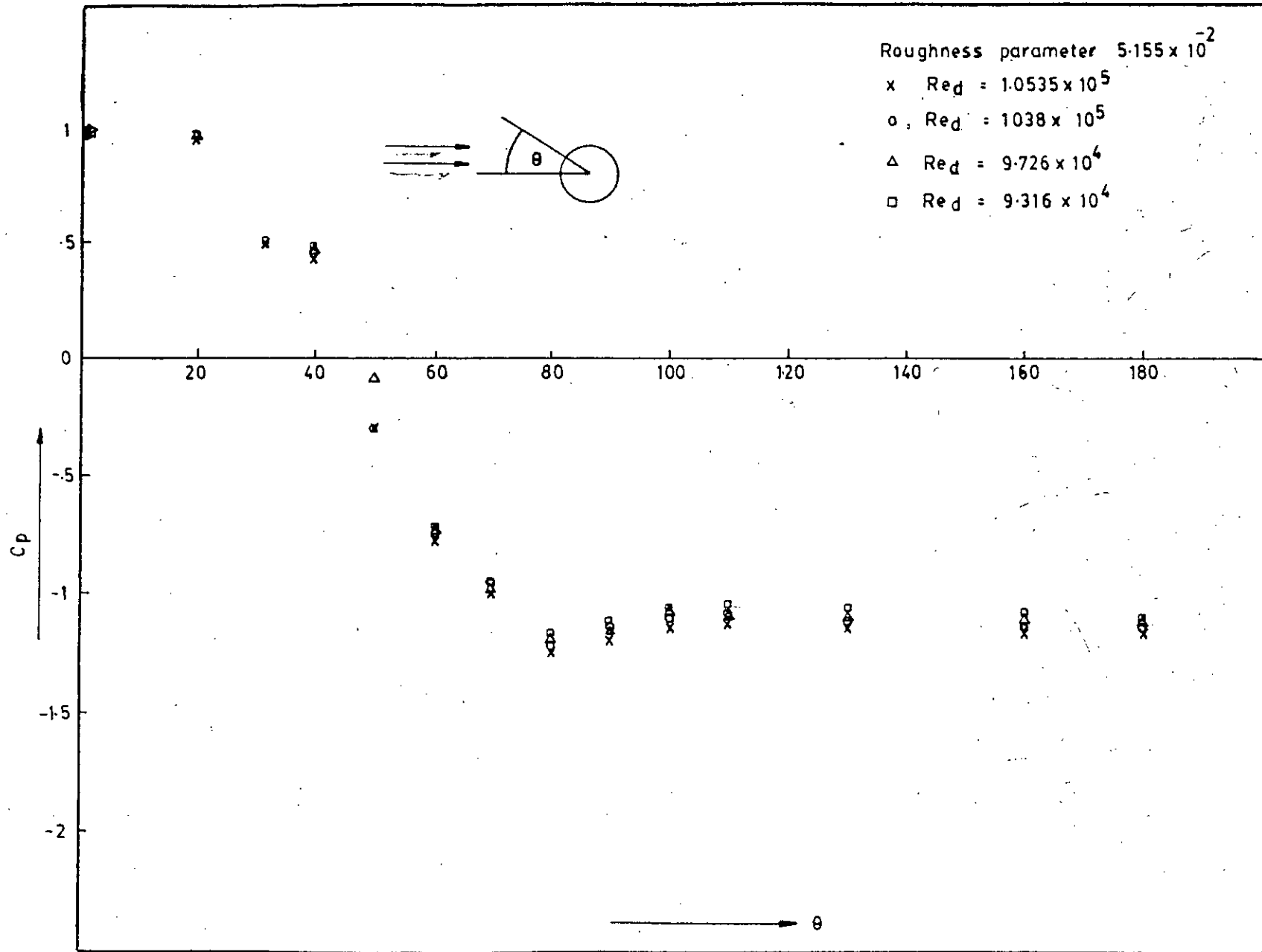
Fig. 5-2-1-c   Pressure distribution around cylinder
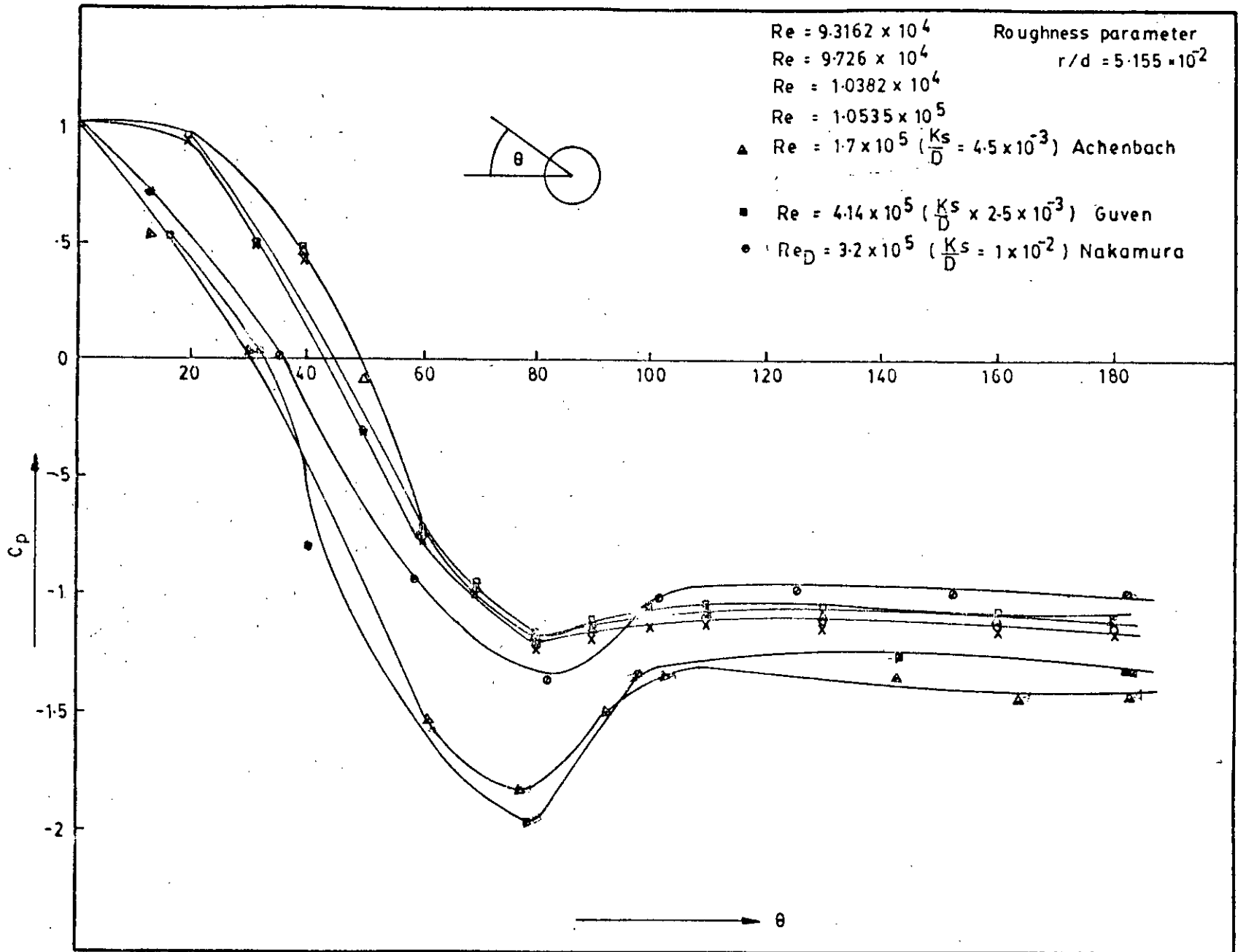
Fig. 5-2-1-d Pressure distribution around cylinder
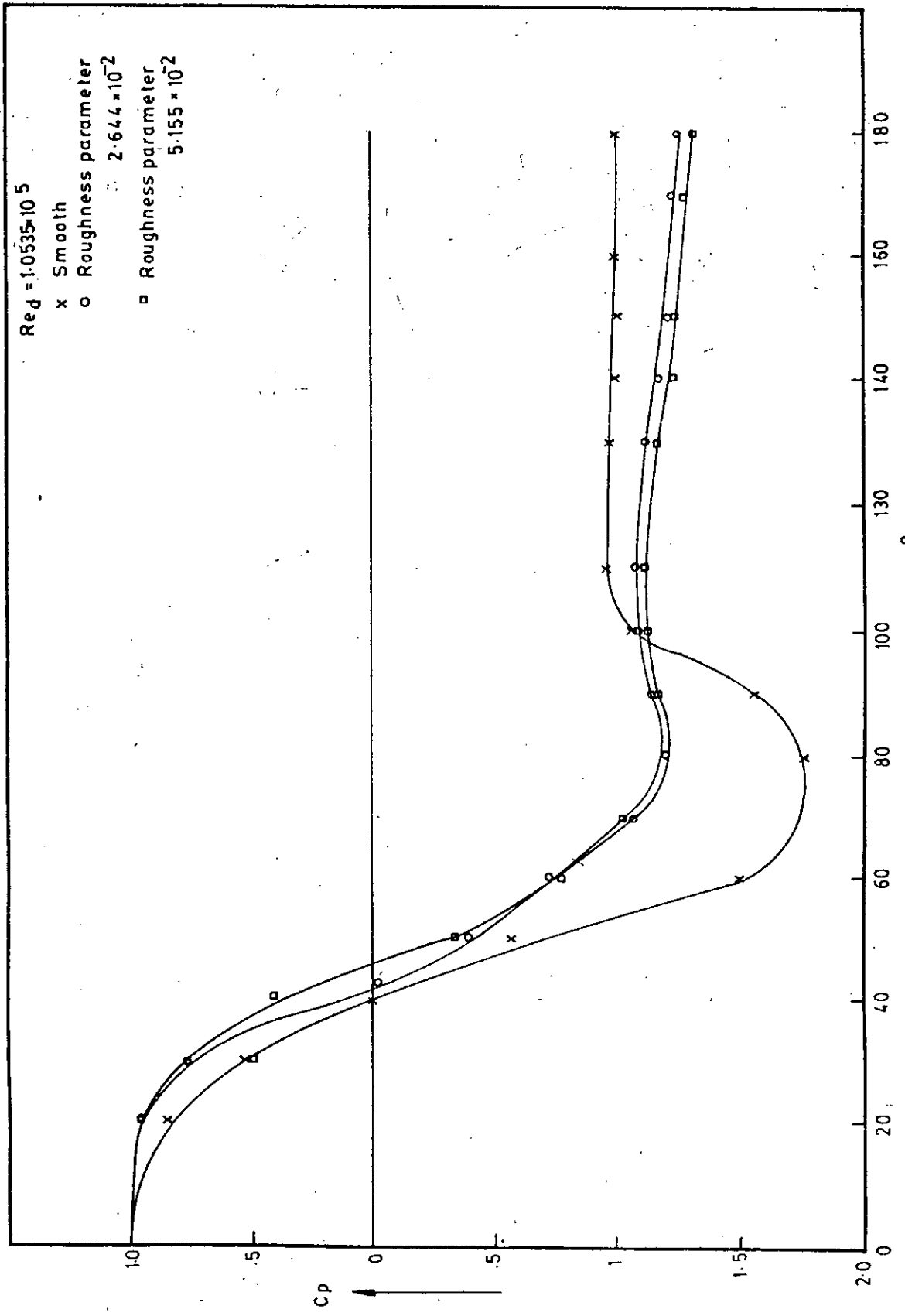
Fig. 5-2-+e Pressure distribution around the cylinder
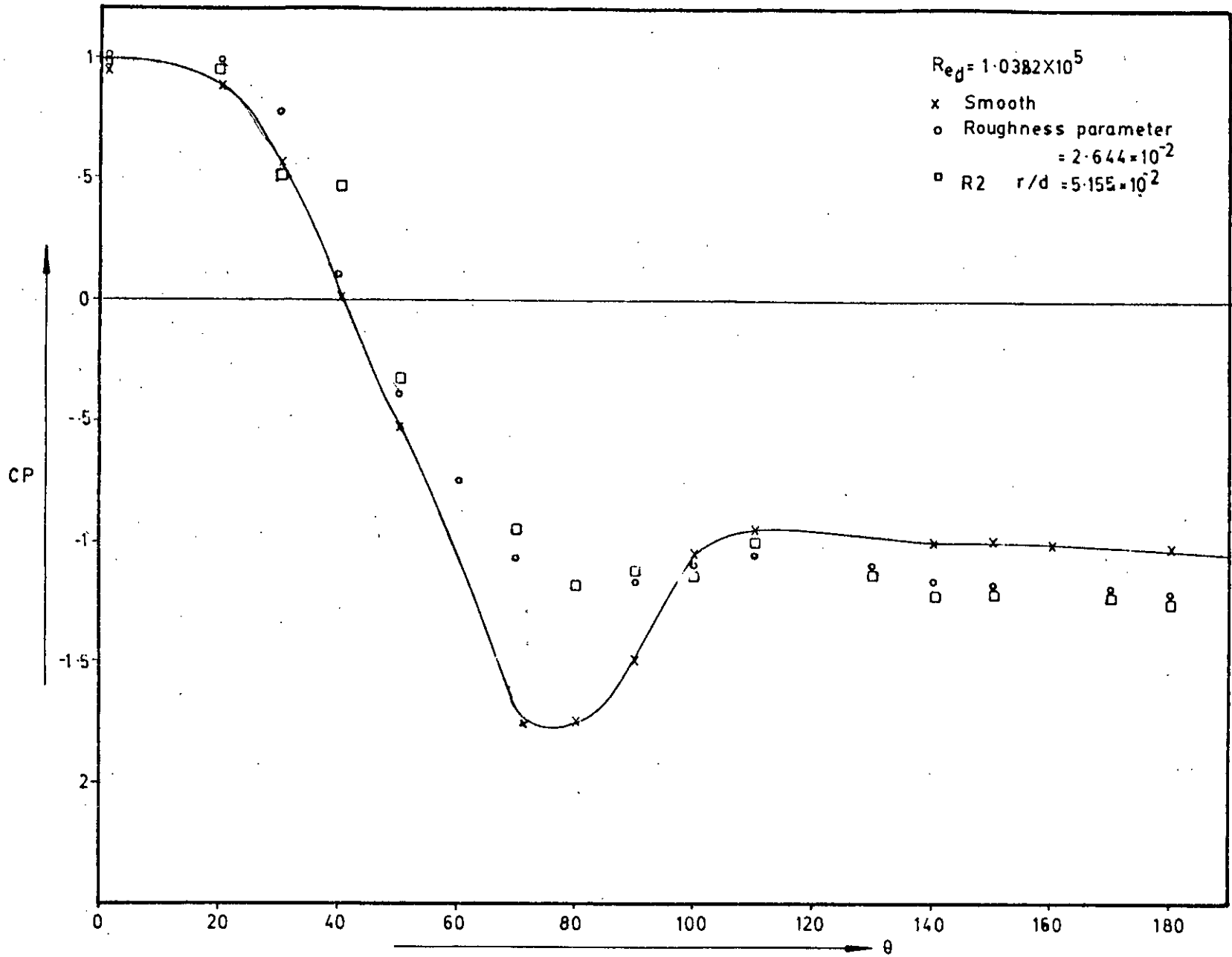
Fig.5-2-1-f   Pressure distribution around the cylinder

The figure shows a plot of CP versus θ.

Legend:
$R_{ed} = 1 \cdot 0382 \times 10^{5}$

x   Smooth

o   Roughness parameter
$= 2 \cdot 644 \times 10^{-2}$

□   R2 $r/d = 5 \cdot 155 \times 10^{-2}$

CP axis values: 1.0, .5, 0, -.5, -1, -1.5, 2

θ axis values: 0, 20, 40, 60, 80, 100, 120, 140, 160, 180
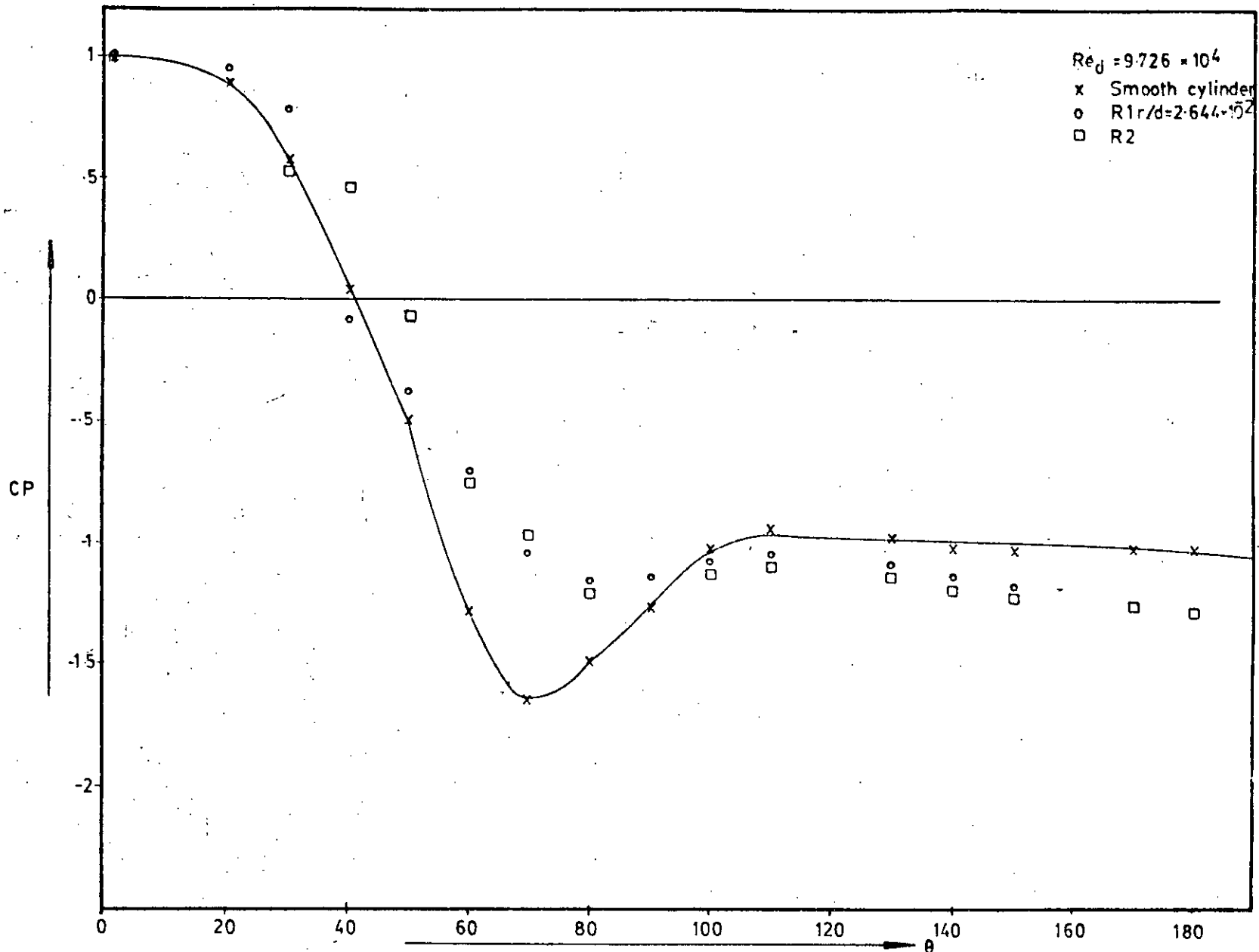
Fig.5-2-1-g   Pressure distibution around the cylinder
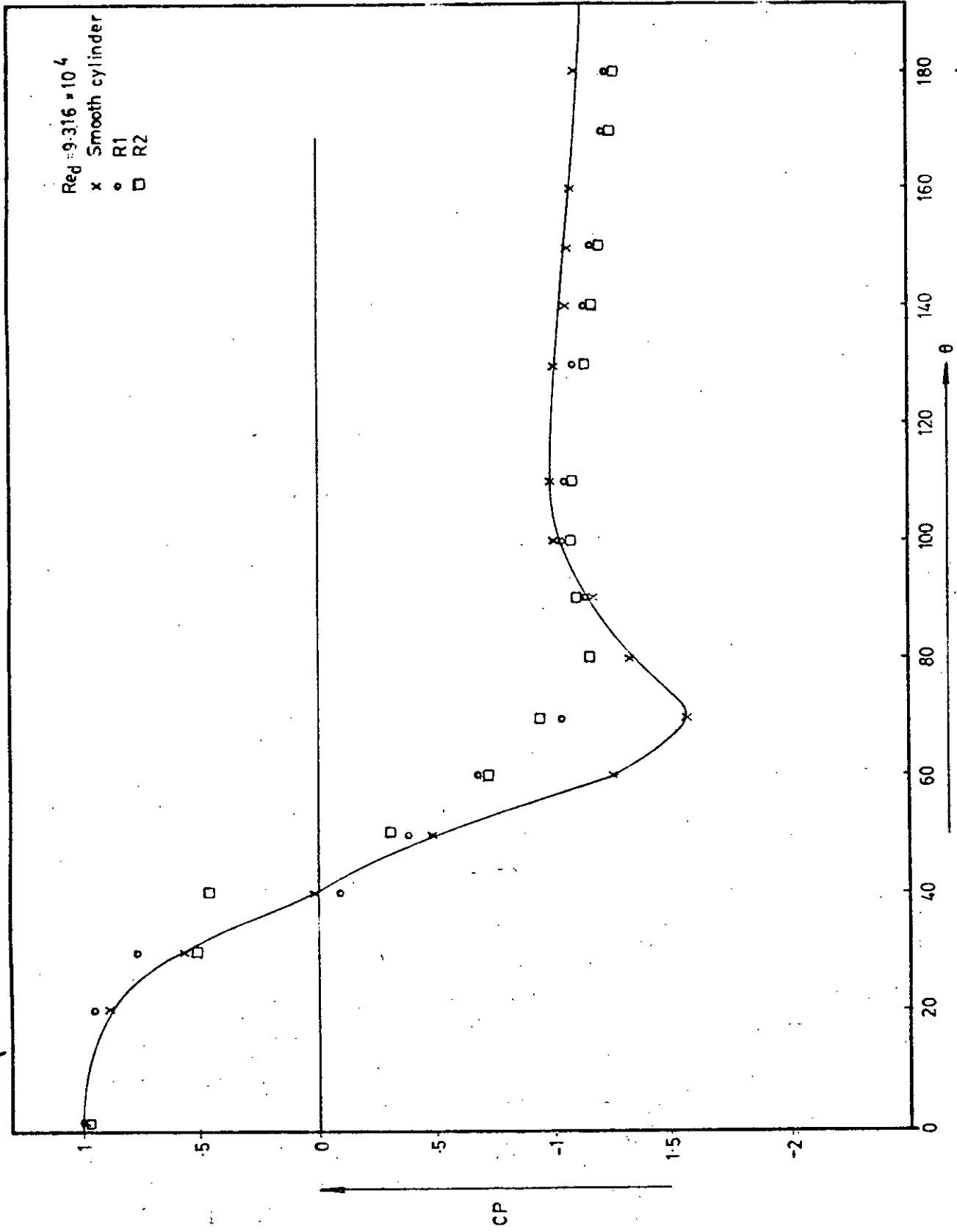
Fig. 5-2-1-h Pressure distribution arond the cylinder
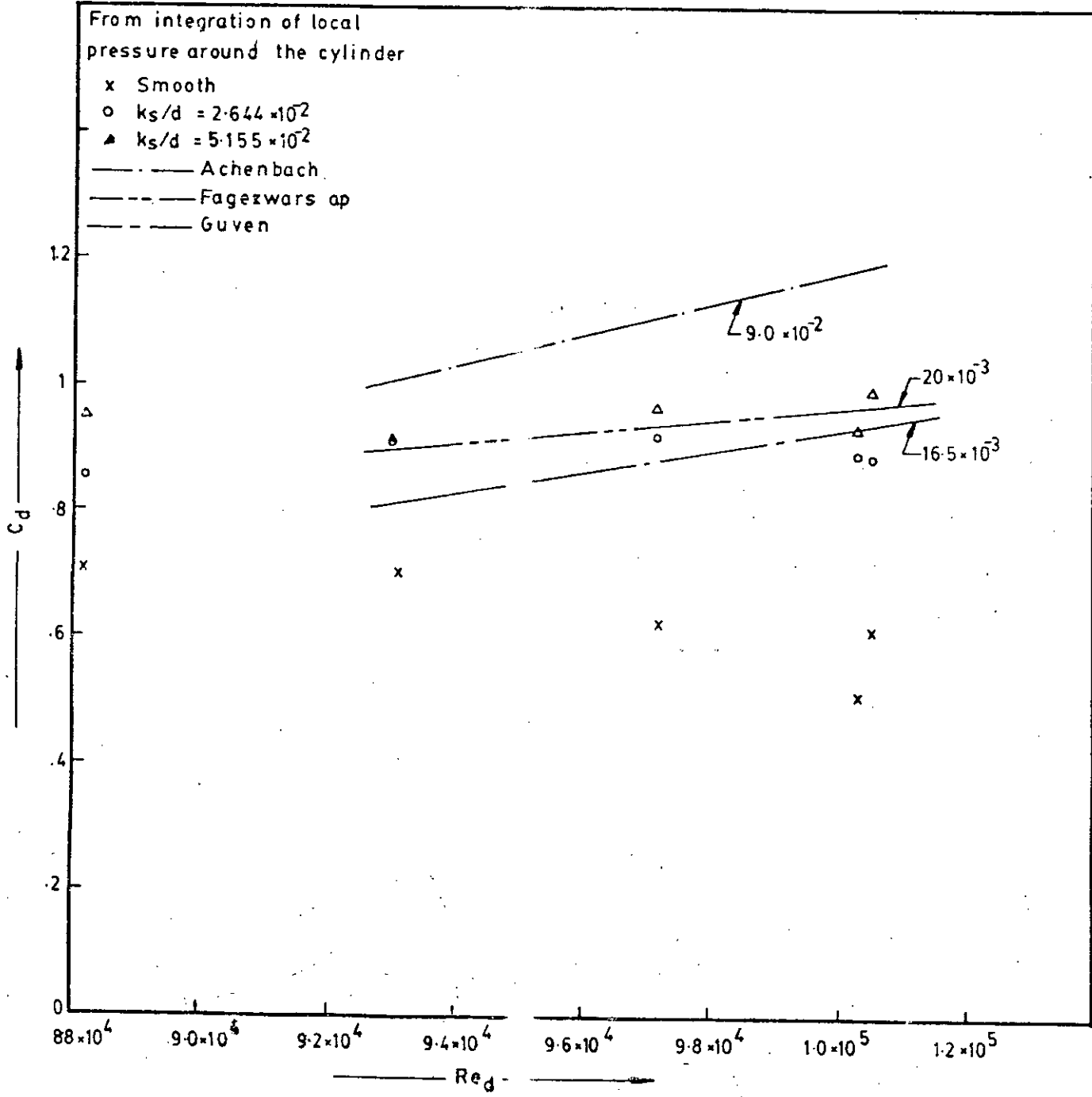
Fig. 5-2-2-a Variation of drag coefficie with Reynolds number
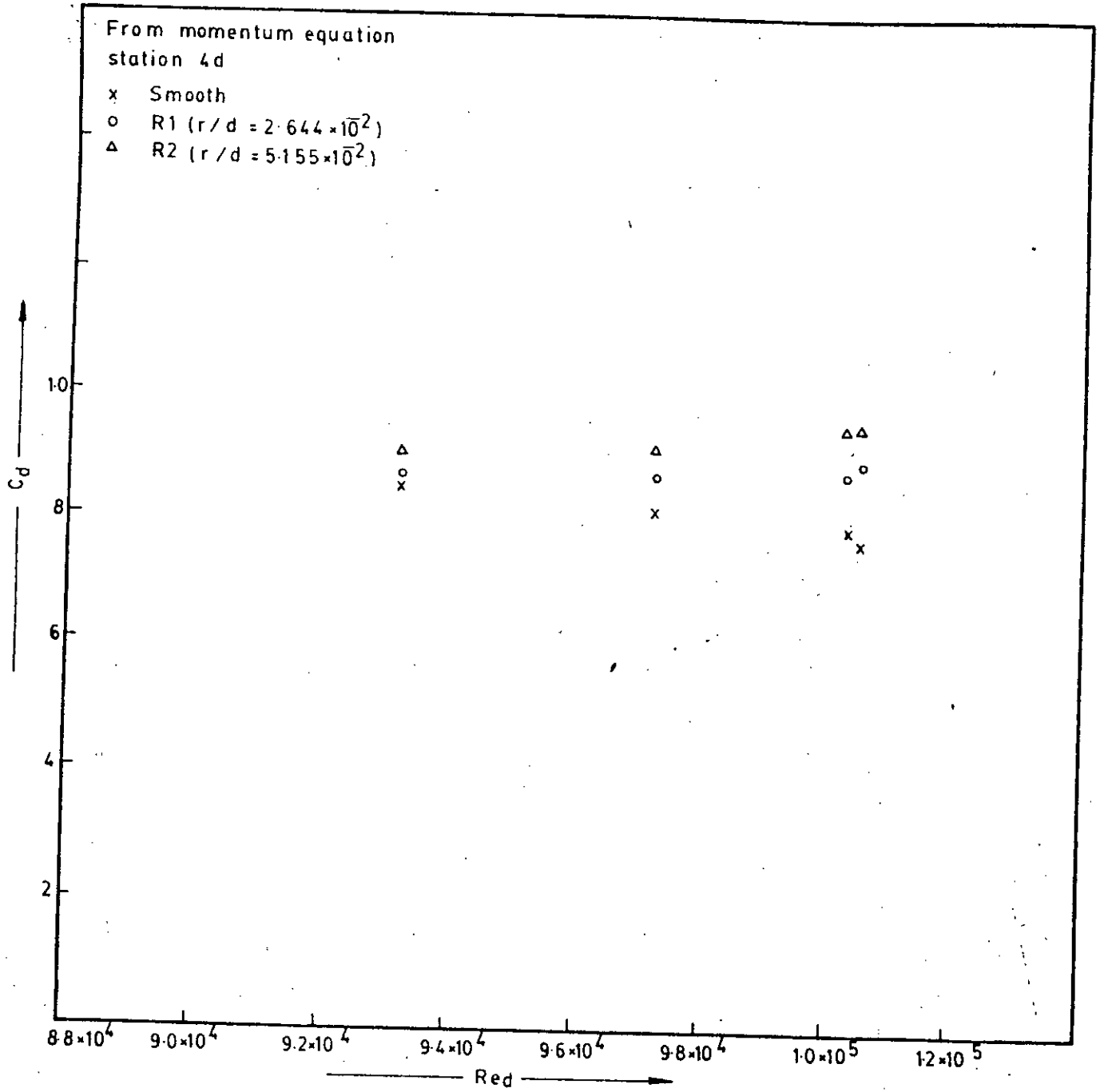
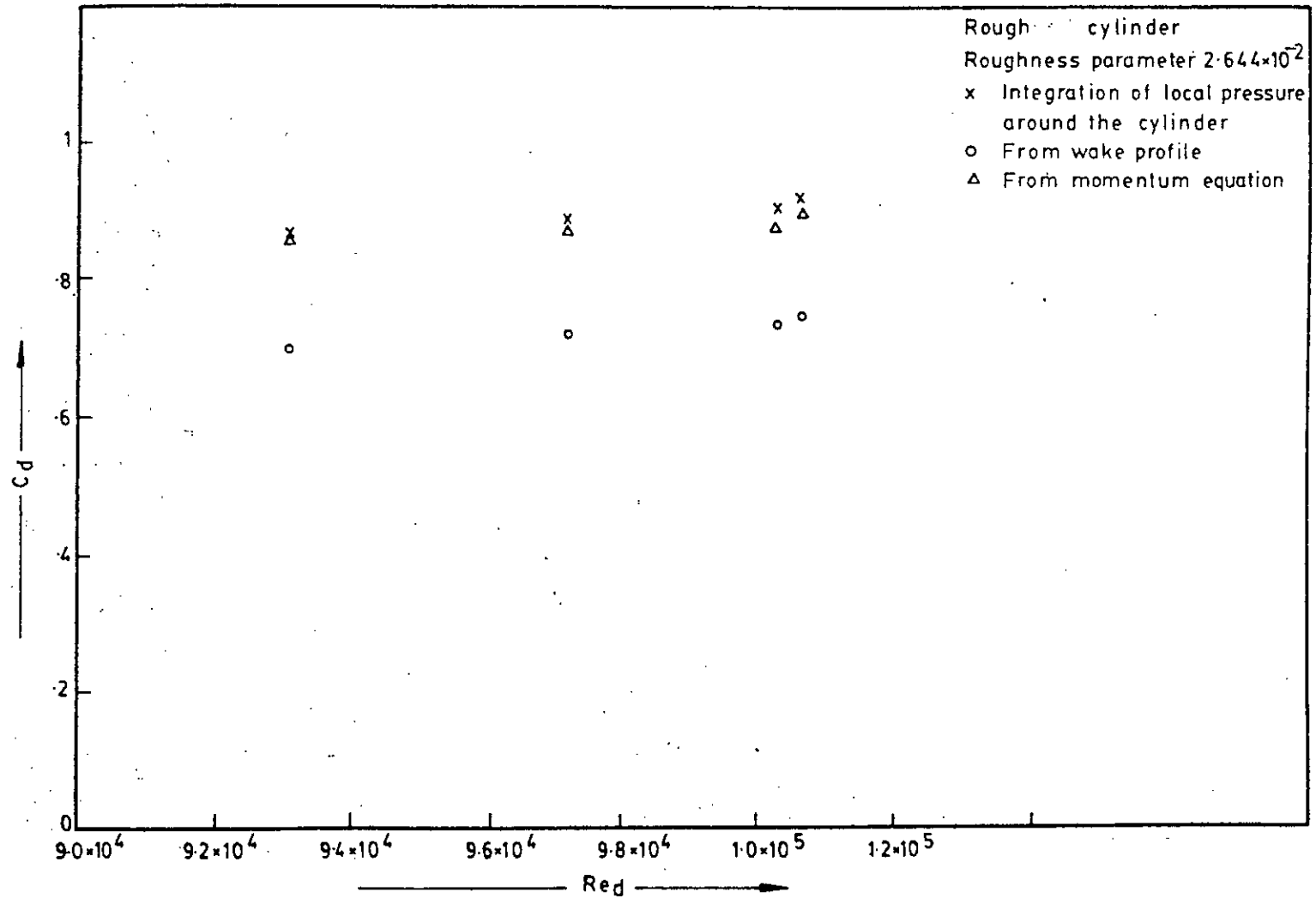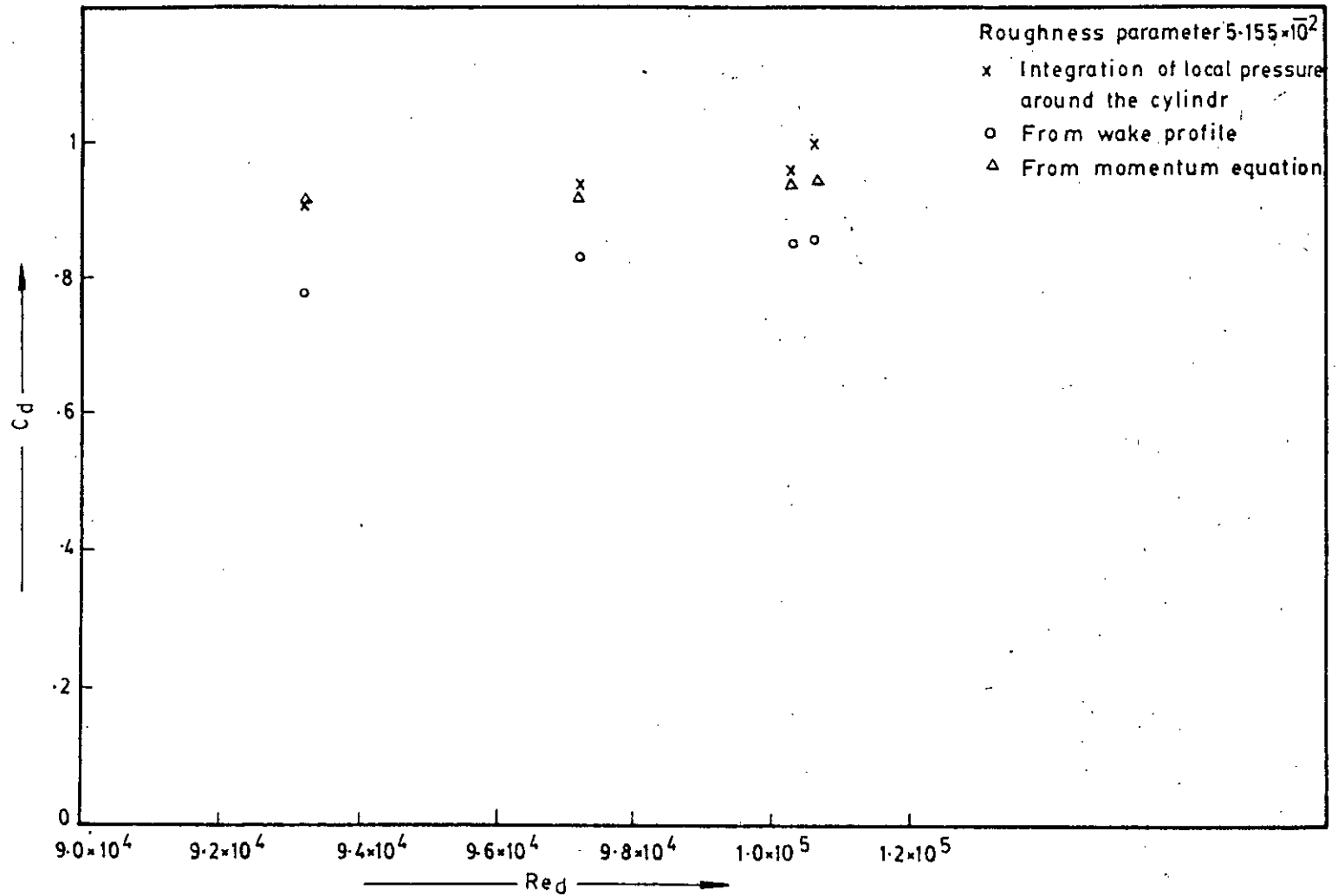Fig. 5-2-2-b Variation of drag coefficient with Reynolds number

From momentum equation
station 6d
x   Smooth
o   R1 ($r/d = 2.644 \times 10^{2}$)
△   R2 ($r/d = 5.155 \ 10^{2}$)
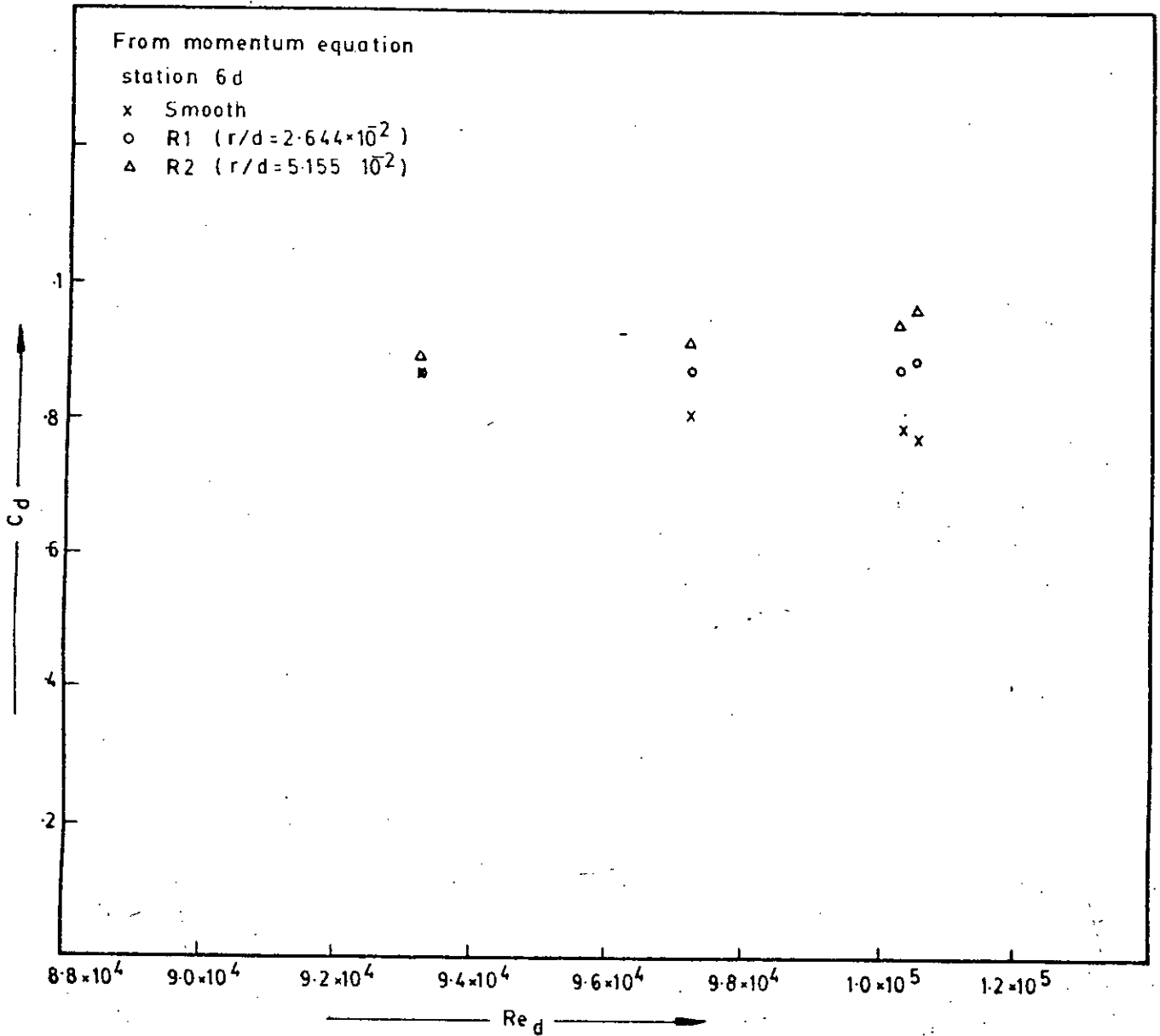
Fig. 5-2-2-c   Variation of drag coefficient with Reynolds number
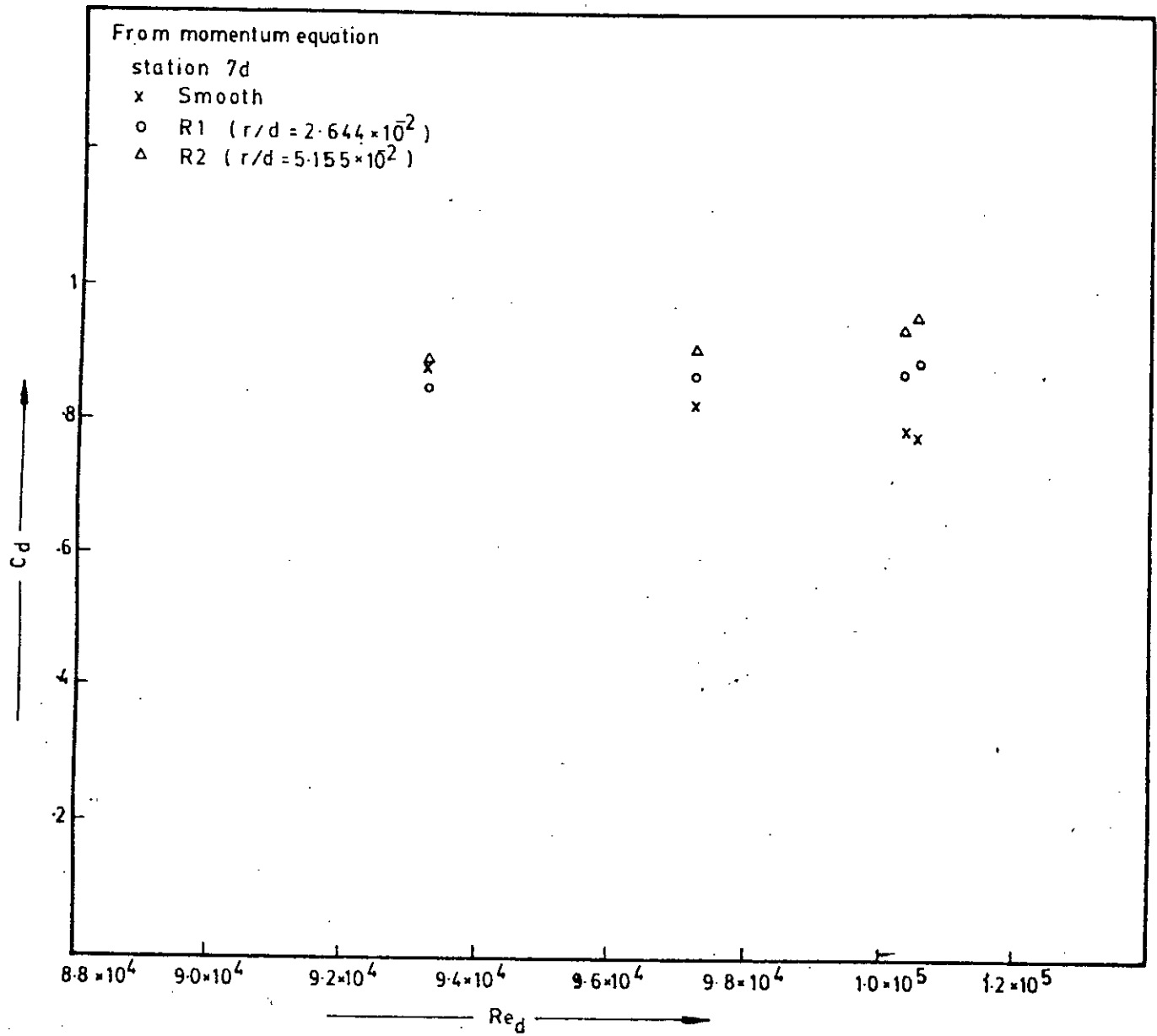
Fig. 5-2-2-d   Variation of drag coefficient with Reynolds number
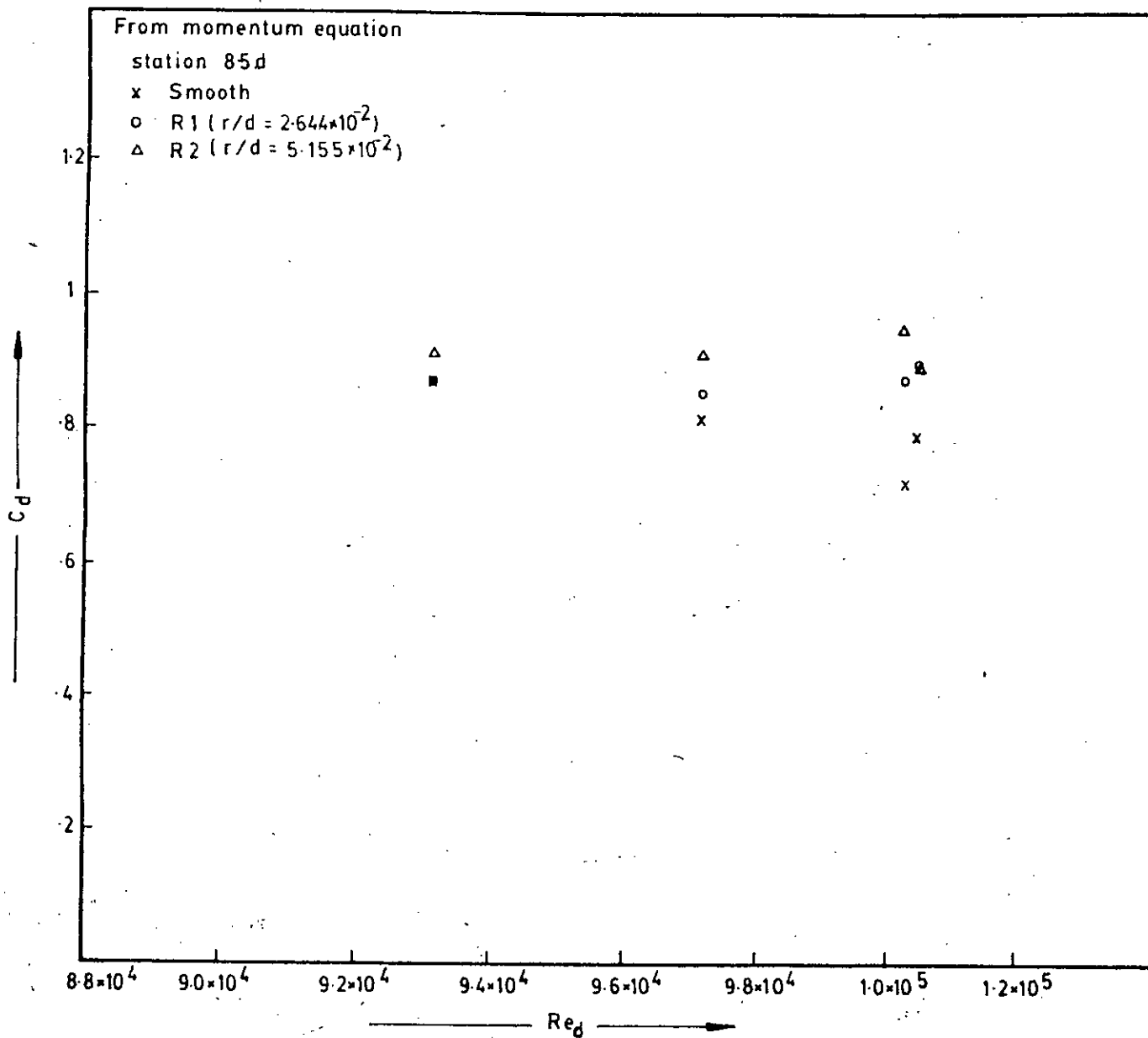
Fig. 5-2-2-e Variation of drag coefficient with Reynolds number

From momentum equetion
station   12·5 d
x   Smooth
o   R1 (r/d = 2·644 ×10⁻²)
Δ   R2   r /d = 5·155 ×10⁻²)
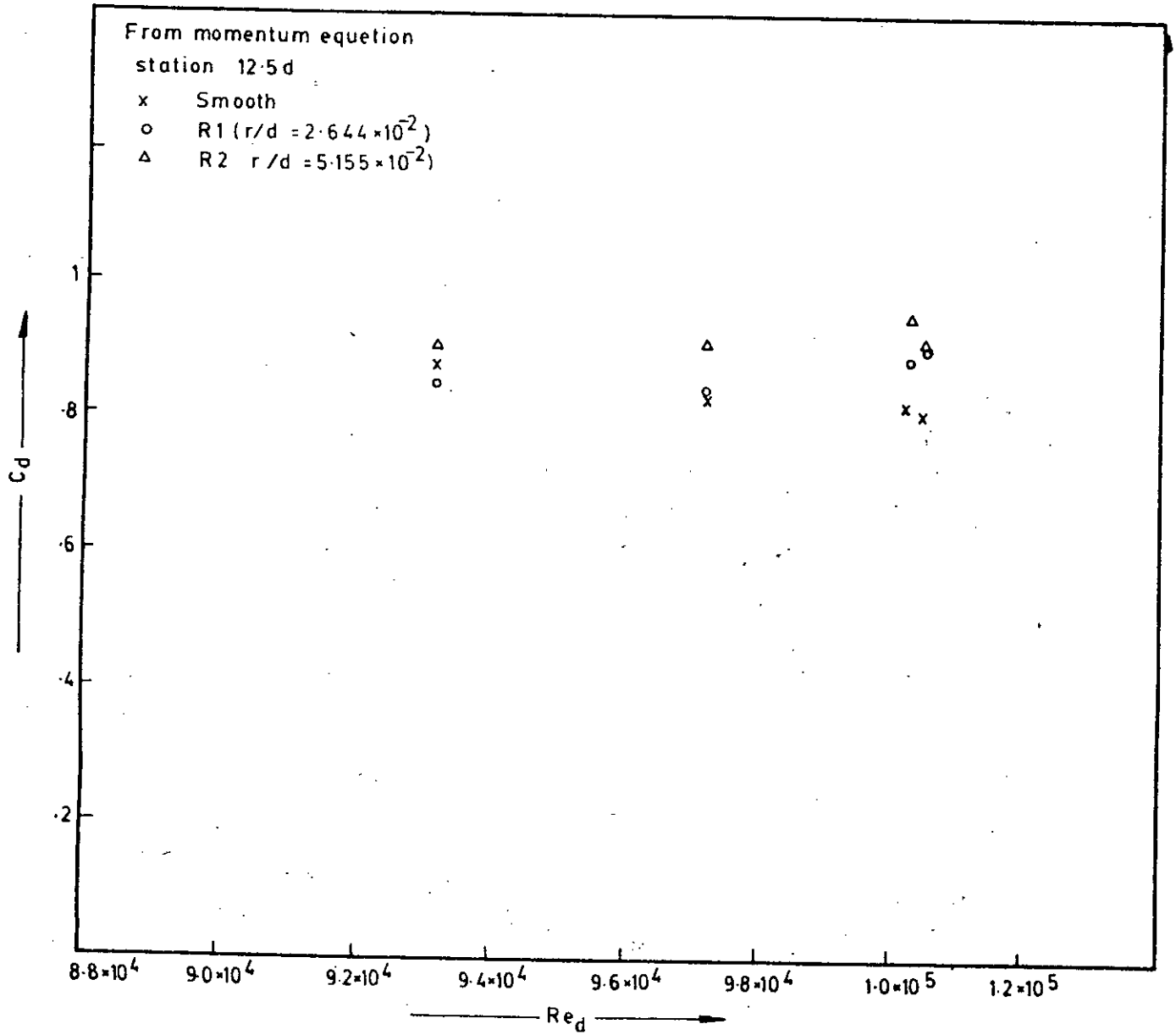
Fig. 5-2-2-f   Variation of drag coefficient with Reynolds number
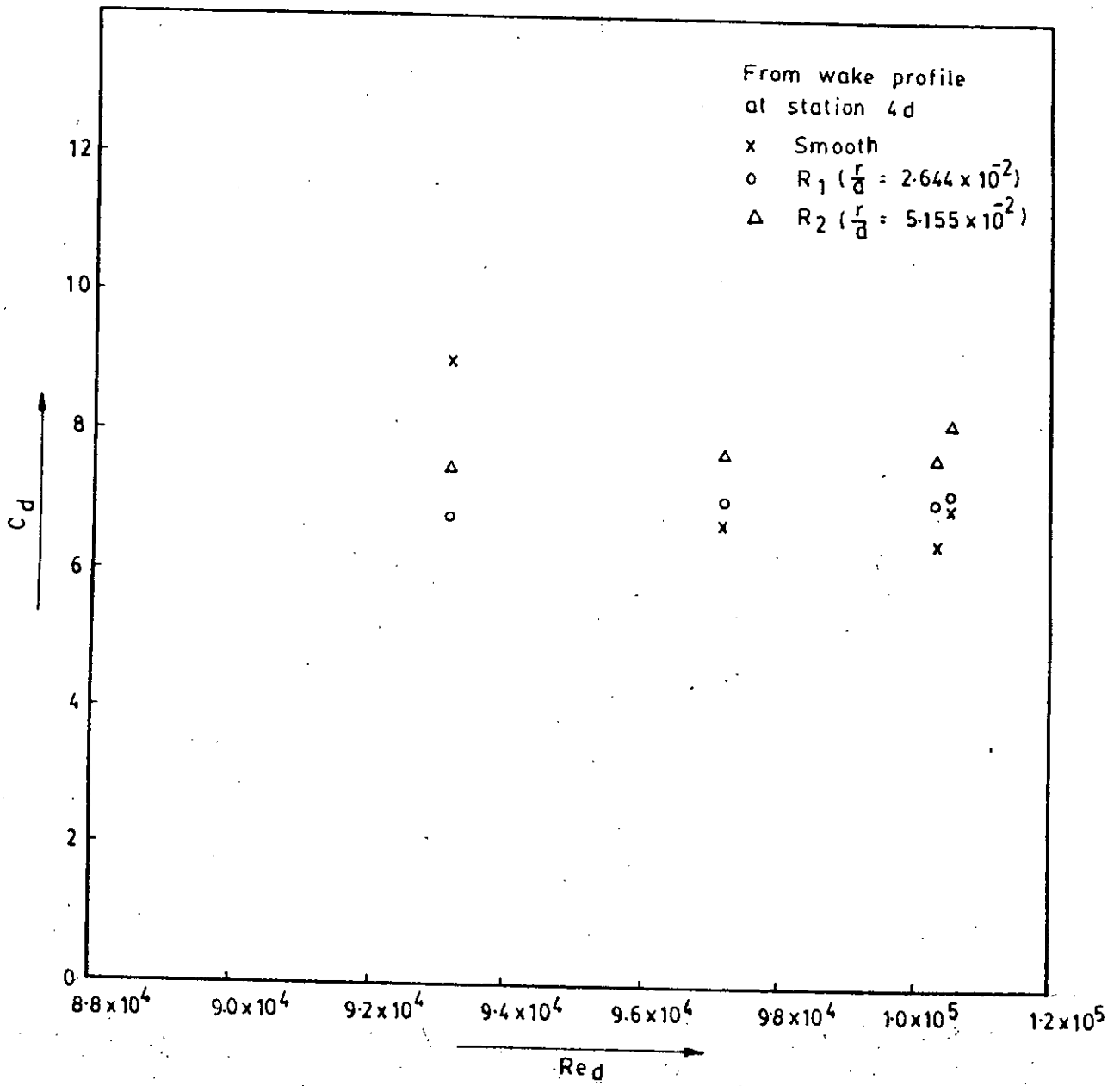
Fig. 5-2-2-g. Variation of drag coefficient with Reynolds number
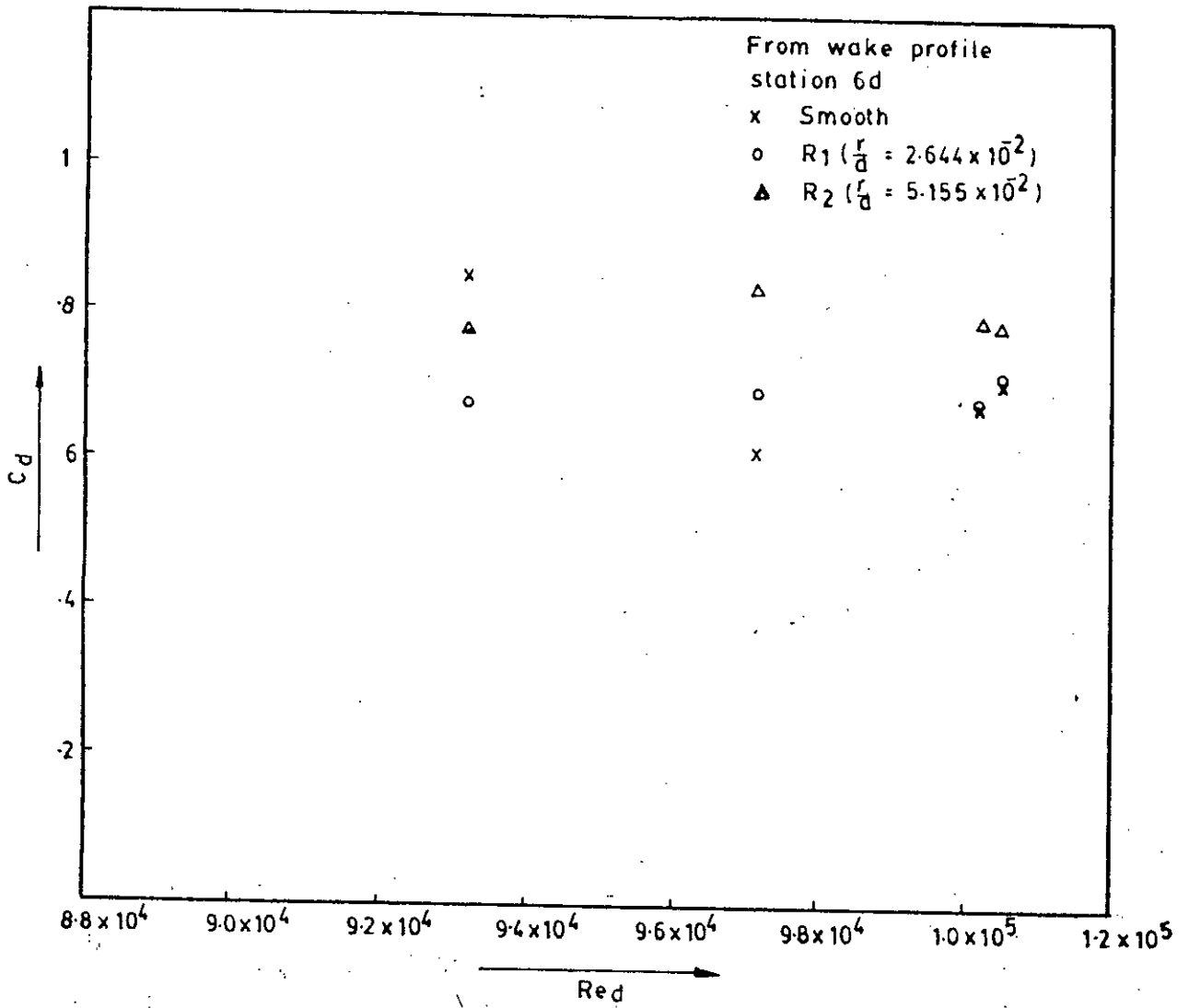
Fig. 5-2-2-h   Variation of drag coefficient with Reynolds number
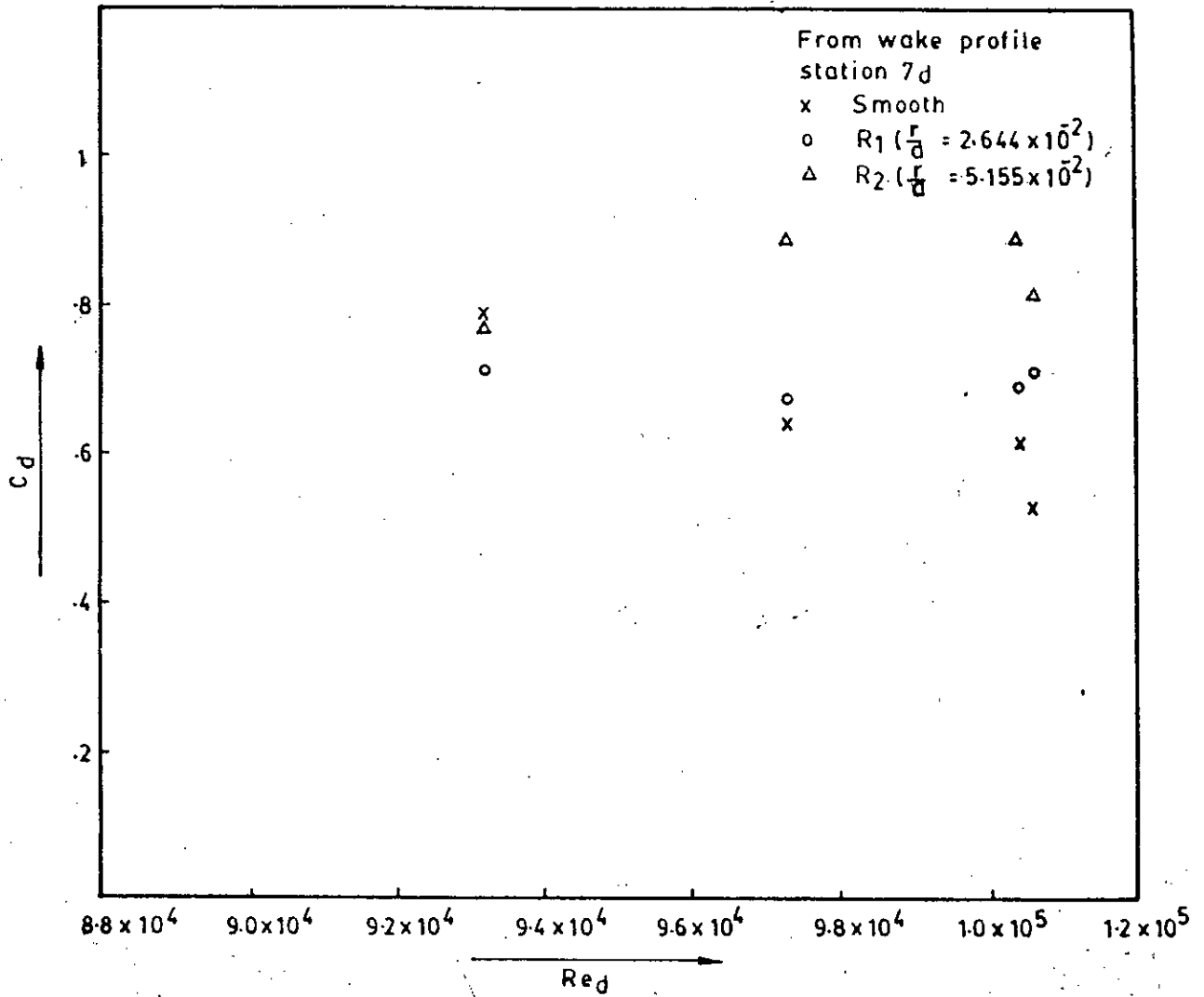
Fig. 5-2-2-i Variation of drag coefficient with Reynolds number
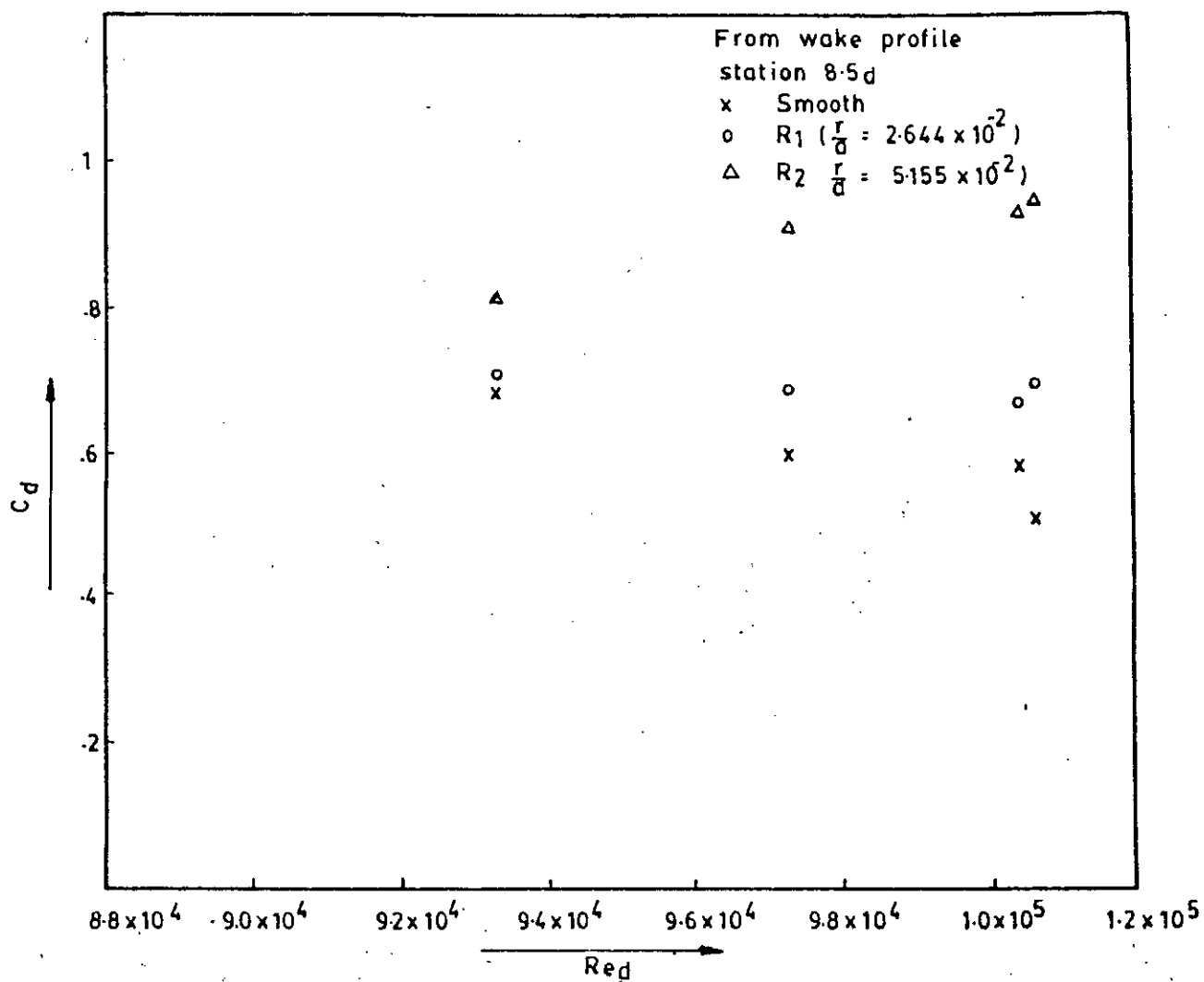
Fig. 5-2-2-j   Variation of drag coefficient with Reynolds number
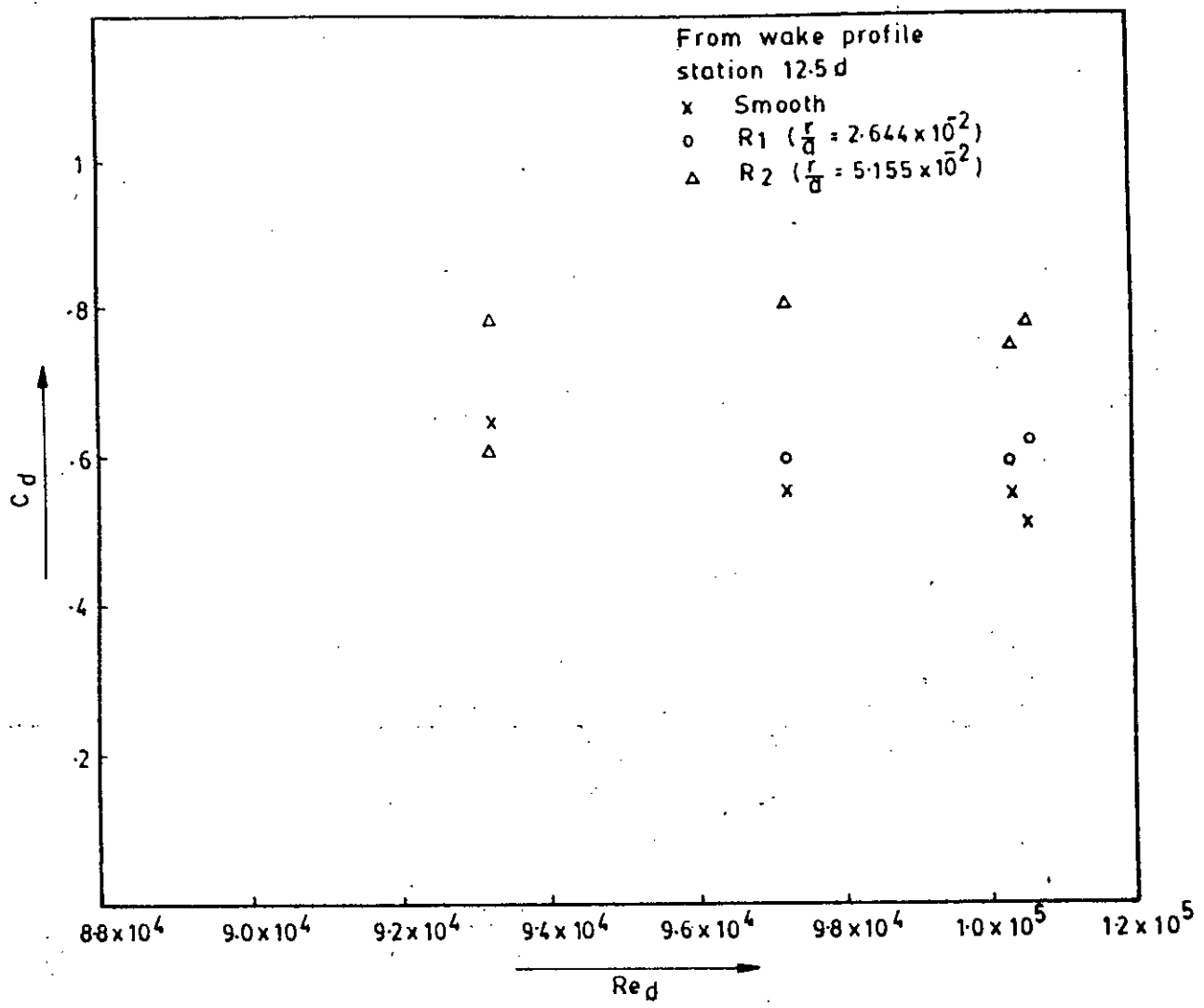
Fig. 5-2-2-k   Variation of drag coefficient with Reynolds number
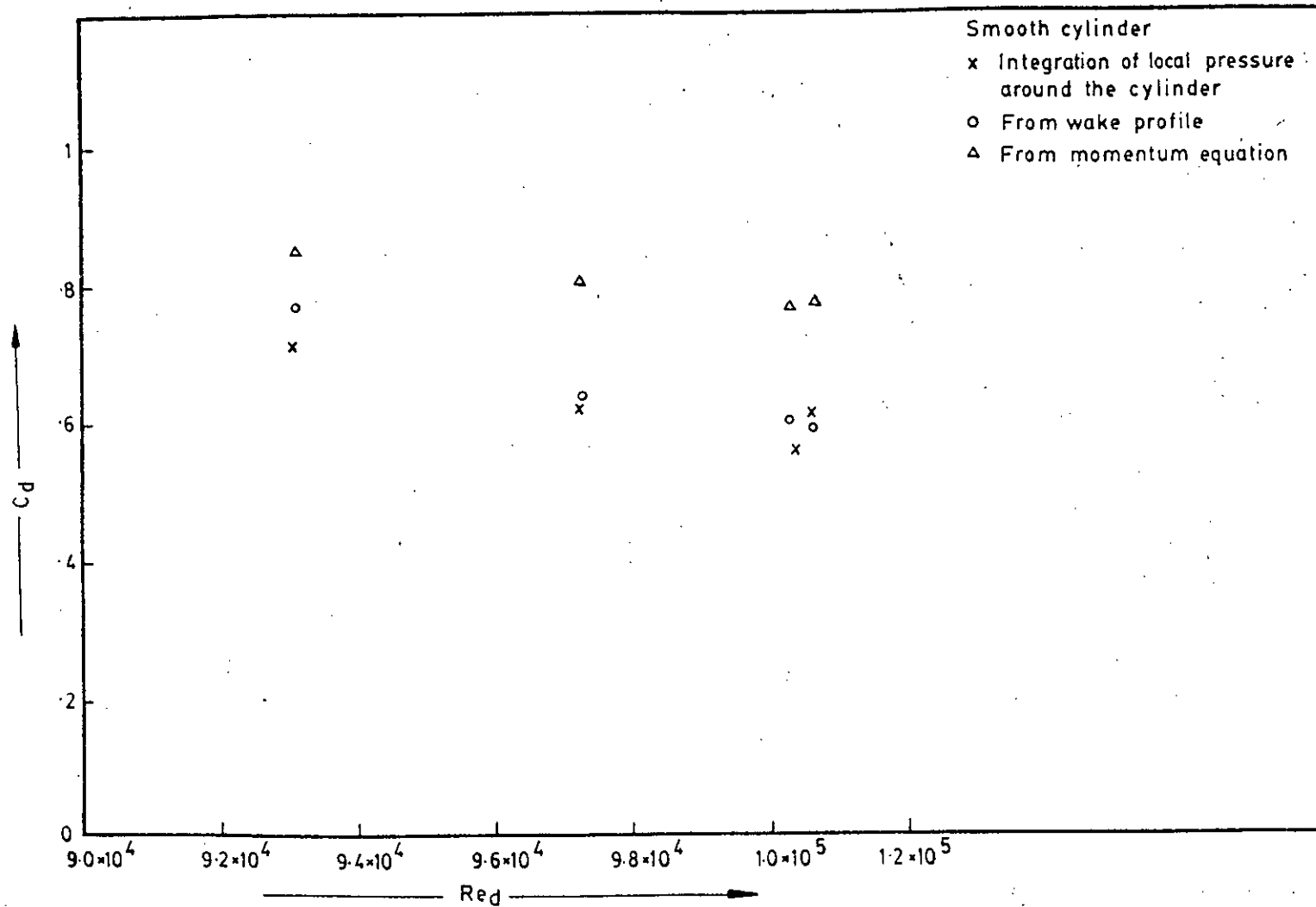
Fig.5-2-2-m Variation of drag coefficient with Reynolds number

Fig. 5-2-2-n Variation of drag coefficient with Reynolds number

Fig. 5-2-2-o Variation of drag coefficient with Reynolds number
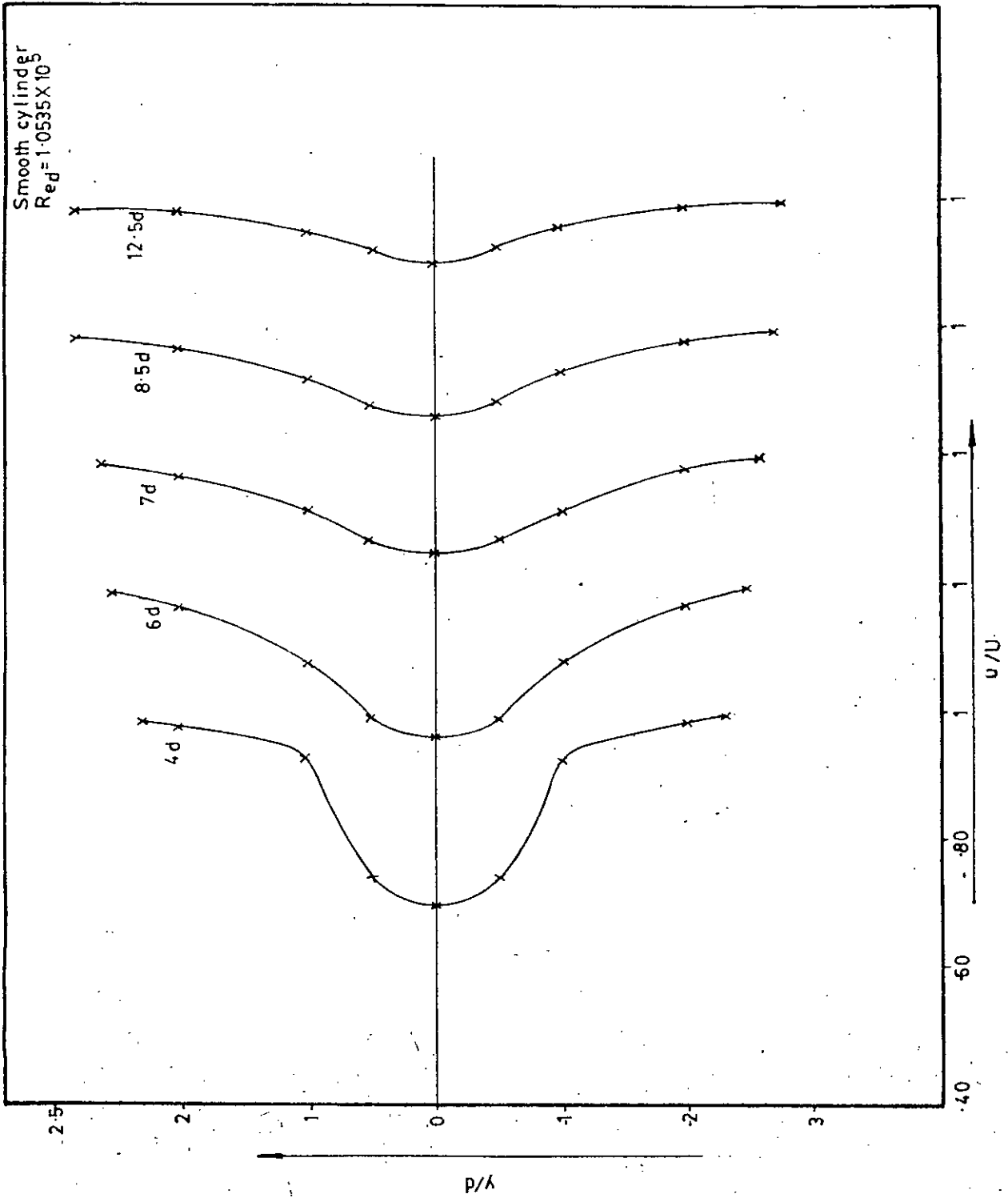
Fig. 5-3-1-a Mean velocity distribution in wake

Smooth cylinder
$R_{ed} = 1.038 \times 10^5$
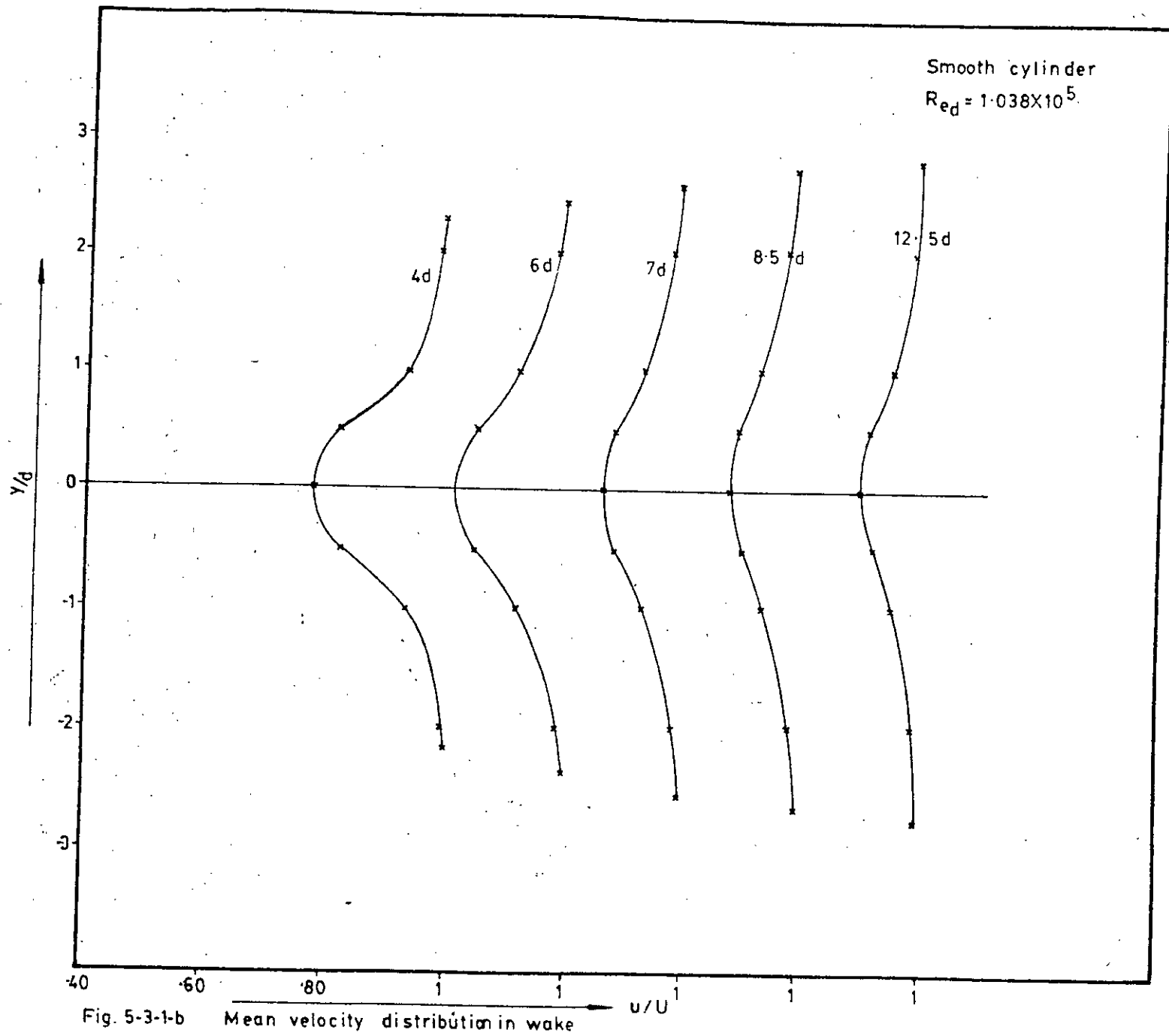
Fig. 5-3-1-b   Mean velocity distribution in wake
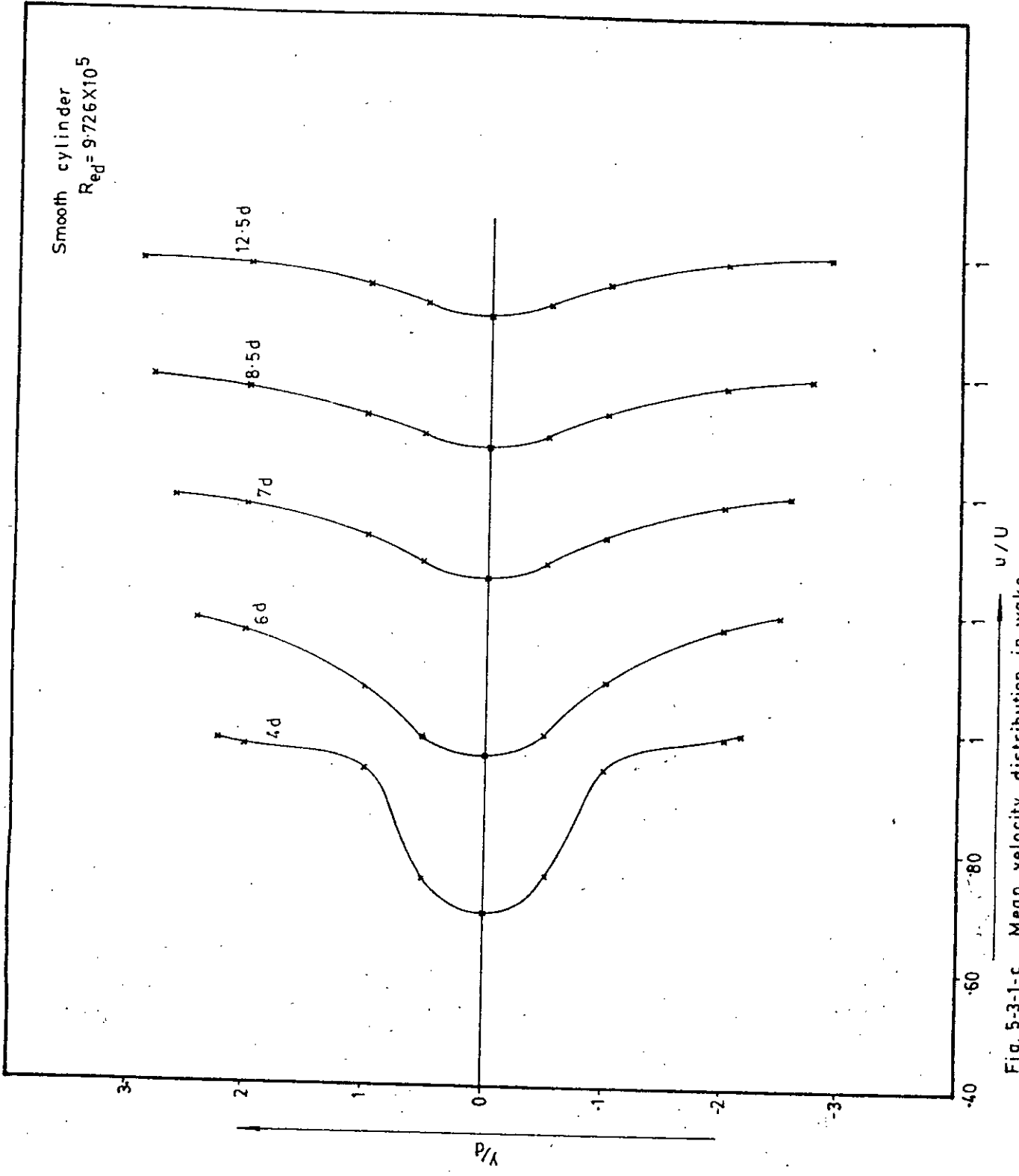
Fig. 5-3-1-c   Mean velocity distribution in wake

Smooth cylinder
$R_{ed} = 9{\cdot}316 \times 10^4$
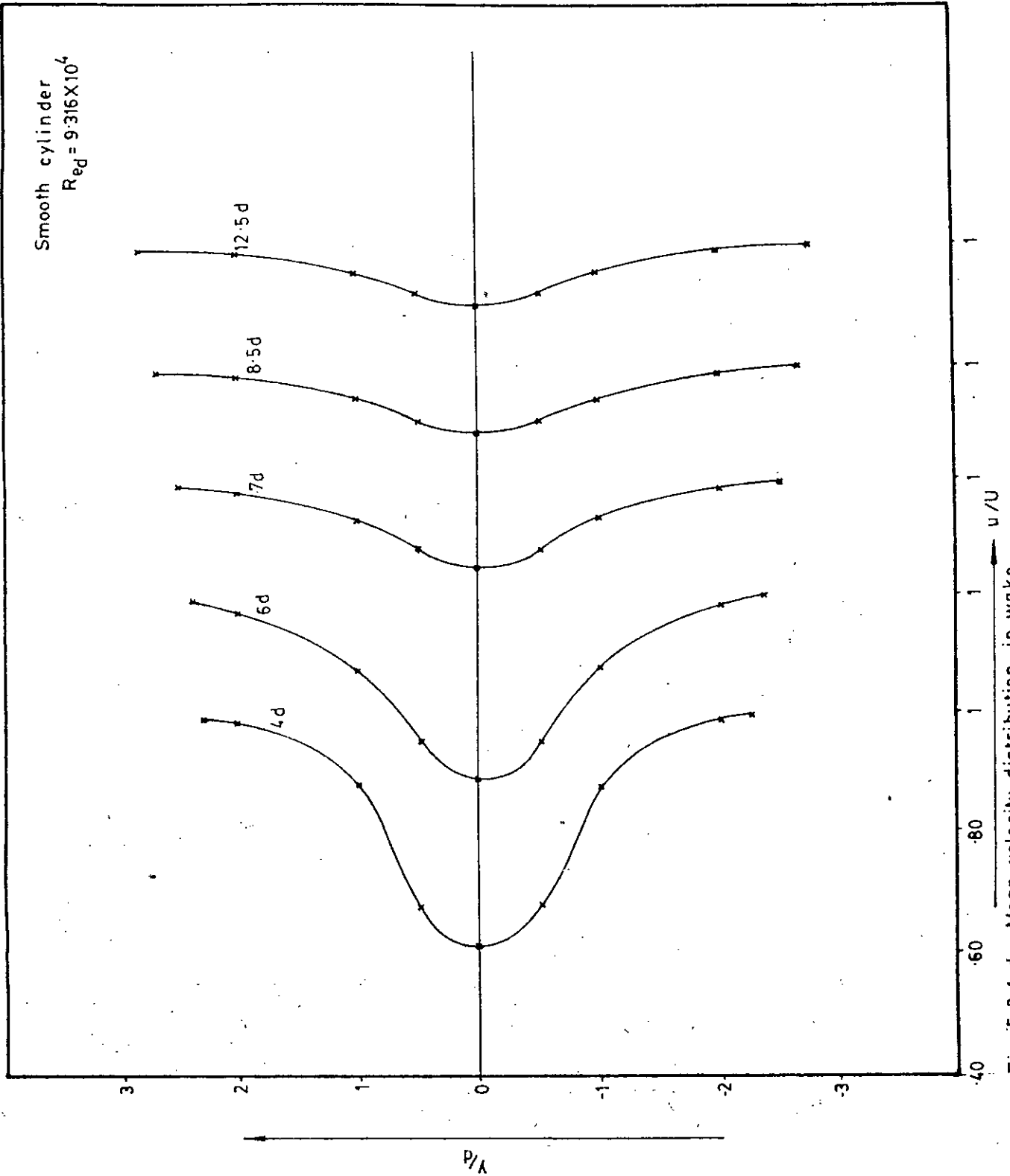
Fig. 5·3·1·d   Mean velocity distribution in wake
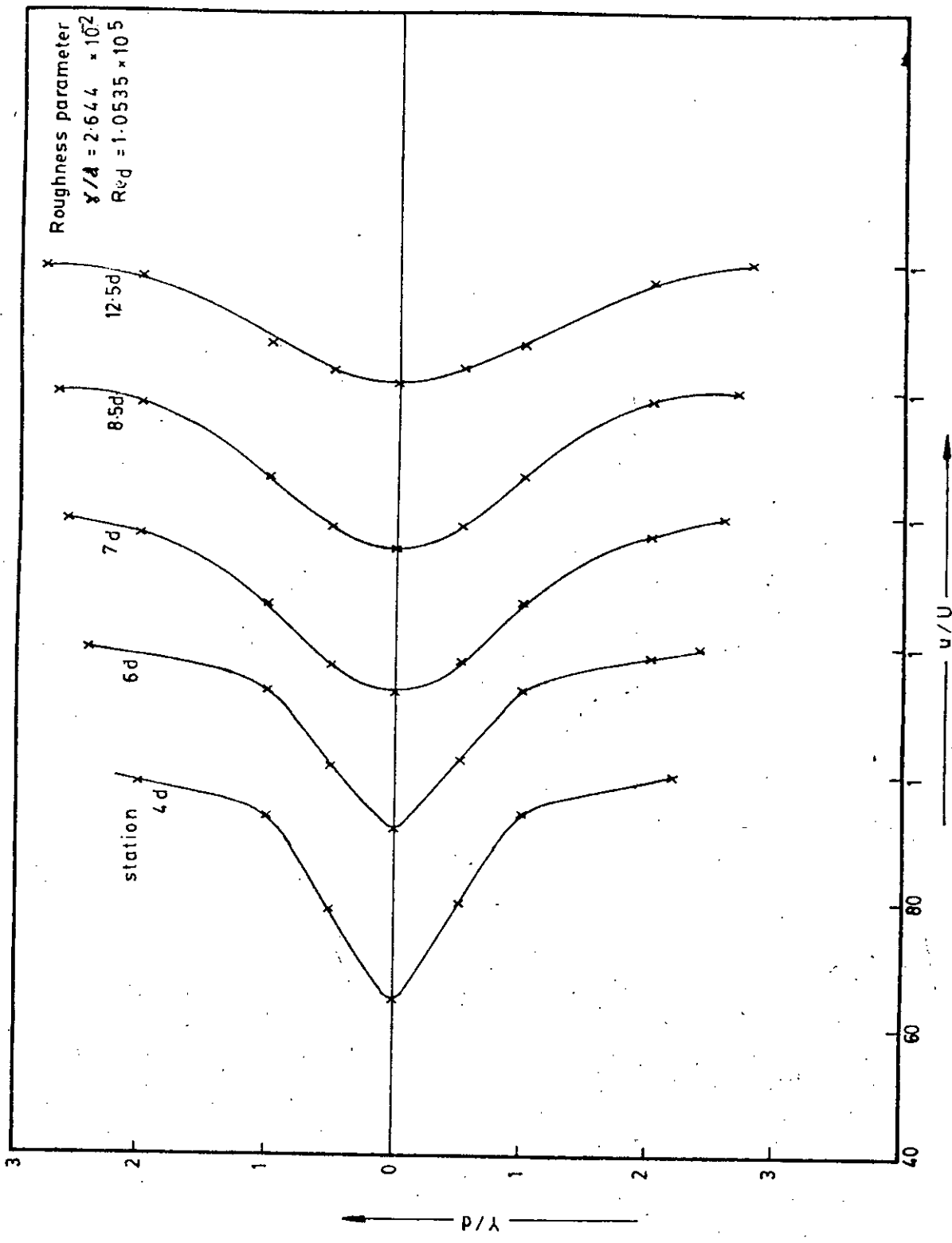
Fig. 5-3-1-e Mean velocity distribution in wake
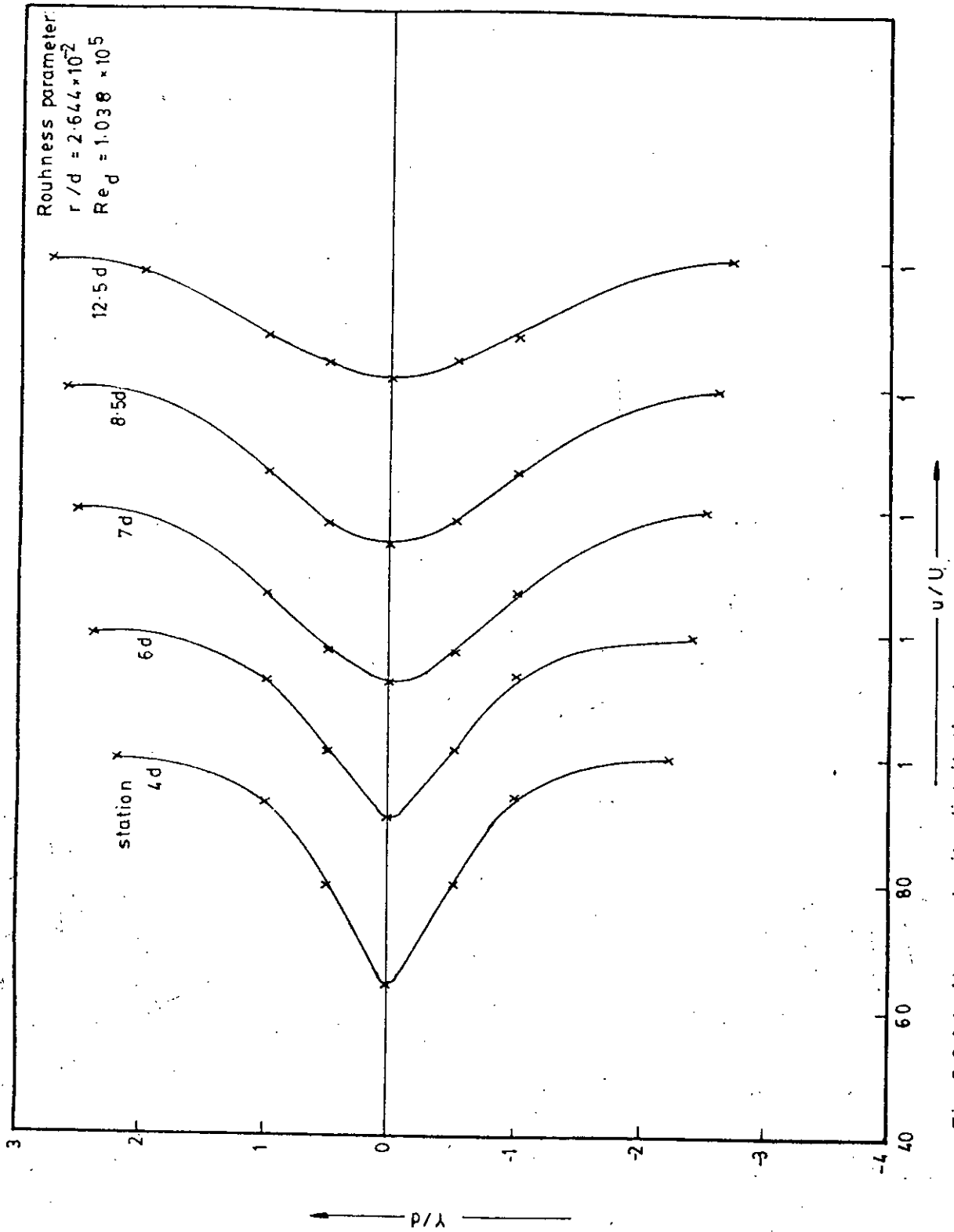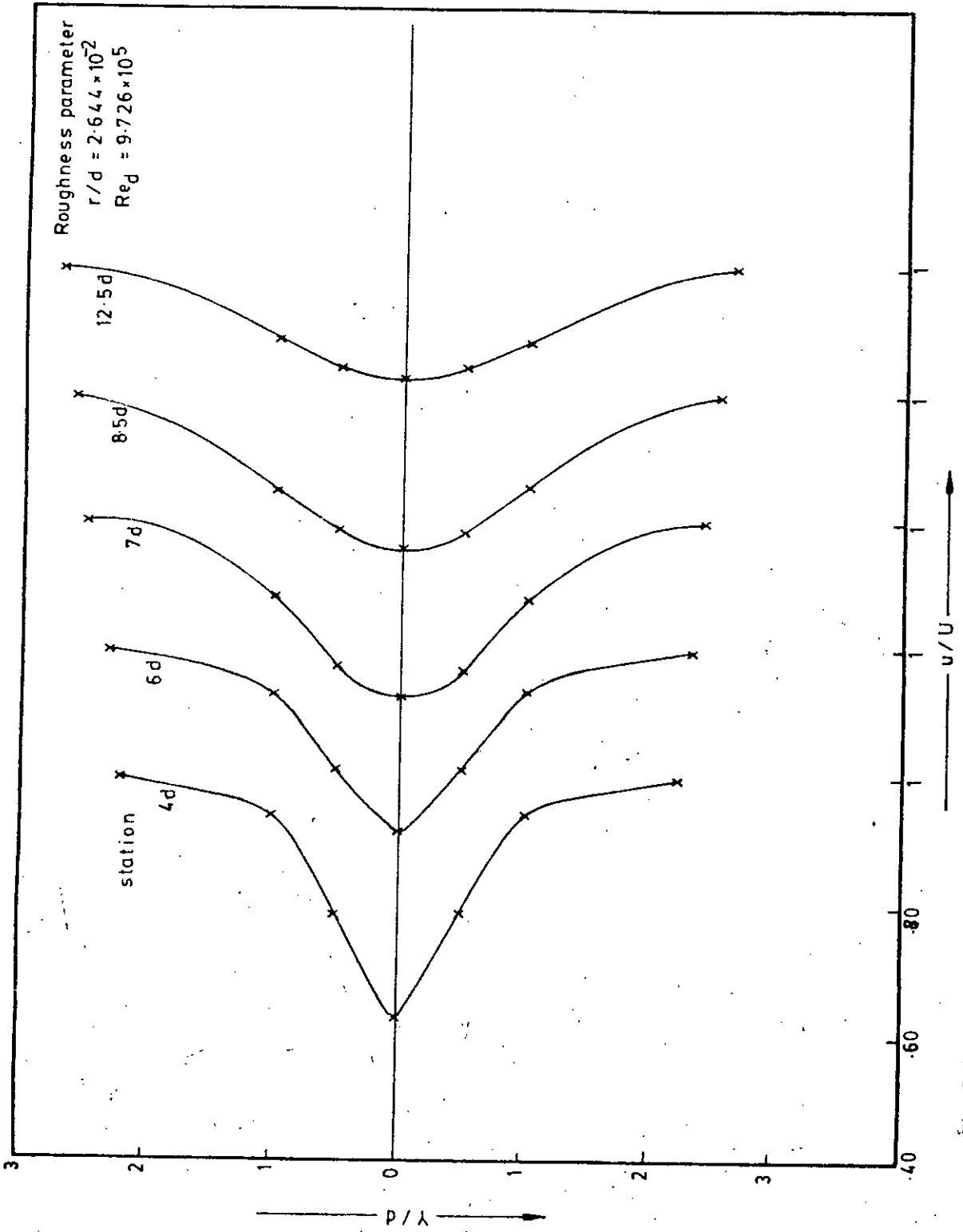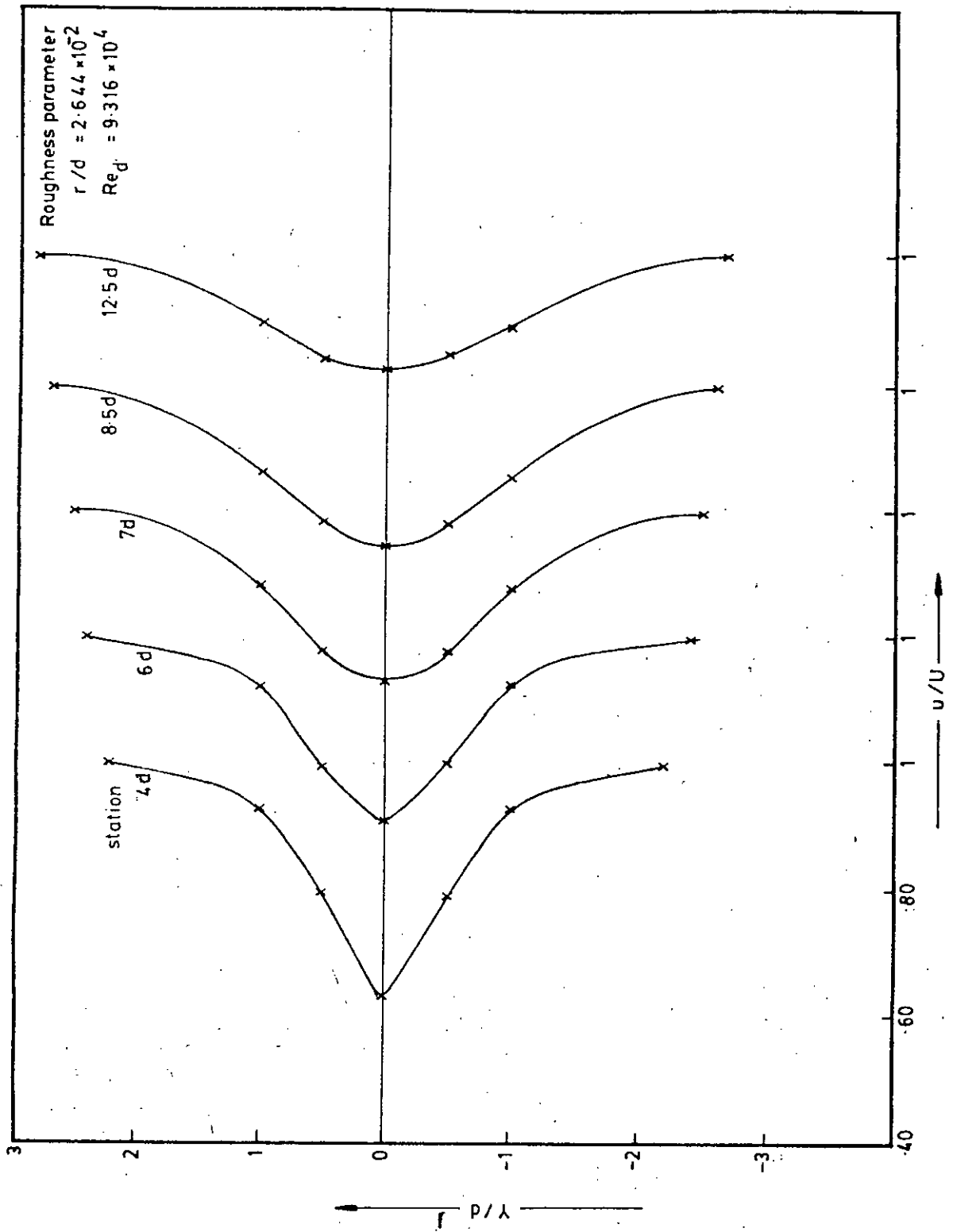
Fig. 5-3-1-f Mean velocity distribution in wake

Roughness parameter
$r/d = 2.644 \times 10^{-2}$
$Re_d = 9.726 \times 10^5$

12·5d

8·5d

7d

6d

station 4d

Fig. 5-3-1-g Mean velocity distribution in wake

u / U

y / d

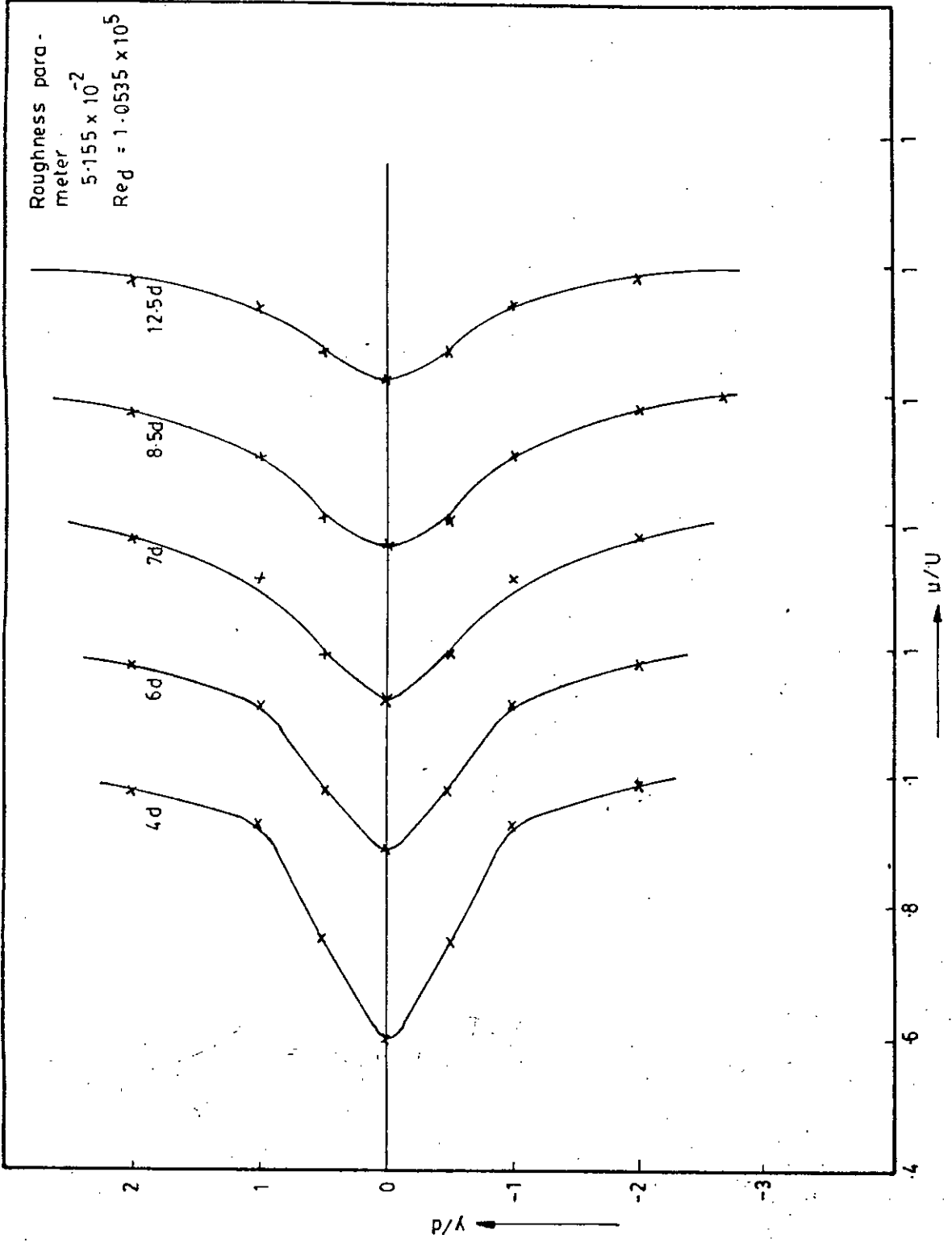Fig. 5-3-1-h   Mean velocity distribution in wake

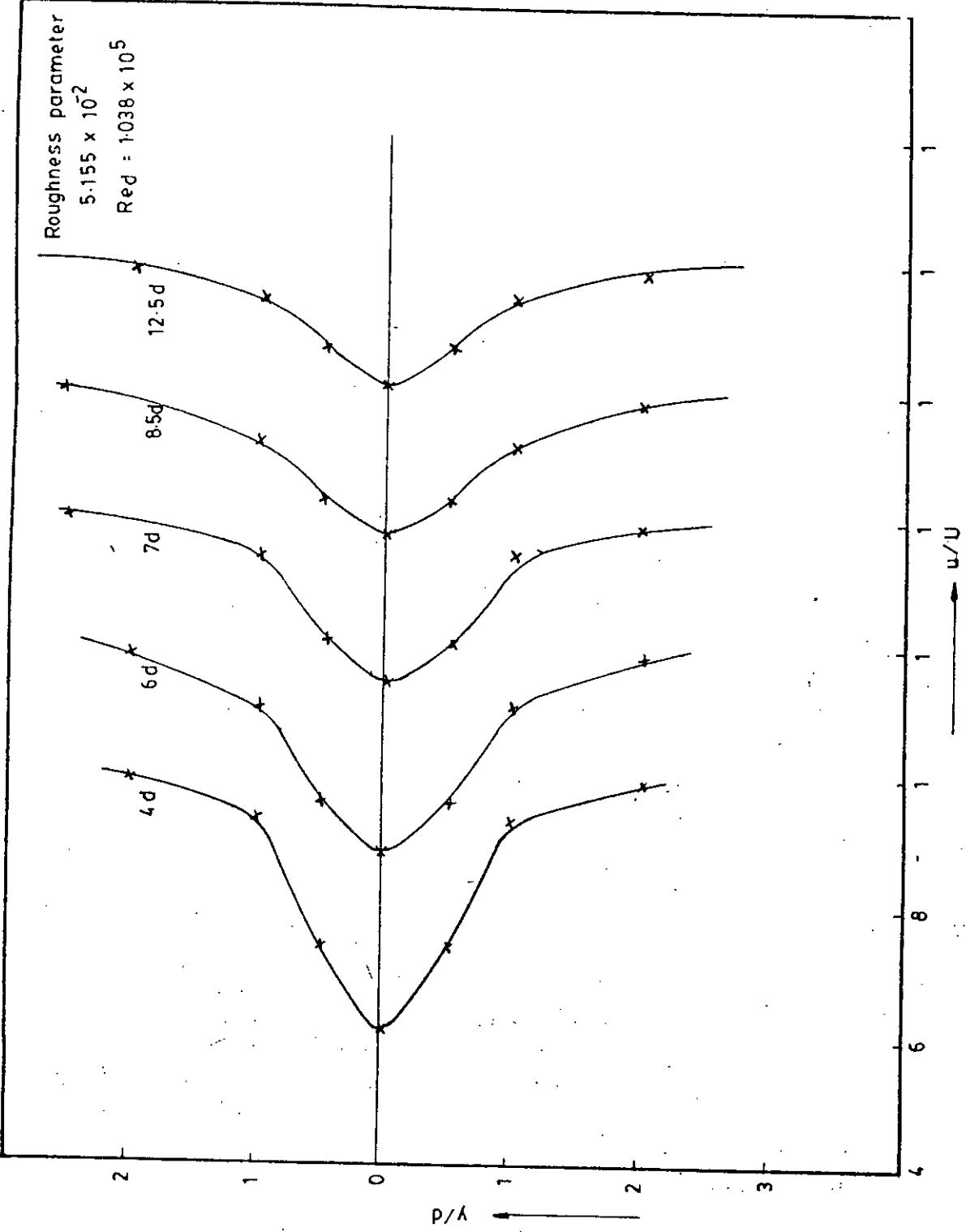Fig. 5-3-1-i   Mean velocity distribution in wake
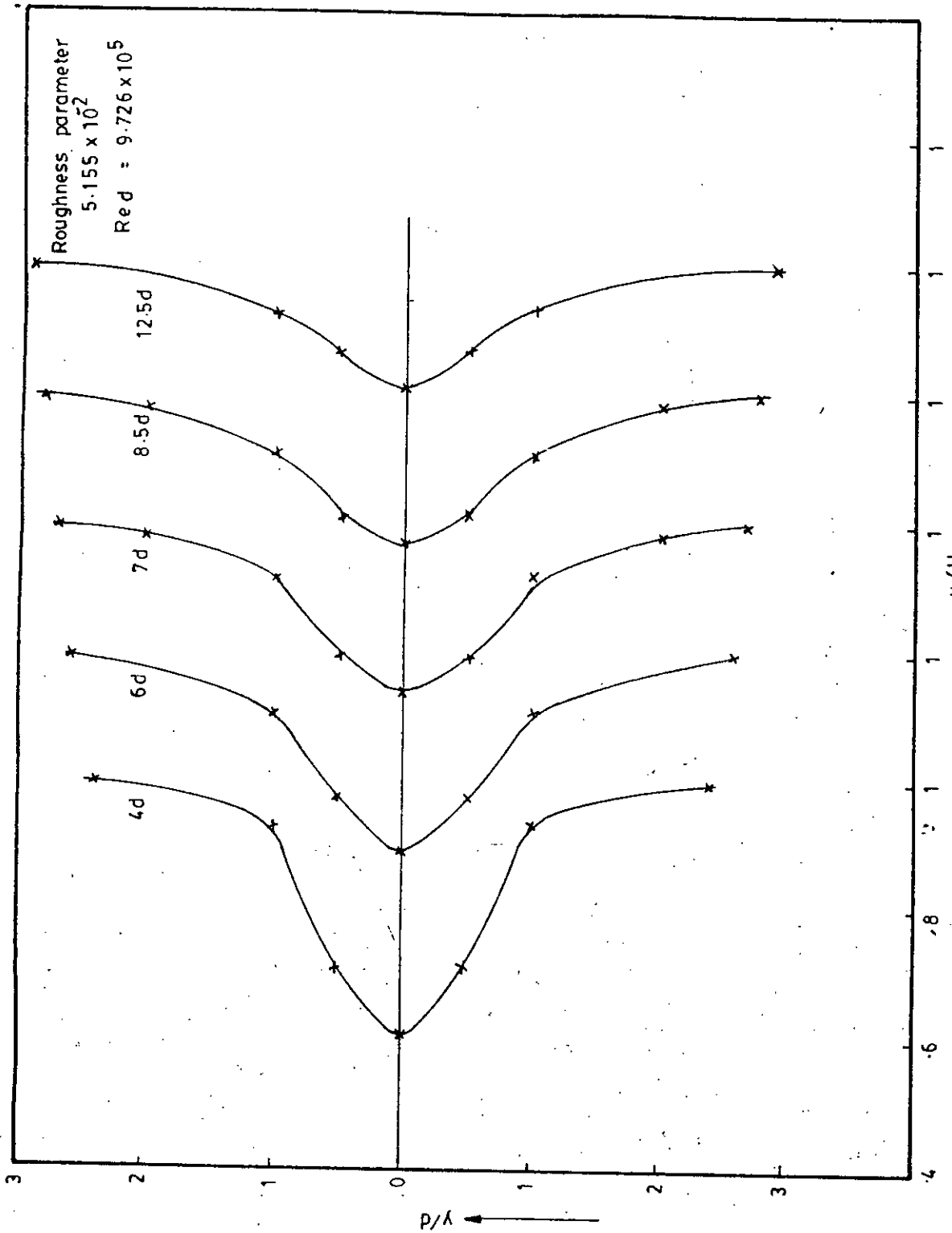
Fig. 5-3-1-j Mean velocity distribution in wake
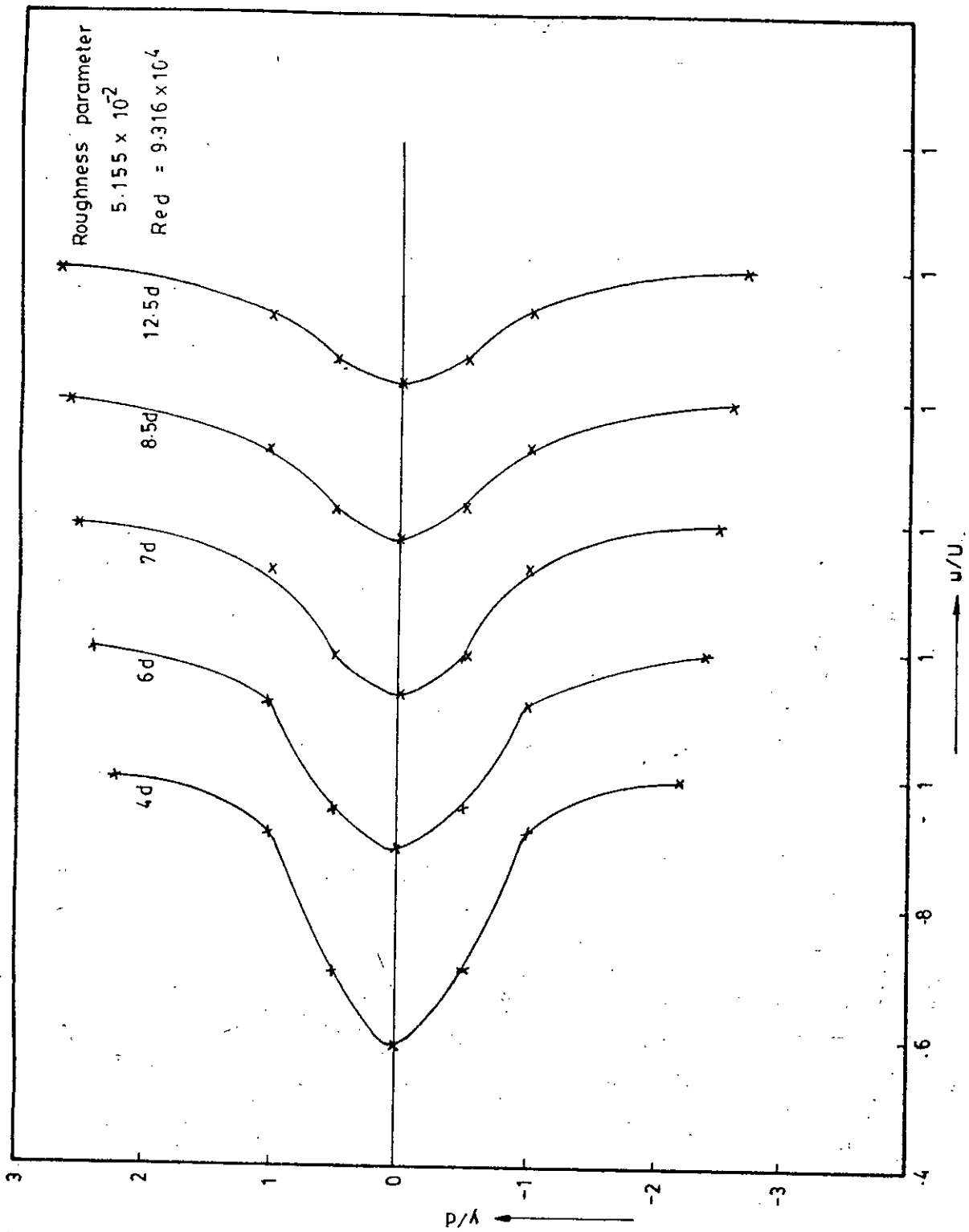
Fig. 5-3-1-k   Mean velocity distribution in wake
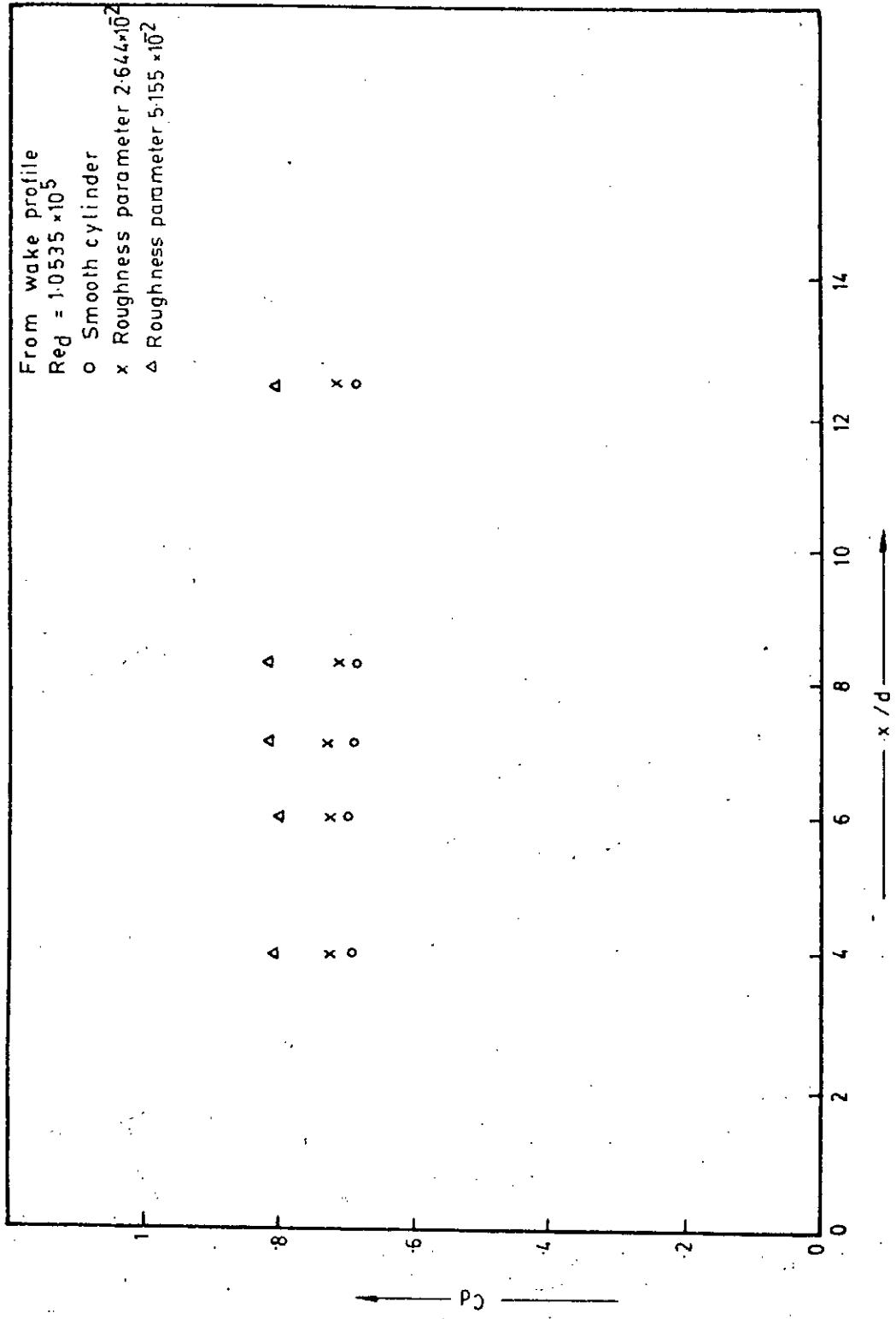
Fig. 5-3-1-1   Mean velocity distribution in wake

From wake profile
Red = 1.0535 ×10^5
o Smooth cylinder
x Roughness parameter 2.644×10^{-2}
△ Roughness parameter 5.155 ×10^{-2}

Fig. 5-3-1-m Variation of Cd with the axial distance

From wake profile
Red = 9·316 × 10⁴
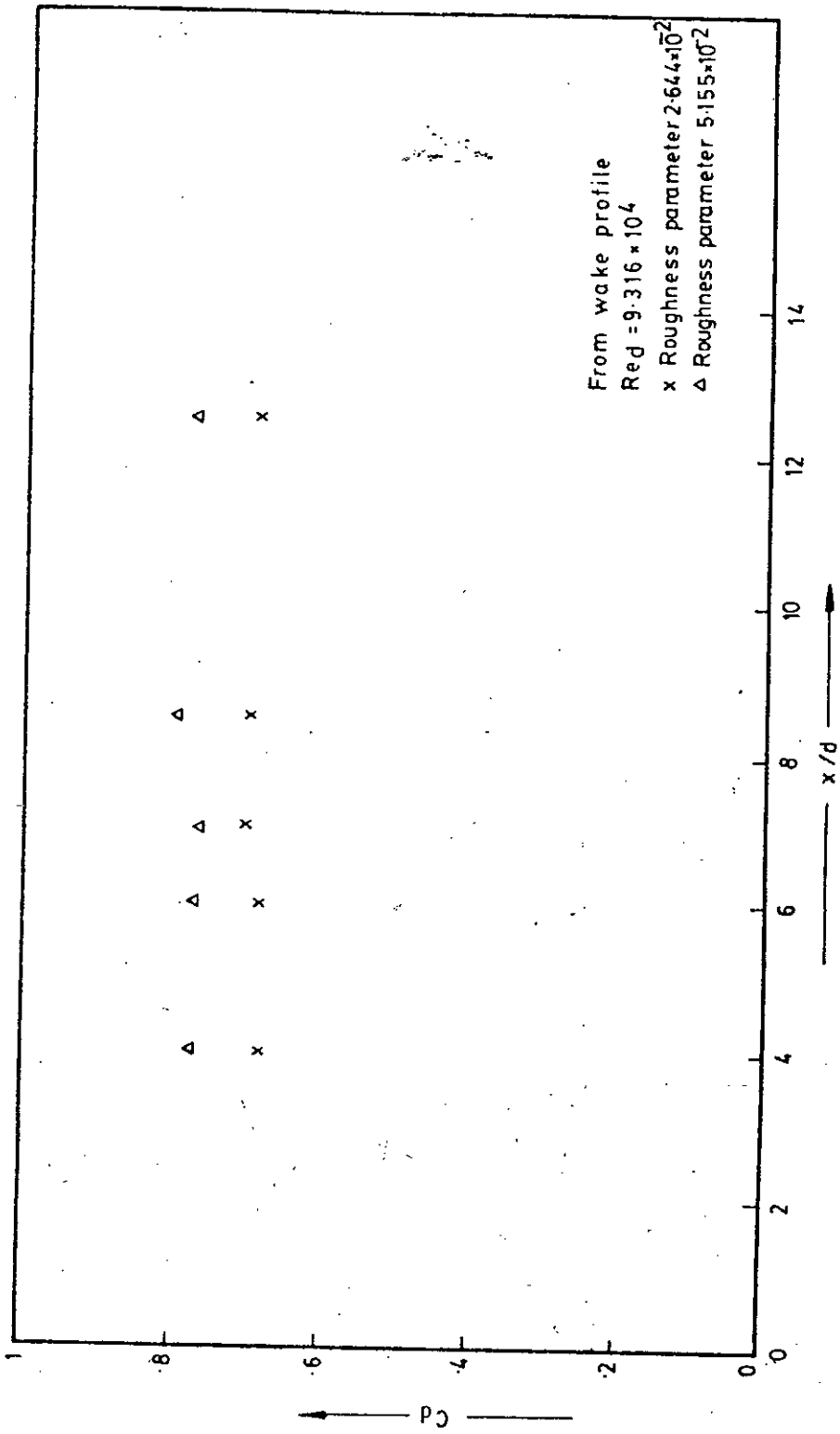x Roughness parameter 2·644×10⁻²
△ Roughness parameter 5·155×10⁻²

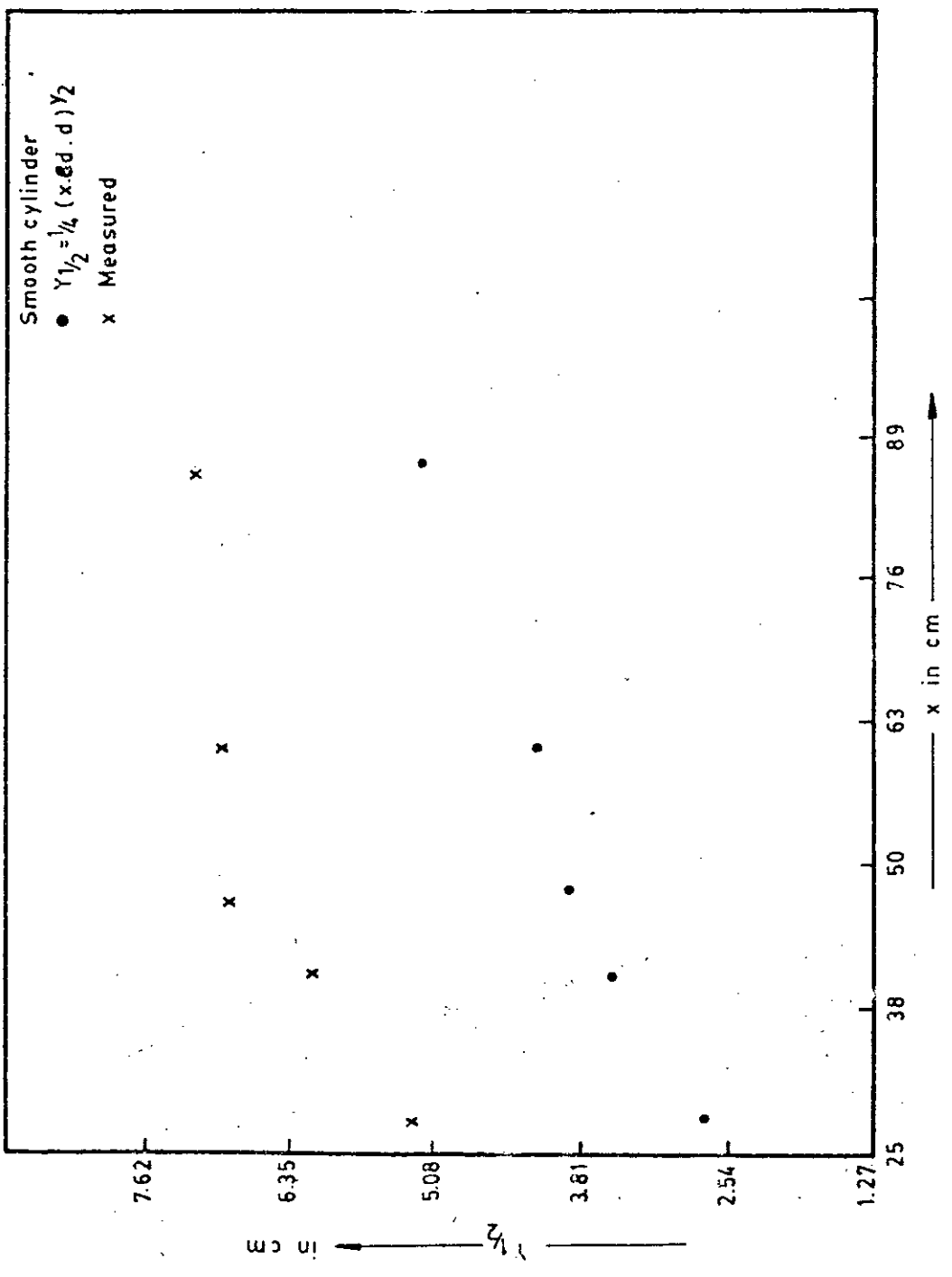Fig. 5-3-1-n Variation of Cd with the axial distance

Fig. 5-3-2-a Variation of half width with axial distance

Fig.5-3-2-b Velocity distribution along centre line of wake

Fig. 5-3-2-c Velocity distribution along centre line of wake

$r/d = 5.155 \times 10^2$

x	$Re_d = 1.0535 \times 10^5$
o	$Re_d = 1.038 \times 10^5$
□	$Re_d = 9.726 \times 10^4$
△	$Re_d = 9.316 \times 10^4$

U_c/U

1·0

·90
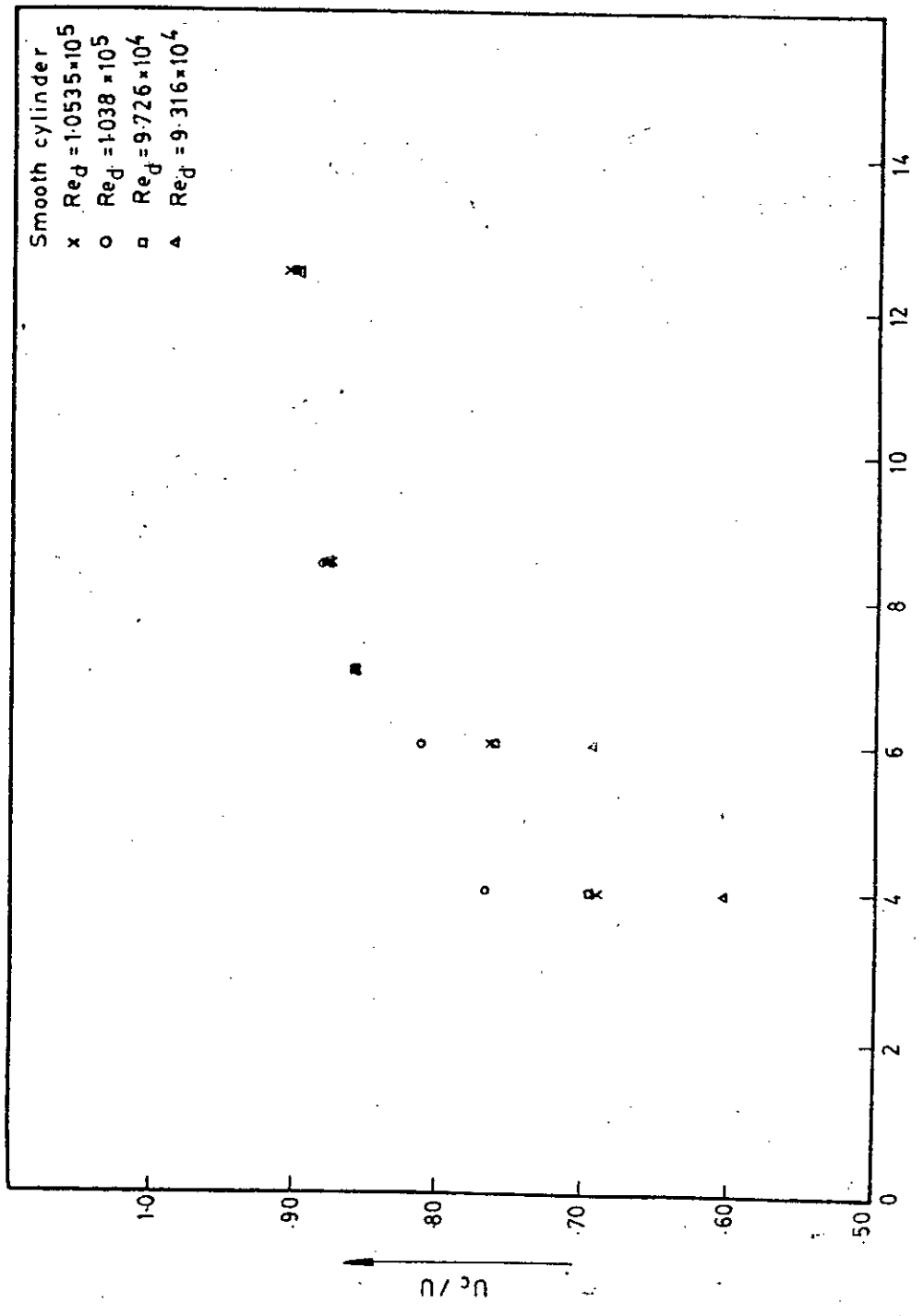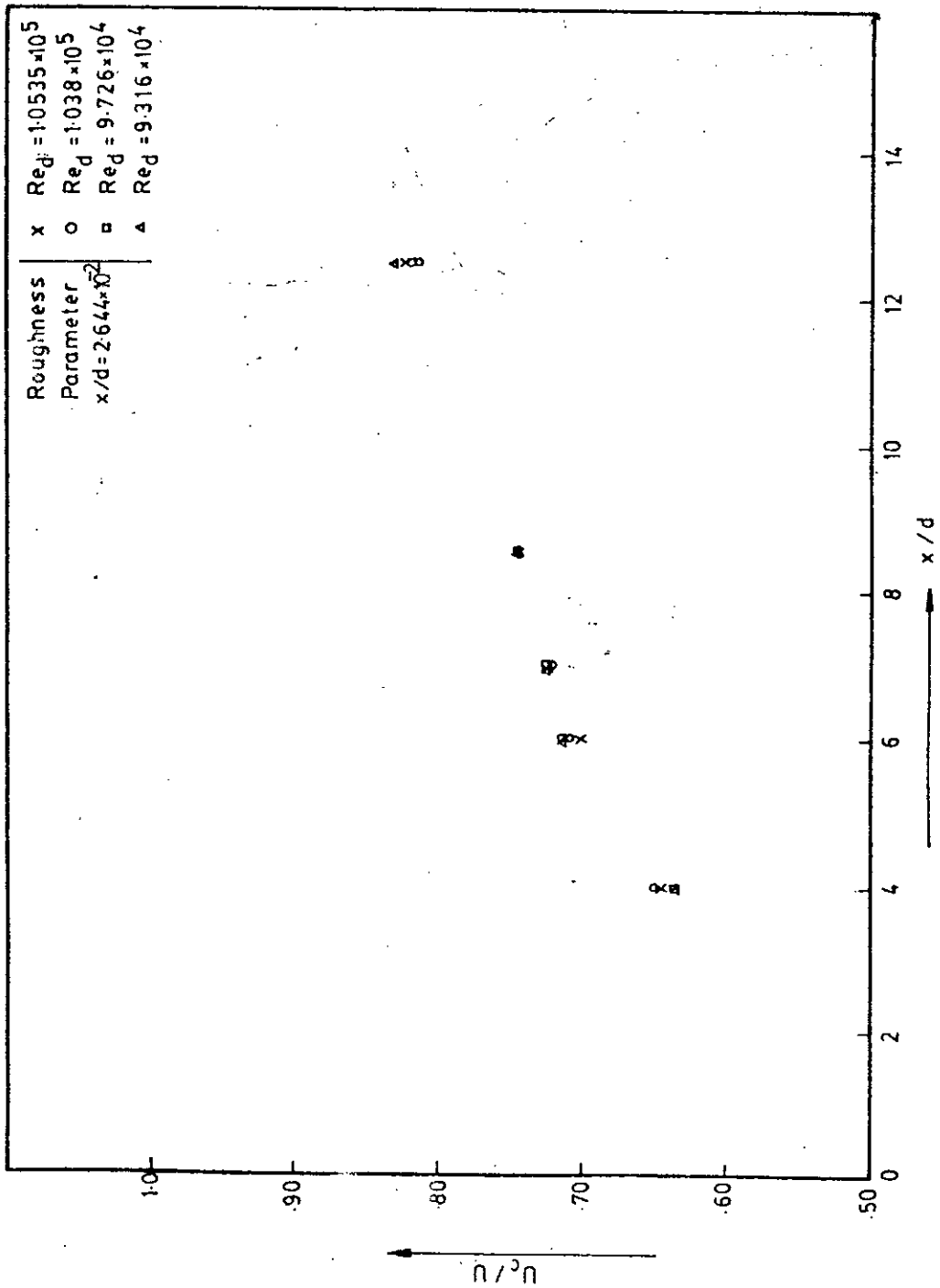
·80

·70

·60

·50

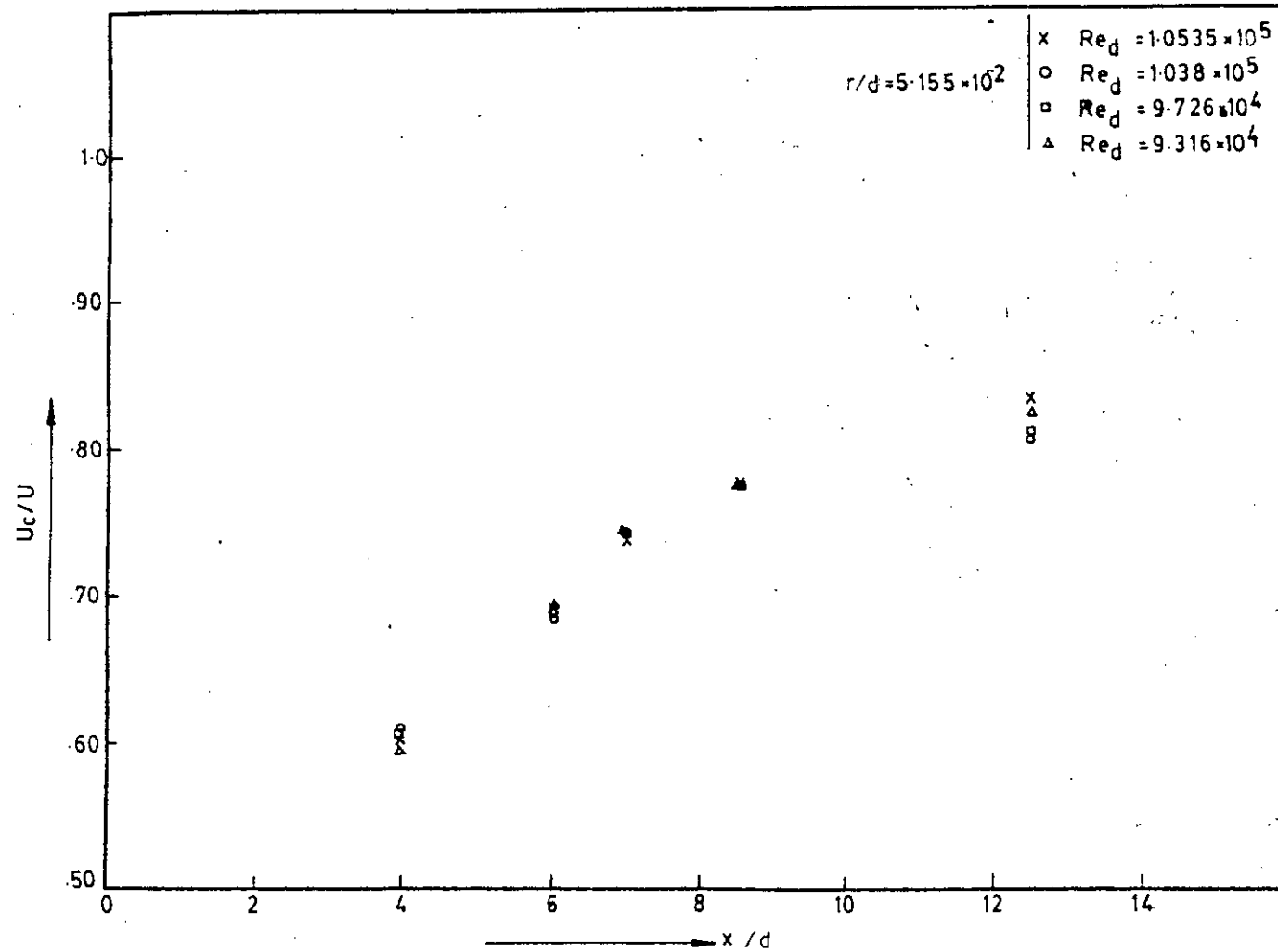0   2   4   6   8   10   12   14

x/d

Fig. 5-3-2-d Velocity distribution along centre line of wake
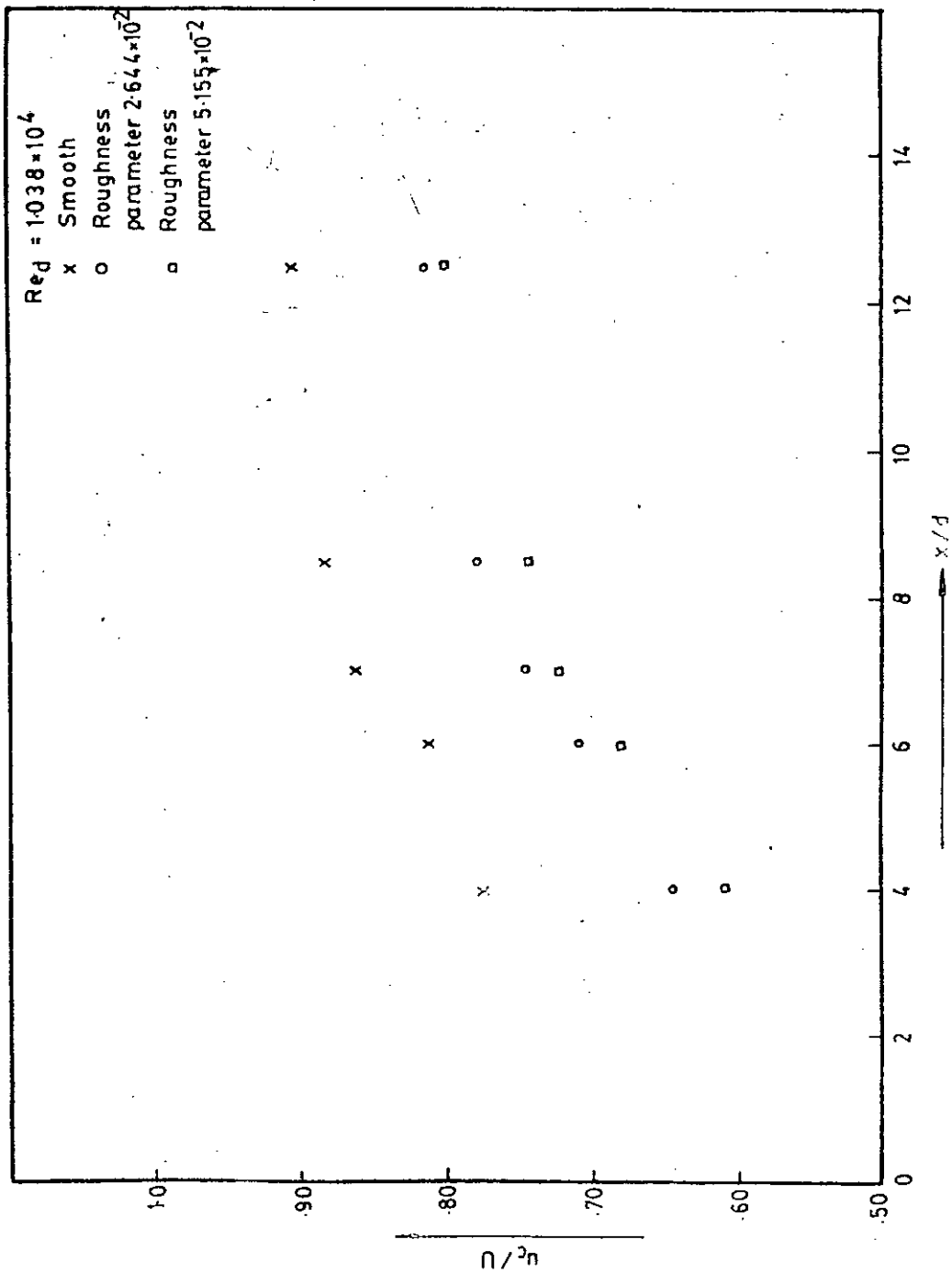
Fig. 5-3-2-e Velocity distribution along centre line of wake

Fig. 5-3-3-a Dimensionless velocity profile in the wake behind a cylinder.
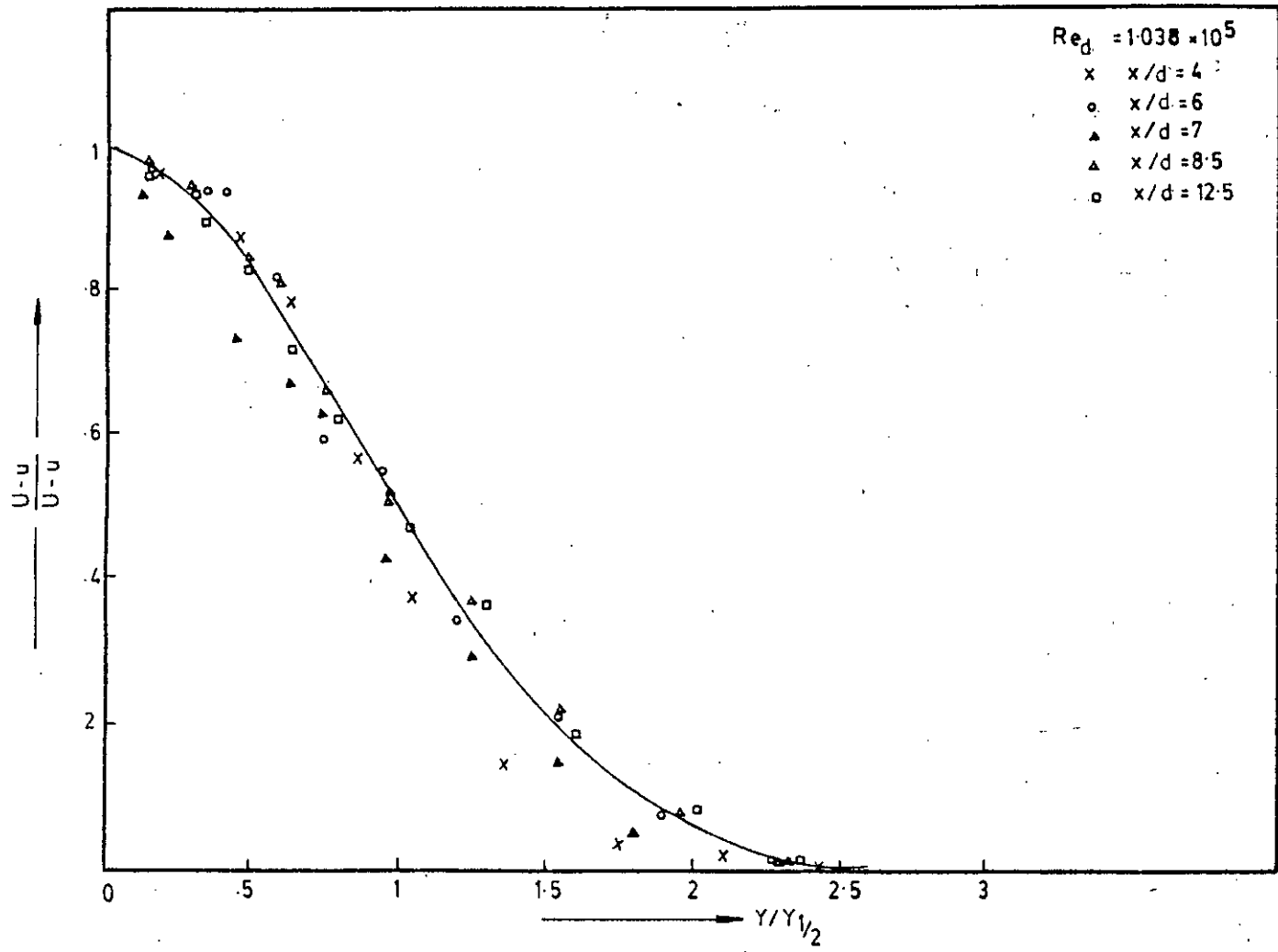
Fig.5-3-3-b Dimensionless velocity profiles in the wake behind a cylinder
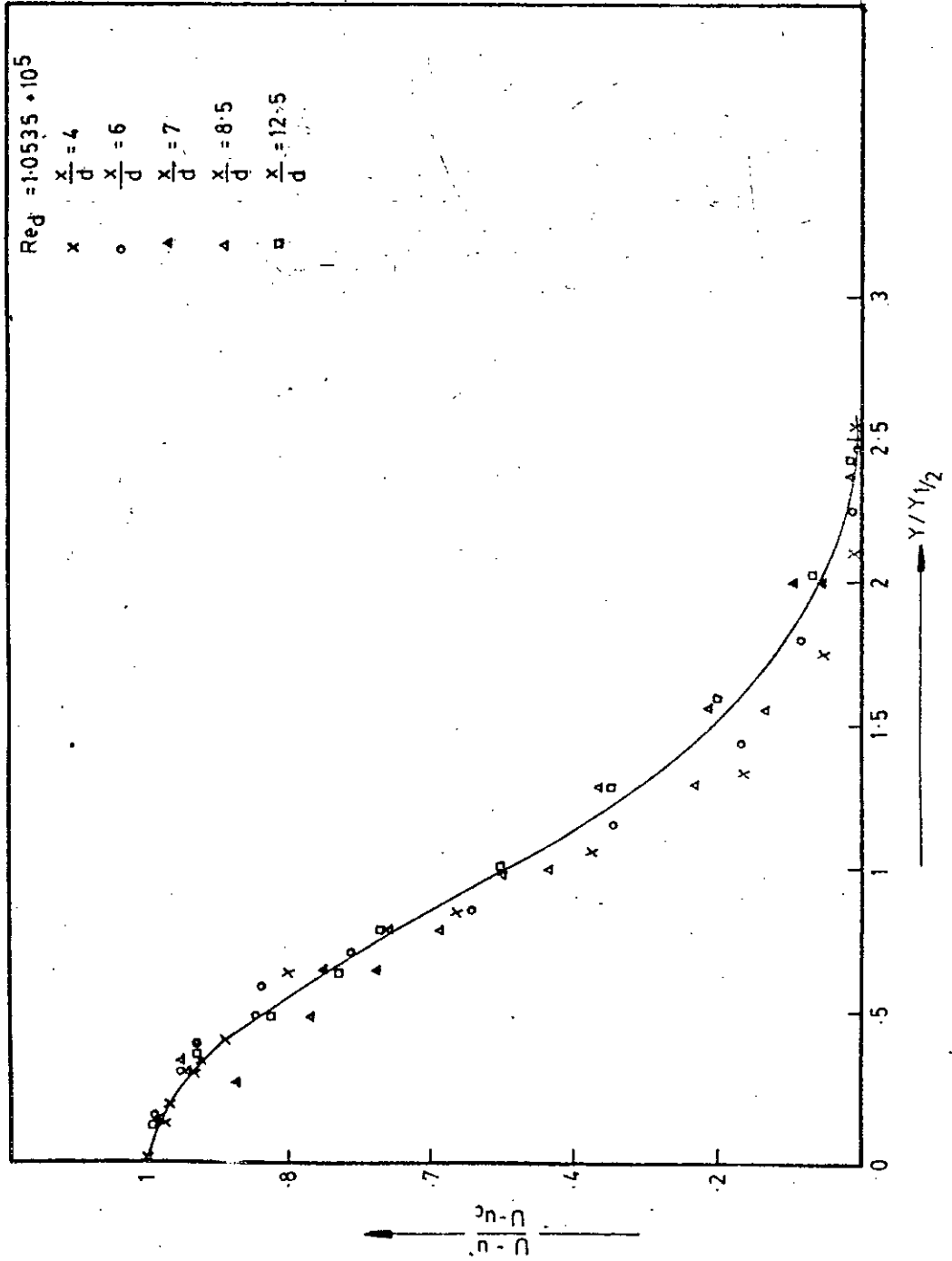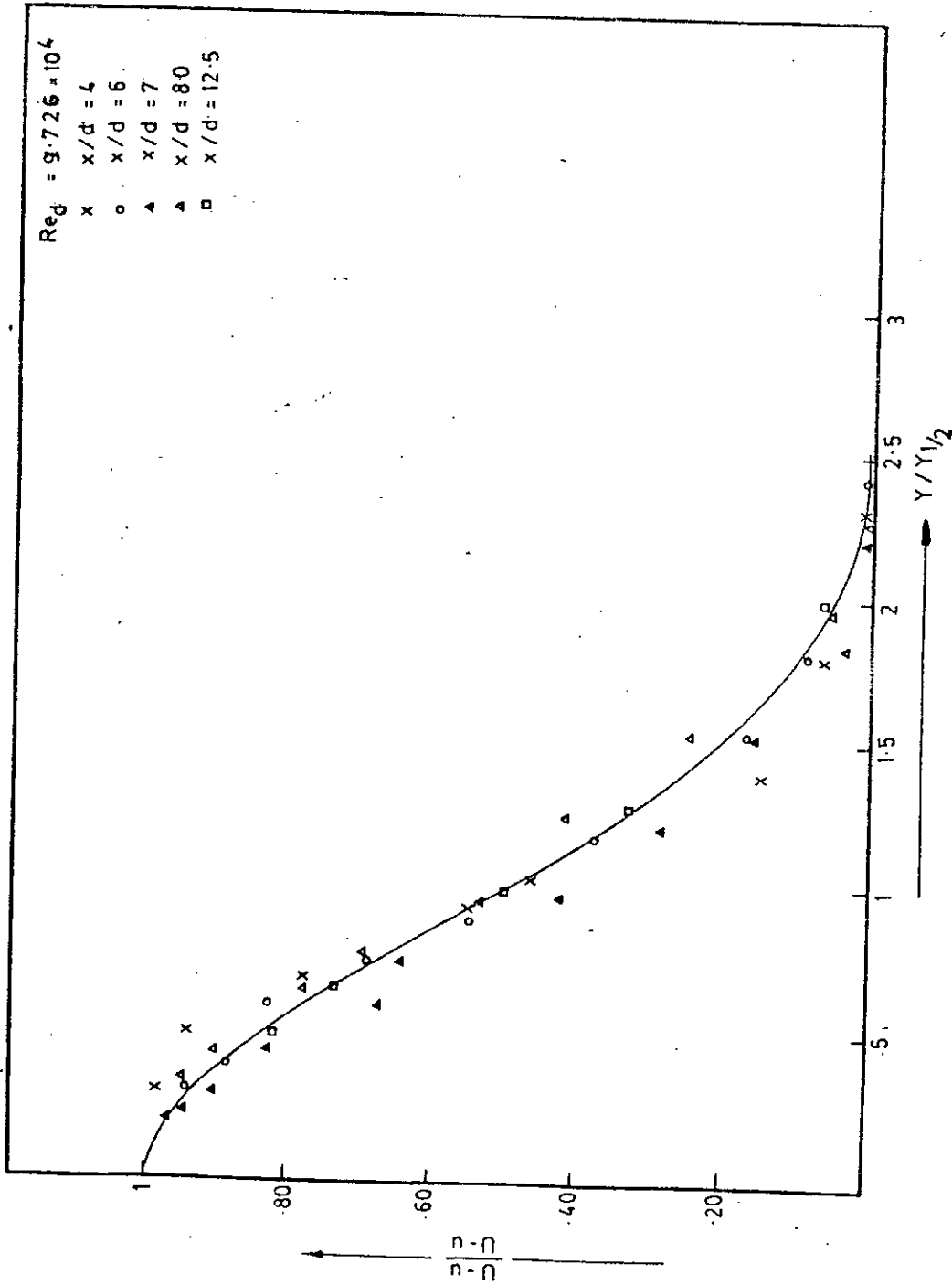
Fig. 5-3-3-c Dimensionless velocity profile in the wake behind a cylinder
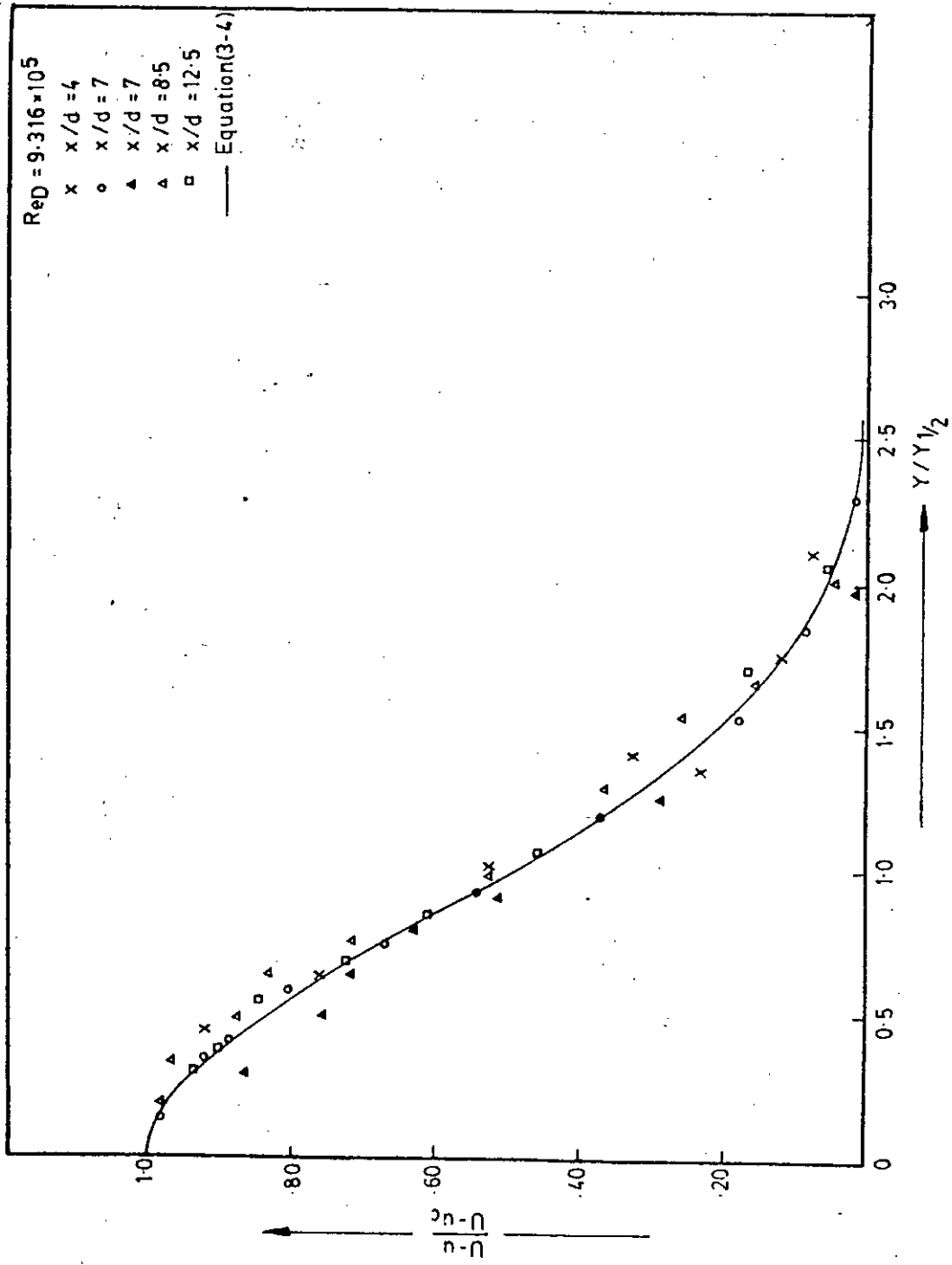
Fig. 5-3-3-d Dimensionless velocity profile in the wake behind a cylinder

Smooth cylinder
x/d = 12·5

rms deviation

Red
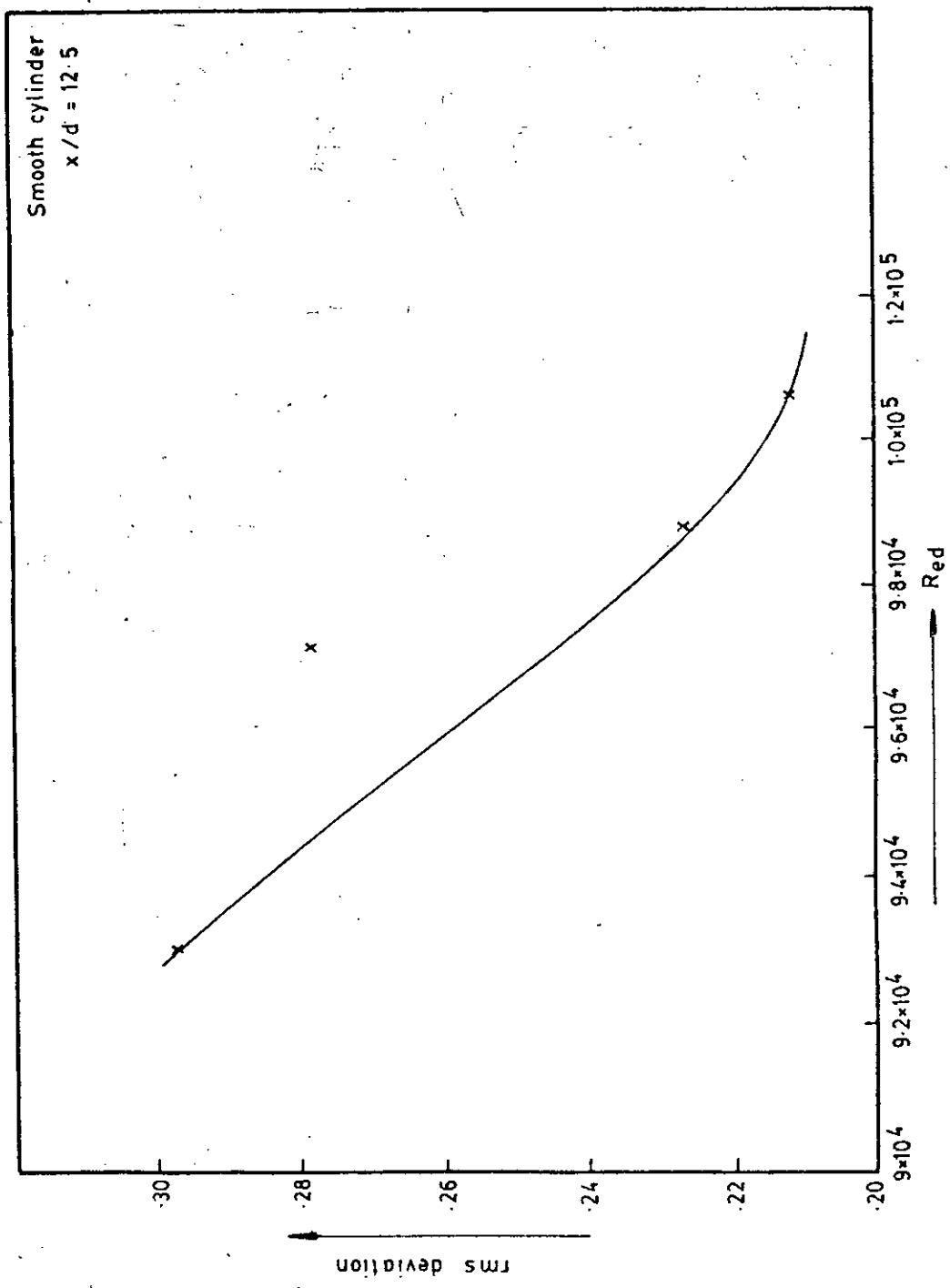
Fig. 5-3-3-e Variation of rms deviation with reynolds no.

Direction of Flow
Flow pattern around the cylinder.

Fig. 5-4-a
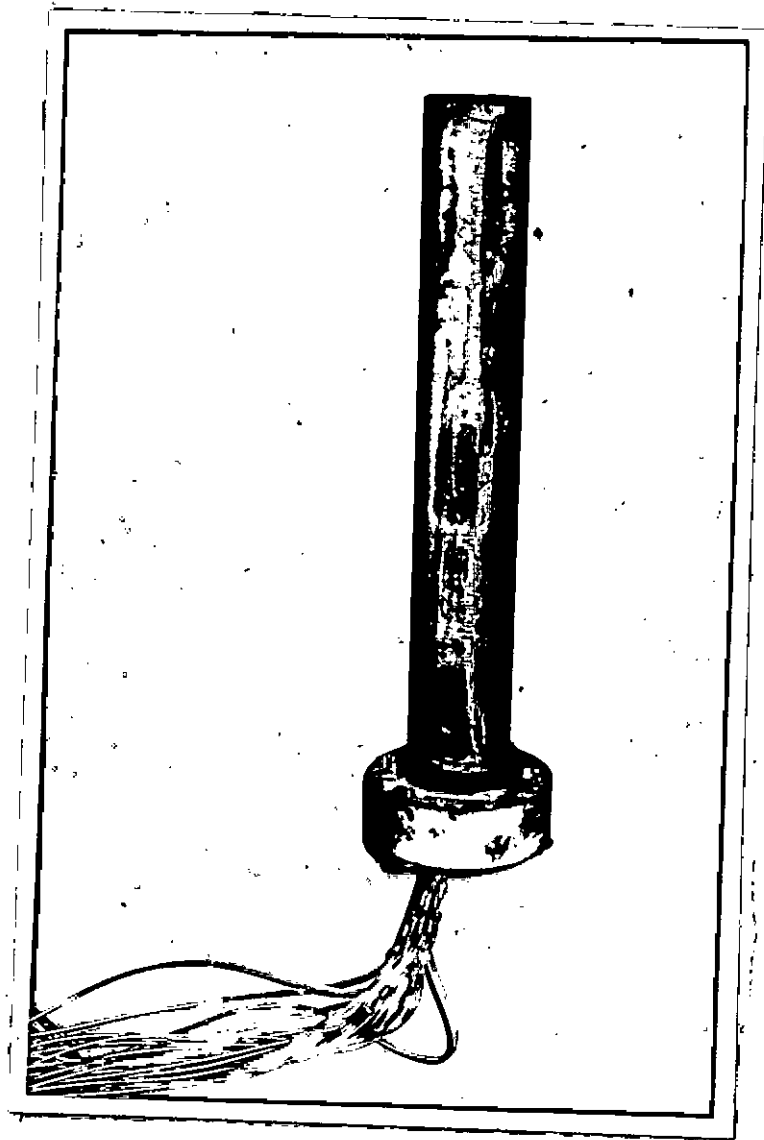
Direction of Flow

Flow pattern around the cylinder

Fig. 5-4-b
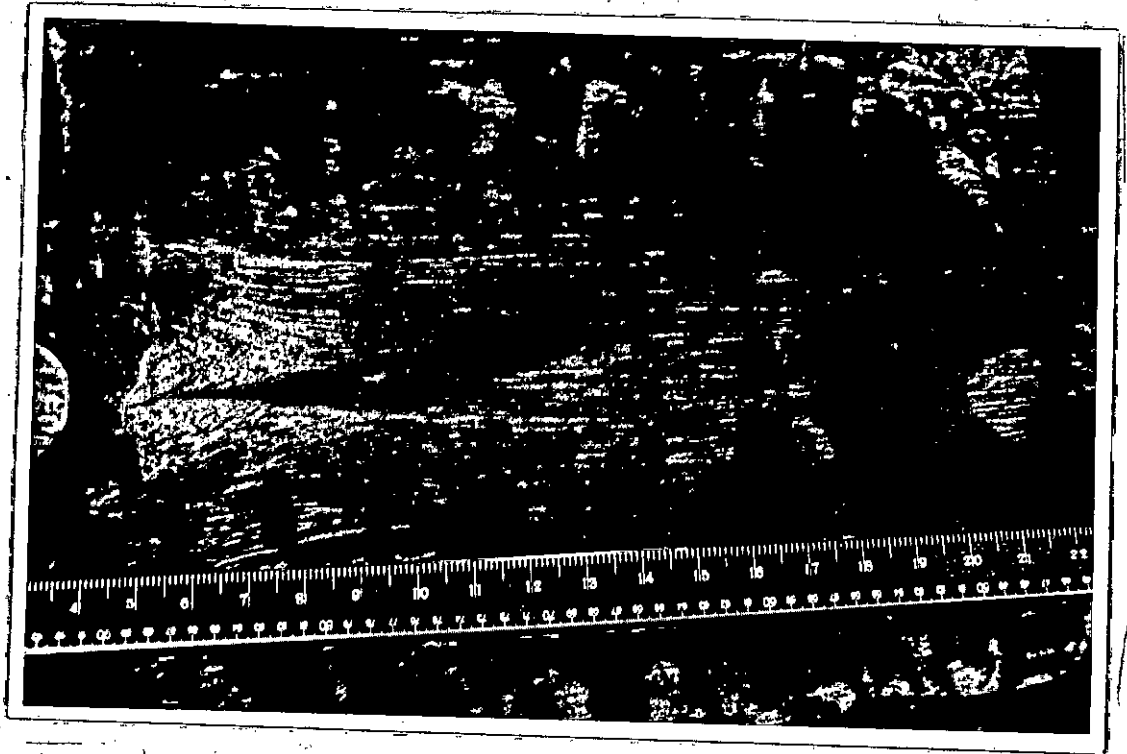
Direction of Flow

Flow pattern behind the cylinder

Fig. 5-4-c

Direction Flow

Flow pattern behind the cylinder (12"×12" WIND TUNNEL, 2.4" PERPEX
CYLINDER)

Fig. 5-4-d

APPENDICES

APPENDIX - A

Determination of Drag Coefficient By Momentum Equation

The cross section of cylinder, test section, the
position of pitot tube and the control volume (marked by
doted line) are presented below.

The flow direction is from left to right
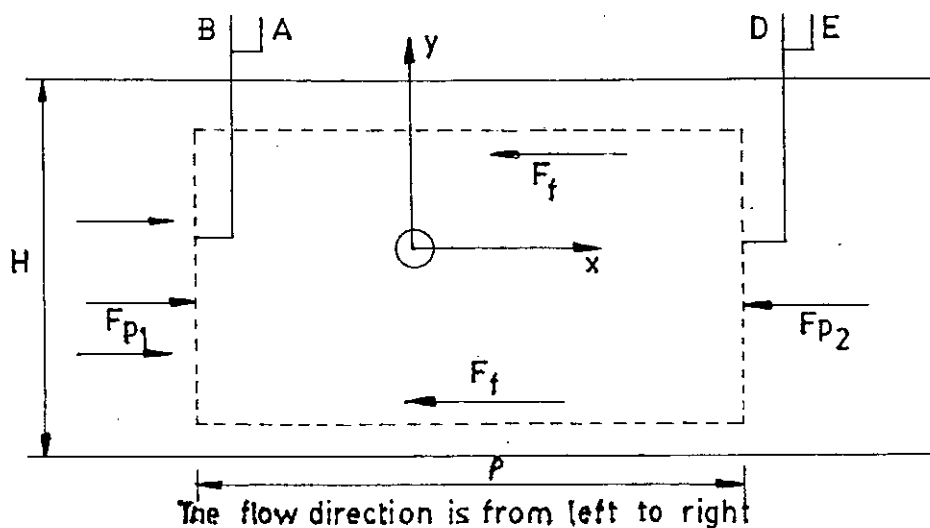
If the momentum equation on the control volume is
applied for steady flow then

$$Fx = \int_A \rho \, V_x \cdot V \cos\alpha \, dA \qquad (A.1)$$

But $F_x = F_{p1} - F_{p2} - 2F_f - D$

Where $F_{p1} = P_1 \cdot h_1 \cdot 1$ Force at section 1; $F_{p2} = \int p_2 dh$
Force at section 2; $F_f = \int \tau_0 \, dl \cdot 1$ friction force; and D is the
drag force. Since no flow takes place across the top and
bottom walls, $V \cos\alpha = 0$ for these surfaces.

So for station (1) $V_x = u$ and $V \cos\alpha = -u$ (because $\cos\alpha = -1$)

and for station (2) $V_x = v$ and $V \cos\alpha = v$.

Therefore, $\int_A \rho V_x . V \cos\alpha \, dA = -\rho_a \int_0^H u^2 dy + \rho_a \int_0^H v^2 dy$

so $\qquad P_1 H - \int_h P_2 dh - 2\int \tau_o dl - D = -\rho_a \int_0^H u^2 dy + \rho_a \int_0^H v^2 dy$

or $\qquad D = P_1 H - \int_H P_2 \, dh + \rho_a \int_0^H u^2 dy - \rho_a \int_0^H v^2 dy - 2\int \tau_o dl$

Since the flow pattern is symmetrical, the reading should be taken from origin to bed surface and multiply the results by 2. So the drag force per unit length becomes

$$D = P_1 . H - 2\int_0^{H/2} P_2 dh + 2\rho_a \int_0^{H/2} u^2 dy - 2\rho_a \int_0^{H/2} v^2 dy - 2\int \tau_o dl$$

$$(A.2)$$

$$\tau_o = \mu \frac{du}{dy}\bigg/_{y=0}$$

velocity gradients are taken at bed and are multiplied by viscosity to get friction stress. Then the drag coefficient is calculated by

$$C_d = \frac{D}{\frac{1}{2}\rho U^2 . d}$$

APPENDIX - B

Determination of Drag Coefficient By the Integration of Local Pressure Around the Cylinder

To the 69.85 mm diameter cylinder, the nineteen holes are made to the upper half part at an interval of 10°. The arrangement of the holes and the flow conditions are as follows.
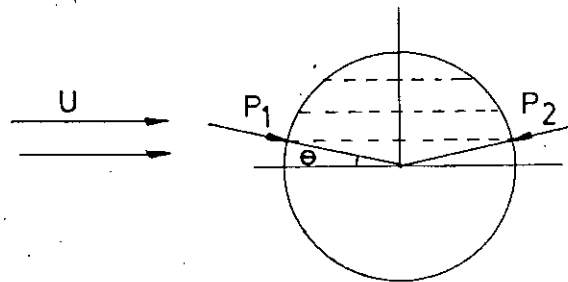
The pressure P_1 in the x direction is $P_1 \cos \theta$ and P_2 acts as $-P_2 \cos\theta$. The drag force acted on the cylinder D is

$$D = \int dD = \int P.dA \qquad dA = R.d\theta \times 1 \qquad (b.1)$$

where dA is the perpendicular area on which the pressure P is taken. So $D = \int (P_1-P_2) \cos \theta . R \, d\theta$. θ varies from 0 to 90° and giving drag for half part of the cylinder; So the total drag is obtained by

$$D = 2 \int_0^{\pi/2} (P_1-P_2) \cos\theta \, R \, d\theta \qquad (B.2)$$

Finally the drag coefficient is calculated by

$$C_d = D/(\tfrac{1}{2}\rho U^2 . d)$$

APPENDIX - C

Determination of Drag Coefficient From the Wake Profile
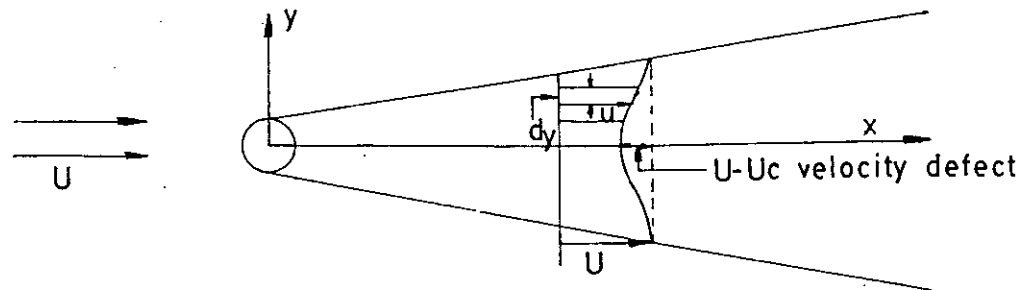
Scheme of wake flow behind a cylinder

A cylinder of diameter d is immersed in a flow stream of velocity U and density ρ. A wake is formed behind the cylinder where the magnitude of velocity is less than U. The centre line velocity is the smallest velocity of the wake. The width of the wake increases with distances from the cylinder (body) and the dip in the velocity profile gradually levels off. The cylinder will be subjected to drag force D during the flow. Now an element dy is taken of the area of the plane (+Y to the flow direction) in the wake and if u is the air velocity in this area, then the total flux of momentum is equal to the drag D. Thus

$$D = l\rho \int_{y=0}^{\alpha} u\ (U-u)\,dy \qquad\qquad (C.1)$$

Where l is the length of the cylinder.

or
$$D = \rho \int u(U-u) \, dy \qquad\qquad (C.2)$$

where D is now force per unit length.

Assuming the static pressure in the undisturbed zone to be zero and the total head as g_O and the total head at a point of measurement as g' it can be written as

$$g_O = \tfrac{1}{2}\rho U^2 \qquad g' = \tfrac{1}{2}\rho u^2$$

Then equation (C.2) becomes by putting the above values

$$D = \rho \int \sqrt{\frac{2g'}{\rho}} \; (\; \sqrt{\frac{2g_O}{\rho}} - \sqrt{\frac{2g'}{\rho}} \;) \; dy$$

$$D = \rho \int \sqrt{\frac{2g'}{\rho}} \cdot \sqrt{\frac{2}{\rho}} \; (\; \sqrt{g_O} - \sqrt{g'}) \; dy$$

$$= \rho 2/\rho \int \sqrt{g'} \; (\; \sqrt{g_O} - \sqrt{g'}) \; dy$$

$$= 2 \int \sqrt{g'} \; (\; \sqrt{g_O} - \sqrt{g'}) \; dy \qquad\qquad (c.3)$$

Now putting $\quad g = \dfrac{g'}{g_O} = \dfrac{\tfrac{1}{2}\rho u^2}{\tfrac{1}{2}\rho U^2} = (\dfrac{u}{U})^2$

Equation (C.3) becomes

$$D = 2 \int \sqrt{g \cdot g_O} \; (\; \sqrt{g_O} - \sqrt{g \cdot g_O}) \; dy$$

$$= 2 \sqrt{g_O} \cdot \sqrt{g_O} \int \sqrt{g} \; (1 - \sqrt{g}) \; dy$$

$$= g_o \int 2 \sqrt{g} \ (\ 1- \sqrt{g}) \ dy$$

$$= \tfrac{1}{2} \rho U^2 \int 2. \ u/U \ (\ 1-u/U) \ dy \qquad\qquad (C.4)$$

But the coefficient of drag C_D is defined as

$$C_D = \frac{D}{\tfrac{1}{2} \rho U^2 . d} \qquad\qquad (C.5)$$

Where D is the drag per unit length of the cylinder.

Comparing equation (C.4) and (C.5) it is obtained

$$C_D = \int 2 \frac{u}{U} \ (\ 1- \frac{u}{U} \ ) \ d(\ \frac{y}{d} \ ) \qquad\qquad (C.6)$$

So by measuring velocity distribution in the wake of the cylinder and by applying equation (C.6) the drag coefficient is calculated.

APPENDIX - D

Determination of Wall Shear Velocity

The law of the wall for smooth surface is

$$u/U^* = \frac{1}{k} \log \frac{yU^*}{\nu} + B' \qquad (D.1)$$

where k and B' are universal consts, k also known as Von karman's constant. The numerical values are k = .41 & B' = 4.9. These are the average values found by clauser from various sources.

Now multiplying both sides of (D -1) by $U^*/U = \sqrt{C_f/2}$

The equation becomes

$$\frac{u}{U^*} \times \frac{U^*}{U} = \frac{1}{.41} \times \log \frac{yU^*}{\nu} \times \sqrt{\frac{C_f}{2}} + 4.9 \times \sqrt{\frac{C_f}{2}}$$

$$\frac{u}{U} = \frac{1}{.41} \log \{\frac{y}{\nu} (U. \sqrt{\frac{C_f}{2}})\} \times \sqrt{\frac{C_f}{2}} + 4.9 \times \sqrt{\frac{C_f}{2}}$$

$$= 5.6 \sqrt{\frac{C_f}{2}} \log \frac{yU}{\nu} + 5.6 \sqrt{\frac{C_f}{2}} \{\log \sqrt{\frac{C_f}{2}} + 875 \}$$

$$= 5.6 \sqrt{\frac{C_f}{2}} \log \frac{yU}{\nu} + C \qquad (D.2)$$

$$= m \log yU/\nu + C$$

or Y = m X + C which is a linear equation $\qquad (D.3)$

where Y = u/U

and $m = 5.6 \sqrt{C_f/2}$, slope of the curve and

and $C = 5.6 \sqrt{C_f/2} \{\log \sqrt{C_f/2} + .875\}$, intercept of the curve with the ordinate.

By plotting. u/U versus yU/ν for all the points in semi log scale, the value of m could be calculated from which the value of $\sqrt{C_f/2}$ can be calculated.

By putting the value of $\sqrt{C_f/2}$ in the equation

$$U^* = \sqrt{\frac{C_f}{2}} \cdot U,$$ the value of shear velocity U* can be found out .

Plotting U/U* versus yU^*/ν in semi-log scale, the equation (D.1) the law of the wall can fairly be proved and a straight line will be drawn indicating developed flow.

APPENDIX - E

Uncertainty Analysis

Some errors are introduced during the measurement, such as for atmospheric changes, measuring instruments, the probe settings. Uncertainties thus crept into the measurements of velocity and pressure is analysed in the way as suggested by Kline and McClintock (25).

E.1 Uncertainty in Mean Velocity Measurements:

The draft gauge was calibrated for water head reading for manometric fluid petrol of density .834. But during the experiment kerosin was used of density .7851. So the actual height indicates the multiplication of the measured height by $\frac{.7851}{.834}$. When air was flowing with a velocity of U cm/sec and a pitot static tube was placed parallel to the flow, the velocity was found from the dynamic head h_w cm of water recorded by the Elison draft gauge from the relation

$$u = \sqrt{\frac{2.g.h_w.\gamma_w}{\gamma_a}} \times \frac{.7851}{.834} \qquad (E.1.1)$$

where γ_w and γ_a were the specific wts of water and air respectively. If the sensing point of the pitot static tube had a misalignment of θ from the direction fof flow due to adjustment error, then the measured velocity would be

$$u = \sqrt{\frac{2g \cdot h_w \cdot \gamma_w}{\gamma_a}} \times \frac{.7851}{.834} \cdot \sec \theta \qquad (E.1.2)$$

Using $P = \gamma_a RT$ (E.1.3) where P, R and T are pressure, gas constant and absolute temperature of air respectively, then velocity u becomes

$$u = \sqrt{2g \cdot h_w \gamma_w \times RT/p} \times (.7851/.834) \sec \theta$$

$$= \sqrt{\frac{2g \cdot R \cdot \gamma_w}{\quad}} \times \frac{.7851}{.834} \times \sqrt{h_w \cdot T/p} \sec \theta$$

$$= C \sqrt{h_w \ T/p} \ \sec \qquad (E.1.4)$$

But the variation of specific wt. of water during measurements does not arise since the temperature difference becomes very small.

If $\quad u = f (\alpha_1, \alpha_2, \ldots, \alpha_n)$ \hfill (E.1.5)

Then the mean $\mu_u = f (\bar{\alpha}_1, \bar{\alpha}_2, \ldots \bar{\alpha}_n)$ \hfill (E.1.6)

and the variance $\quad \sigma^2_u = \leqq (\frac{\partial u}{\partial \alpha_i})^2 \sigma \alpha_i$ \hfill (E.1.7)

In terms of objective coefficients of variance

$$\delta^2_u = \frac{\sigma^2 u}{\mu^2 u} = \Sigma \ (\frac{\partial u}{\partial \alpha_i} \cdot \frac{\bar{\alpha}_i}{\mu_u})^2 \ , \ (\frac{\sigma \alpha_i}{\bar{\alpha}_i})$$

$$\simeq \quad \sum_{i=1}^{n} \quad \left(\frac{\partial u}{\partial \alpha_i} \cdot \frac{\bar{\alpha}_i}{\mu_u} \right)^2 \quad \delta^2{}_{\alpha i} \tag{E.1.8}$$

where δ_u is the coefficient of variance (C.O.V.) and $\delta\alpha_i$ is the C.O.V. of free variables α_i.

It may be noted that C.O.V. is often used as measure of uncertainties.

Here $u = f(T, p, h_w, \theta)$

So the uncertainty in velocity measurement can be expressed as

$$\sigma_u = \left(\frac{\partial u}{\partial p} \cdot \sigma_p \right)^2 + \left(\frac{\partial u}{\partial T} \cdot \sigma_T \right)^2 + \left(\frac{\partial u}{\partial hw} \cdot \sigma_{hw} \right)^2 + \left(\frac{\partial u}{\partial \theta} \cdot \sigma_\theta \right)^2$$

$$\tag{E.1.9}$$

Where σ_p, σ_T, σ_{hw} and σ_θ are uncertainties associated with pressuere, temperature manometer reading and alignment of the probe with flow direction.

To get the uncertainties involved in the different variables the respective partial derivatives are now found out. Again writing equation (E.1.4) in the form

$$u = C \sqrt{h_w \cdot T/P} \ \ \sec \theta \tag{E.1.10}$$

where $\quad C = \sqrt{2g} . R . \gamma_w \quad x \dfrac{.7851}{.834}$ $\hspace{2cm}$ (E.1.11)

The partial derivatives of U are found to be

$$\frac{\partial u}{\partial p} = C \sqrt{h_w . T} . \sec \theta \ x - \tfrac{1}{2} \ P^{-3/2}$$

$$= - C/2 \sqrt{h_w \ T/P^3} \ . \ \sec \theta \hspace{2cm} (E.1.12)$$

and $\dfrac{\partial u}{\partial T} = C \sqrt{h_w/P} \ . \ \sec \theta . \ \tfrac{1}{2} \ . \ T^{-\frac{1}{2}}$

$$= C/2 \sqrt{h_w/TP} \quad \sec \theta \hspace{2cm} (E.1.13)$$

and $\dfrac{\partial u}{\partial h} = C \sqrt{T/P} . \ \sec \theta . \ \tfrac{1}{2} h_w^{-\frac{1}{2}}$ $\hspace{2cm}$ (E.1.14)

$$\frac{\partial u}{\partial \theta} = C \sqrt{h_w . T/P} . \ \sec\theta \ . \ \tan \theta \hspace{2cm} (E.1.15)$$

Putting these equations to (E.1.19) we get

$$\sigma_u = \{ (-C/2 \sqrt{\frac{h_w . T}{P^3}} . \ \sec \theta . \ \sigma_p)^2 + (C/2 \ \sec \theta \sqrt{\frac{h}{TP}} \ \sigma_T)^2$$

$$+ (C/2 . \sqrt{T/Ph} \ . \ \sec \theta . \ \sigma_h)^2 \ (+C \sqrt{h_w T/P} . \ \sec \theta . \tan\theta \ \sigma_\theta)^2 \}^{\frac{1}{2}}$$

$$= \{ C^2/4 . \frac{h_w T}{P^3} (\sec \theta)^2 . \ \sigma_p^2 + C^2/4 . \ h/T.P. \ (\sec \theta)^2 . \ (\sigma_T)^2$$

$$+ \frac{C^2}{4} . \ T/P.h_w . \ \sec^2\theta \ \sigma_{hw}^2 + C^2 . h_w T/P. \ \sec^2\theta \ . \ \tan^2\theta \ \sigma_\theta^2 \}^{\frac{1}{2}}$$

$$= C/2 \quad \cos \theta \{ \, (\frac{h_w T}{p^3}) \; \sigma_p^2 \; + \; (\frac{h_w}{T \cdot P}) \cdot \; \sigma_T^2 \; + (\frac{T}{p \cdot h_w}) \sigma_{hw}^2 + \; 4 (\frac{h_w T}{p})$$

$$\sigma_\theta^2 \cdot \tan^2 \theta \, \}^{\frac{1}{2}} \qquad\qquad (E.1.16)$$

Now dividing equation (E.1.12) by (E.1.6) the uncertainty in velocity measurement takes the form

$$\frac{\sigma u}{u} = \frac{1}{2} \{ \frac{\sigma^2 p}{p^2} + \frac{\sigma^2 T}{T^2} + \frac{\sigma^2 hw}{hw^2} + 4\sigma \theta^2 \cdot \tan^2 \theta \}^{\frac{1}{2}}$$

The direction is taken for objective uncertainties. There is also subjective uncertainties which is considered 5%, so the final uncertainties form becomes

$$\frac{\sigma u}{u} = \frac{1}{2} \; (\frac{\sigma p^2}{p^2} + \frac{\sigma T^2}{m^2} + \frac{\sigma hw^2}{hw^2} + 4\sigma \theta^2 \; \tan^2 \theta + \Delta \delta^2)^{\frac{1}{2}}$$

Now during an experimental run, the following conditions were observed.

$$P = 76.2 \text{ cm} \pm .127 \text{ cm of Hg.}$$
$$T = 83^\circ \pm 2^\circ F$$
$$h_w = 6.35 \text{ cm} \pm .0254 \text{ cm of water}$$
$$\theta = 0^\circ \pm 2^\circ$$

The corresponding uncertainty in velocity measurement becomes

$$\sigma_u / u = .0123 \text{ or } 1.23\%.$$

E.2 Uncertainty for Pressure Measurements:

The wall static pressures (cylinder) measured from the surface tappings were the gage pressure below atmospheric pressure. If P be the absolute static pressure and P_a be the atmospheric pressure, then the recorded pressure be

$$P_r = P_a - P \qquad\qquad (E.2.1)$$

and the absolute static pressure

$$P = P_a - P_r \qquad\qquad (E.2.2)$$

The recorded pressure is nothing but $\gamma_w h_w'$. So that

$$P = P_a - \gamma_w h_w' \qquad\qquad (E.2.3)$$

Since in manometer, kerosine is used in lieu of petrol, so hw' becomes

$$= h_w \times \frac{.7851}{.834}$$

$$P = P_a - \frac{\gamma_w h_w}{100} \times \frac{.7851}{.834} \qquad\qquad (E.2.4)$$

where h_w is in cm. of water

Since the change of density of water is negligble, so the uncertainty in surface static pressure measurement is

$$\sigma_p = \left\{ \left(\frac{\partial P}{\partial P_a} \cdot \sigma_{pa} \right)^2 + \left(\frac{\partial P}{\partial h_w} \cdot \sigma_{hw} \right)^2 \right\}^{\frac{1}{2}} \qquad (E.2.5)$$

Now $\quad \frac{\partial P}{\partial P_a} = 1$

$$\frac{\partial P}{\partial h_w} = -\gamma_w \frac{.7851}{.834} \times \frac{1}{100}$$

$$\sigma_p = \left\{ \sigma_{pa}^2 + \gamma_w^2 \left(\frac{.7851}{.834} \times \frac{1}{100} \right)^2 \cdot \sigma_{hw}^2 \right\}^{\frac{1}{2}} \qquad (E.2.6)$$

$$\frac{\sigma_p}{P} = \frac{\left\{ \sigma_{pa}^2 + \gamma_w^2 \left(\frac{.7851}{.834 \times 100} \right)^2 \sigma_{hw}^2 \right\}^{\frac{1}{2}}}{P_a - h_w \gamma_w \frac{.7851}{.834} \times \frac{1}{100}}$$

But for short interval $\sigma_{pa} = 0$

$P = 101,325 \ N/m^2$

$\gamma_w = 1000 \ kg/m^3$

$h_w = 6.45 \ cm \pm .0254 \ cm \ of \ H_2O$

$\sigma_p/P = 1.139 \times 10^{-6} \qquad i.e., \ .00011389\%.$

However the pressure recording was greatly related to the freeness from the sand grain particles of the pressure holes. When static pressure at the downstream and upstream side was measured by pitot static tube, the recorded static pressure was subjected to error of misalignment. If h was the manometer

reading, then the recorded pressure would be

$$Pr = \gamma_w \cdot \frac{h_w}{100} \times \frac{.7851}{.834} - \frac{\gamma_a}{2g} U^2 \cdot \cos^2 (90^\circ - \theta) \qquad (E.2.7)$$

which can be reduced to the form

$$Pr = \frac{\gamma_w}{100} \times \frac{.7851}{.834} h_w - \frac{1}{2g \cdot R} \cdot \frac{P_a \cdot U^2}{T} \sin^2 \theta \qquad (E.2.8)$$

h being measured in cm of water

So $\qquad Pr = P_1 + P_2 \qquad\qquad (E.2.9)$

where $\qquad P_1 = \frac{\gamma_w}{100} \times \frac{.7851}{.834} h_w = C_1 h_w \qquad (E.2.10)$

and $\qquad P_2 = - \frac{1}{2g \cdot R} \cdot \frac{P_a \cdot U^2}{T} \sin^2 \theta = C_2 \frac{P_a U^2}{T} \sin^2 \theta \qquad (E.2.11)$

If σ_{P1} and σ_{P2} are uncertainties in P_1 and P_2 respectively then accordingly

$$\sigma_{P1} = (\partial_{P1}/\partial h) \cdot \sigma_{hw} \qquad (E.2.12)$$

But $\qquad (\partial_{P1}/\partial h) = C_1 \qquad\qquad (E.2.13)$

$$\frac{\sigma_{P1}}{P_1} = \frac{C_1 \sigma_{hw}}{C_2 h_w} = \frac{\sigma_{hw}}{h_w} \qquad (E.2.14)$$

and $\sigma_{P2} = \{ (\frac{\partial P_2}{\partial p} \cdot {}_p)^2 + (\frac{\partial P_2}{\partial T} \cdot \sigma_T)^2 + (\frac{\partial P_2}{\partial u} \cdot \sigma_u)^2 + (\frac{P_2}{\partial \theta} \cdot \sigma_\theta)^2 \}^{\frac{1}{2}}$

$$(E.2.15)$$

But
$$\frac{\partial P_2}{\partial P_a} = C_2 \cdot \frac{U^2}{T} \sin^2 \theta \qquad \text{(E.2.16)}$$

and
$$\frac{\partial P_2}{\partial T} = - \frac{C_2 P_a U^2}{T^2} \sin^2 \theta \qquad \text{(E.2.17)}$$

and
$$\frac{\partial P_2}{\partial u} = \frac{2C_2 P_a \cdot U}{T} \sin^2 \theta \qquad \text{(E.2.18)}$$

and
$$\frac{\partial P_2}{\partial \theta} = \frac{2C_2 P_a U^2}{T} \sin \theta \cdot \cos \theta \qquad \text{(E.2.19)}$$

So the equation (E.2.15) becomes by putting these value

$$\sigma_{P2} = \{ C_2^2 \cdot \frac{u^4}{T^2} \cdot \sin^4 \theta \cdot \sigma_p^2 + \frac{C_2^2 \cdot P_a^2 \cdot U^4}{T^4} \cdot \sin^4 \cdot \sigma_T^2$$

$$+ 4 \cdot C_2^2 \cdot \frac{P_a^2 \cdot U^2}{T^2} \cdot \sin^4 \theta \cdot \sigma_u^2 + \frac{4C_2^2 \cdot P_a^2 \cdot U^4}{T^4} \cdot \sin^2 \theta \cos^2 \theta \cdot \sigma_\theta^2 \}^{\frac{1}{2}}$$

$$\text{(E.2.20)}$$

Now the uncertainty of P_2 can be written with help of (E.2.11) as

$$\frac{\sigma P_2}{P_2} = \{ (\frac{\sigma P_a}{P_a})^2 + (\frac{\sigma_T}{T})^2 + (\frac{2\sigma_u}{u})^2 + (\frac{2\sigma_\theta}{\tan\theta})^2 \}^{\frac{1}{2}} \qquad \text{(E.2.21)}$$

Now from equation (E.2.9), the uncertainty in measurement of Pr is

$$\sigma_{Pr} = \{ (\frac{\partial Pr}{\partial P_1} \cdot \sigma P_1)^2 + (\frac{\partial Pr}{\partial P_2} \cdot \sigma P_2)^2 \}^{\frac{1}{2}}$$

$$= \{ \sigma_{p1}^2 + \sigma_{p2}^2 \}^{\frac{1}{2}} \qquad \text{(E.2.22)}$$

During the experiment, the following conditions were observed

P = 76.2 cm $\pm$ .127 cm of Hg.

T = 83.0 $\pm$ 2°F

h_w = 6.35 cm $\pm$ .254 cm of H_2O.

θ = 0 $\pm$ 2°

u = 198 cm/sec $\pm$ 3.175 cm/sec

From equations (E.2.10), (E.2.11), (E.2.14), (E.2.21), (E.2.20)

$$P_1 \quad = 59.776$$

$$P_2 \quad = .0084$$

$$\sigma P_1/P_1 = .0416$$

$$\sigma P_2/P_2 = 1.9995$$

$$\sigma P_r \quad = 2.49$$
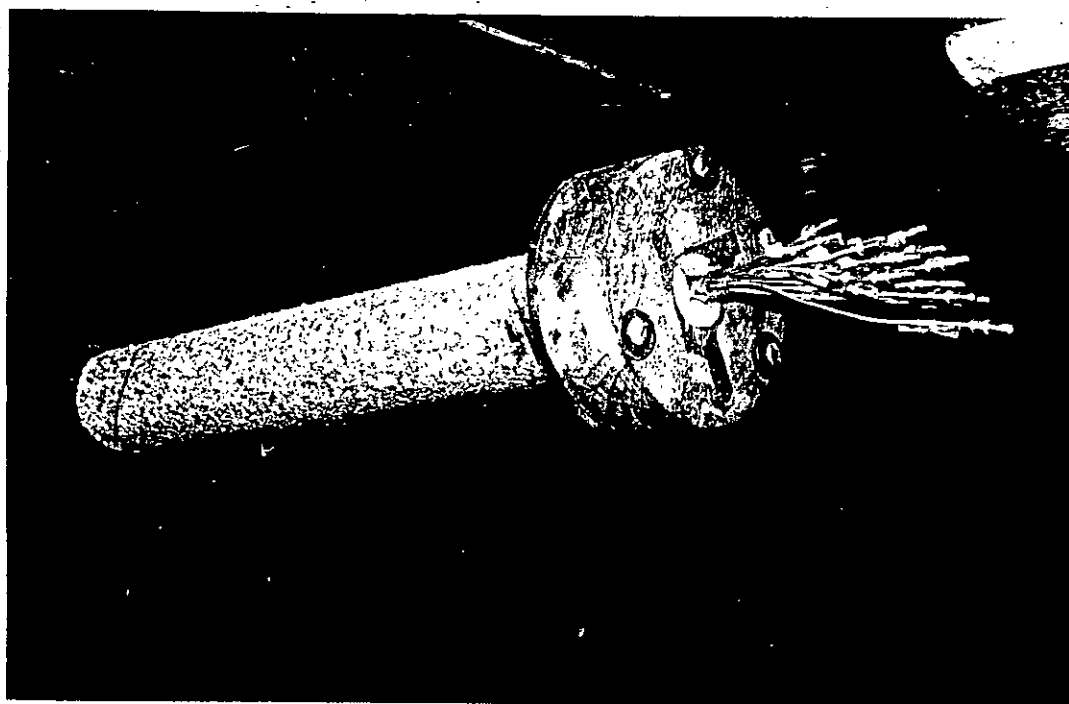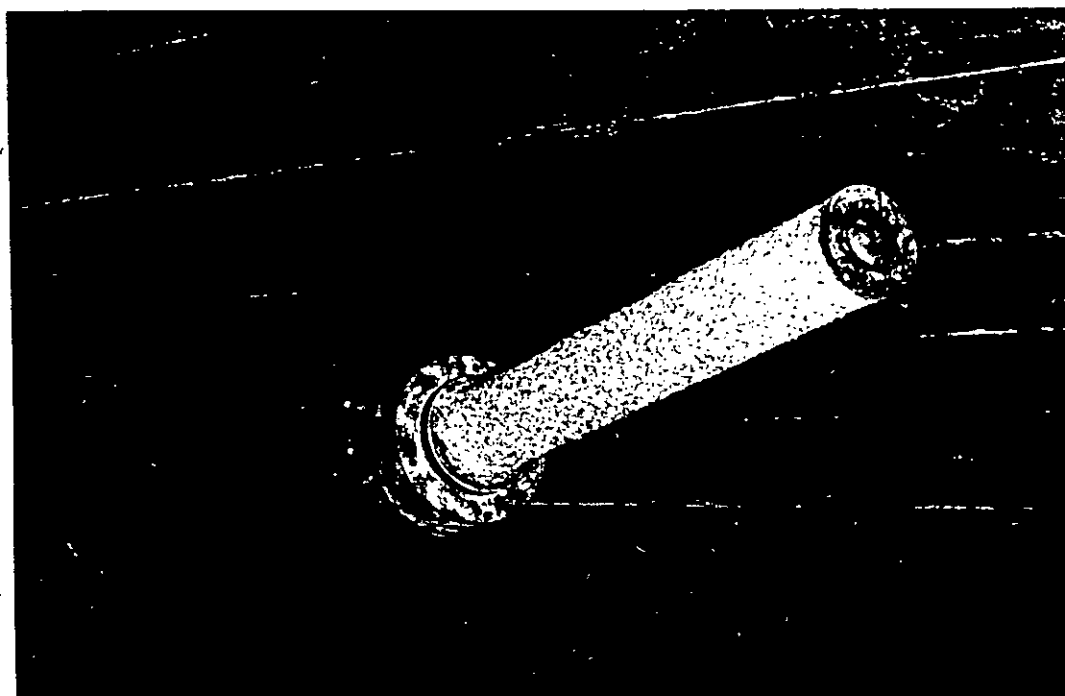
$$\sigma P_r/P_r = 0.0412$$

i.e., uncertainty is 4.12%.

PLATES
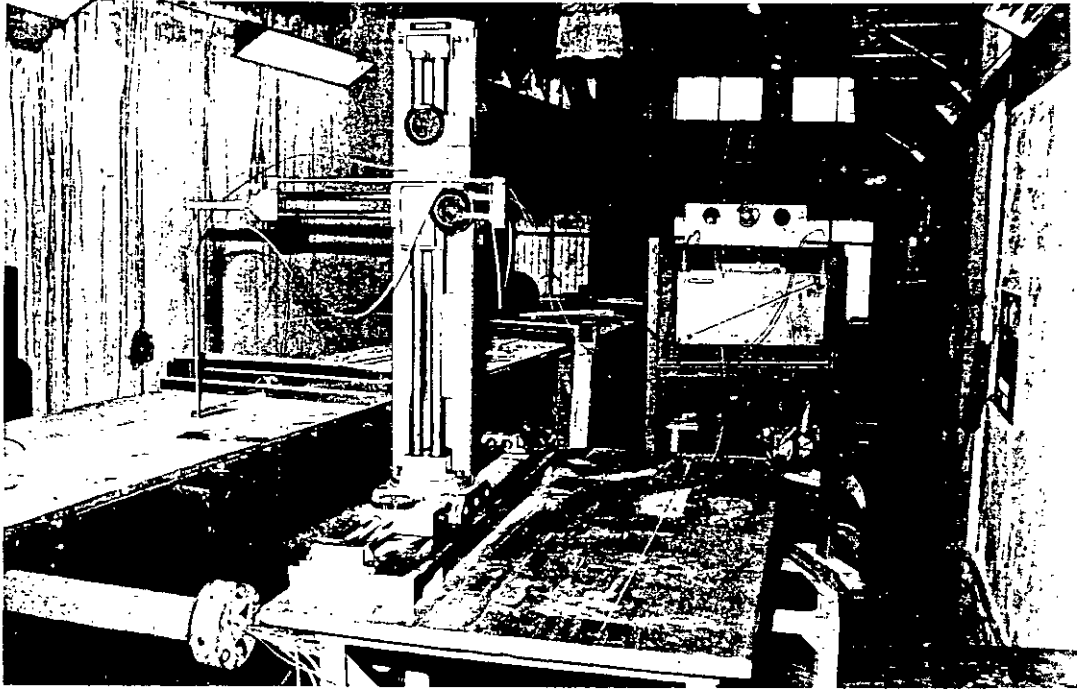
Plate 4-1 Sand roughened cylinder with tappings.

Plate 4-2 Vertical traversing Mechanism with pitot tube connections.
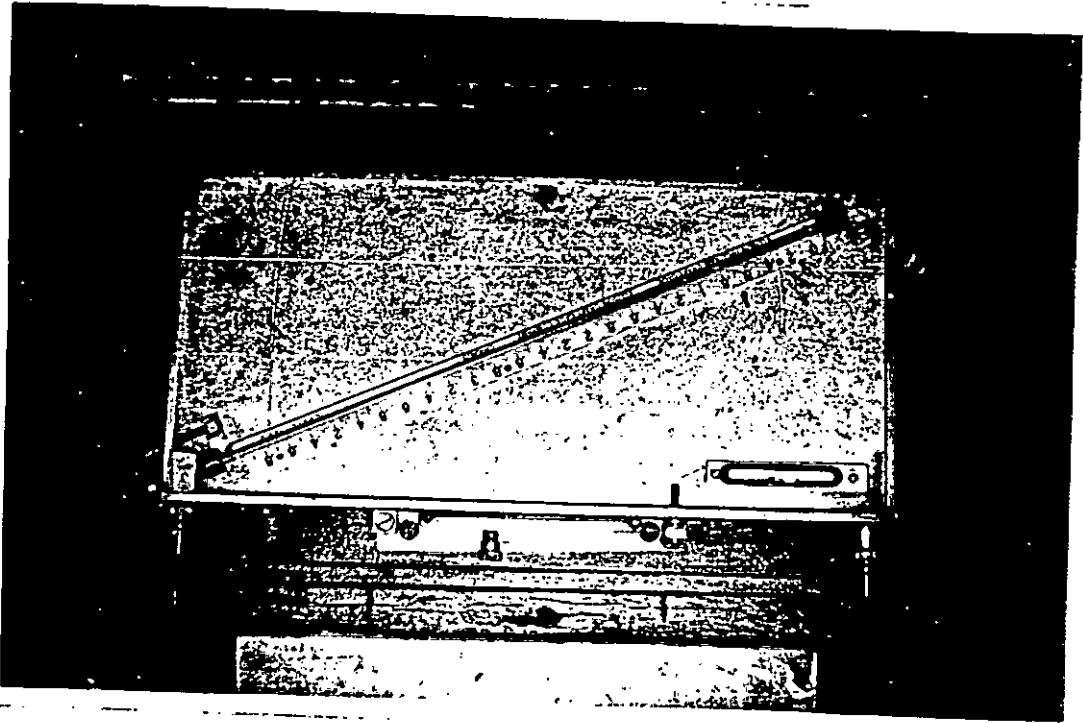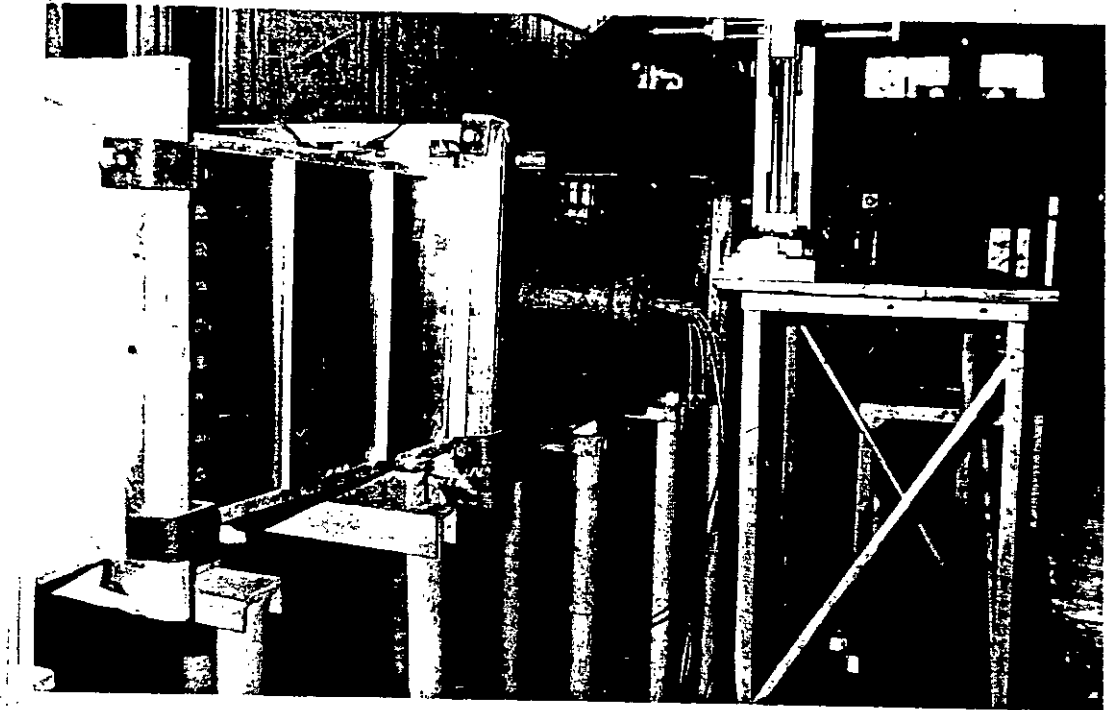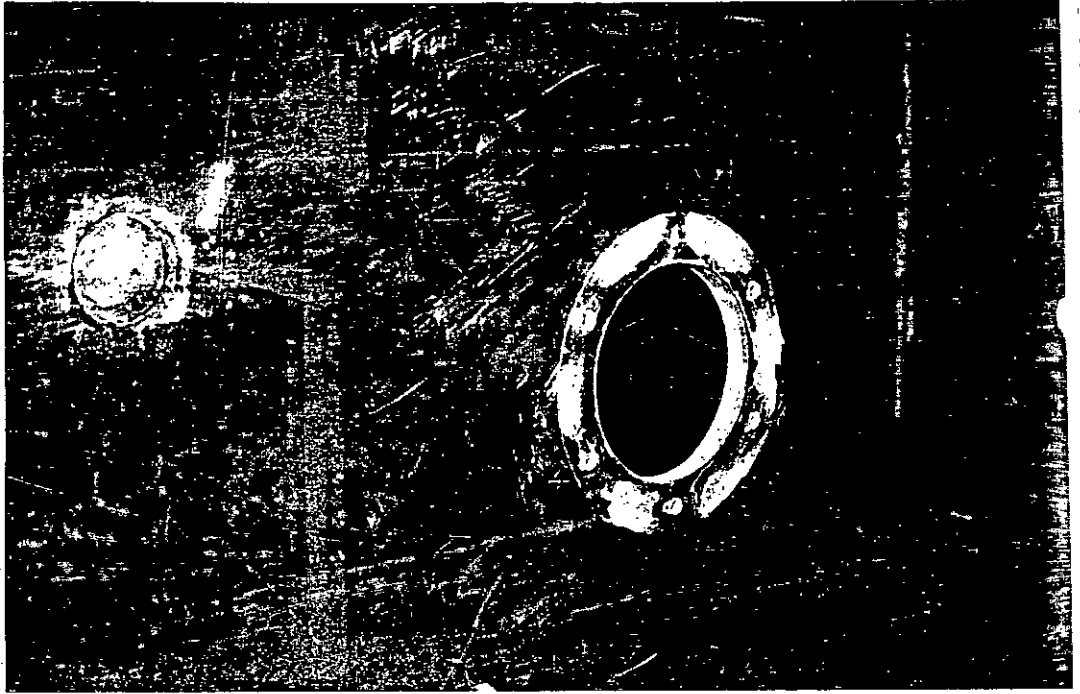
Plate 4-3 Draft Gauge.

Plate 4-4 Position of cylinder in wind tunnel.

Plate 4-5 Holes for inserting cylinder.